MEMS Resonator based Bandpass Filter Design for Wireless Communication Transceiver

THESIS

Submitted in the partial fulfillment of the requirements for the degree of

DOCTOR OF PHILOSOPHY

by

G.MEENAKSHI SUNDARAM

Under the supervision of

Dr. Kamaljit Rangra

BIRLA INSTITUTE OF TECHNOLOGY & SCIENCE
PILANI – 333 031 (RAJASTHAN) INDIA

2015

MEMS Resonator based Bandpass Filter Design for Wireless Communication Transceiver

THESIS

Submitted in the partial fulfillment of the requirements for the degree of

DOCTOR OF PHILOSOPHY

by

G.MEENAKSHI SUNDARAM
(ID.No.2007PHXF415P)

Under the supervision of

Dr. Kamaljit Rangra

Sensors and Nanotechnology Group
CSIR–Central Electronics Engineering Research Institute,
Pilani

BITS Pilani
Pilani | Dubai | Goa | Hyderabad

BIRLA INSTITUTE OF TECHNOLOGY & SCIENCE
PILANI – 333 031 (RAJASTHAN) INDIA

2015

BIRLA INSTITUTE OF TECHNOLOGY & SCIENCE
PILANI – 333 031 (RAJASTHAN) INDIA

CERTIFICATE

This is to certify that the thesis entitled **"MEMS Resonator based Bandpass Filter Design for Wireless Communication Transceiver"** submitted by **G.MEENAKSHI SUNDARAM**, ID.No. **2007PHXF415P** for award of Ph.D Degree of the institute embodies original work done by him under my supervision.

Signature in full of the Supervisor _____

Name : **Dr. Kamaljit Rangra**

Designation : **Chief Scientist and Professor AcSIR**
Sensors and Nanotechnology Group
CSIR–Central Electronics Engineering Research Institute (CERRI), Pilani

Date: _____

Dedicated

to

my parents

Acknowledgements

At the outset, I wish to express the deep sense of gratitude and sincere thanks to my supervisor Dr. Kamaljit Rangra, Chief Scientist and Professor AcSIR , Sensors & Nano-technology Group, CSIR–Central Electronics Engineering Research Institute, Pilani for his valuable guidance, encouragement, suggestions, and moral support throughout the period of this research work. It has been a privilege for me to work and learn under his valuable guidance.

I sincerely express my profound gratitude to Prof. V.S. Rao, Vice-Chancellor, BITS, Pilani for providing me the opportunity to carry out my Doctoral studies at BITS. I convey my honest thanks to Director of BITS-Pilani, Pilani Campus Prof. A.K. Sarkar. I thank Dr. Chandra Shekhar, former Director CEERI, Pilani for Laboratory Support. I thank Prof. G. Raghurama, former Director BITS-Pilani, Pilani Campus for his constant support. I am very much indebted to Prof. S Gurunarayanan, Dean (WILP Division) for their motivation during difficult times.

I also express my gratitude to Prof. S.K. Verma, Dean, Academic Research (Ph.D. Programme) Division and Dr. Hemant R Jadhav, Associate Dean, Academic Research (Ph.D. Programme) Division for providing valuable support throughout the programme.

I also thank to my Doctoral Advisory Committee members Dr. V.K. Chaubey and Dr. Navneet Gupta, Professors, EEE Department, BITS-Pilani who spared their valuable time for reviewing my draft thesis and giving their constructive criticisms and valuable suggestions which have immensely helped in improving the quality of my Ph.D. thesis report.

I would like to thank Prof. Anu Gupta, Head of EEE Department for motivating me throughout my Degree programme.

I also thank all my friends, especially Mr. Mahesh Angira for his constant support during my Ph.D. Thanks are also due to all faculty and staff members of BITS-Pilani, Pilani Campus, especially EEE Department for helping me out at various times. I also thank my students for their support and cooperation.

I would also like to thank Mr. Santosh Kumar Saini, Academic Registration & Counseling Division (ARCD), BITS-Pilani for his help in compilation of thesis.

Last but most importantly, I thank my parents for their care and affection shown towards me. My thanks are also extended to my wife Mrs. Meenakashi Sundareswari and loving daughter Sadhana for their affection.

G.Meenakshi Sundaram

CONTENTS	Page No.

List of Tables

List of Figures

List of Abbreviations

Abbreviations	Description
MEMS	Micro-Electro-Mechanical Systems
RF MEMS	Radio Frequency Micro-Electro-Mechanical Systems
CMOS	Complementary Metal-Oxide Semiconductor
LO	Local Oscillator
LNA	Low Noise Amplifier
IF	Intermediate Frequency
SAW	Surface Acoustic Wave
IDT	Inter Digital Transducers
BAW	Bulk Acoustic Wave
FBAR	Film Bulk Acoustic Resonator
Poly MUMPS	Polysilicon Multi User MEMS Process
FEM	Finite Element Method
IC	Integrated Circuit
BPF	Bandpass Filter
SOIMUMPs	Silicon on Insulator Multi User MEMS Process
VCO	Voltage Controlled Oscillator
PZT	Lead-Zirconate-Titanate
AlN	Aluminum Nitride

Symbols

Q	quality factor
f_0	center frequency
BW_{3dB}	3dB bandwidth
R_x	motional resistance
$\mathrm{R}_{\mathrm{port}}$	port resistance of the vector network analyzer
S_{21}	Transmission parameter
m	mass
γ	damping
k	linear spring constant
f	Force
f_e	electrostatic force
E	Energy
C	Capacitance
v	Voltage
V_p	bias voltage
v_i	alternating excitation voltage
d	Gap
A	overlap area between the resonator and the electrode.
ε_0	vacuum permittivity
i	output current
η	electromechanical coupling coefficient
L_m	motional inductance
C_m	motional capacitance
m_{re}	effective mass

k_{re}	effective stiffness
C_s	feed through capacitance between port 1 and 2
C_p	capacitances coupling the pads to the substrate
ω_{res}	Resonant frequency (radians /sec)
ζ	damping factor
R	disk radius
h	anchor height
d	Air gap between electrode and disk resonator
$\frac{\partial C_1}{\partial r}$	change in electrode-to-resonator overlap capacitance per unit radial displacement at the input port
φ_1	Angle defined by the edges of the input electrode
t	thickness
$\Re(r,\theta)$	zero-to-peak radial displacement amplitude at any point of the disk (r, θ)
ρ	density
σ	Poisson ratio
E	Young's modulus
k	parameter dependent upon Poisson's ratio
k_m	purely mechanical stiffness
k_e	electrical stiffness
α_{si}	thermal expansion coefficient of Silicon
α_e	thermal expansion coefficient of surrounding electrode
L_e	suspended electrode length
$v(r,\theta)$	velocity magnitude at location (r, θ)
C_{re}	Effective damping
η_{e1}, η_{e2}	Electromechanical coupling coefficient for port 1 and2
E_d	Young's modulus of the disk material

σ_{zz}	Normal stress on the substrate
u_z	displacement in the substrate due to the normal stress
Z_0	acoustic impedance
A_c	Coupling beam cross section Area.
β	Phase shift constant
v_p	Phase velocity
x	Displacement
k_{ij}	Normalized coupling coefficient between two consecutive resonators
k_{ri} , k_{rj}	resonator equivalent stiffness
K_{sij}	required spring constant of the coupling beam between i^{th} and j^{th} resonators
B	bandwidth of the filter
W	Width of the coupling beam
C_a, C_b, C_c	T Net work capacitance
$k_r(c)$	resonator stiffness at location c
Ls_a, Ls_b, Cs_c,	T Net work Inductor and capacitance
L_s	Length of V shape coupling beam

Abstract

The recent advances in microelectronics technology and the tremendous growth of the wireless-communication market have drawn muchinterest into radio-frequency MEMS devices (RF MEMS) such as filters, oscillators, and switches, which constitute the ubiquitous components of radio front systems. This thesis presents material selection, design, and characterization of a capacitive micro-machined resonator and filter. The resonator structures such as disk and Lame are studied in detail. Effects of coupling beams in filter response are analyzed with two different coupling structures such as straight and V-shaped beams.

Material selection and design are the two important aspects which govern the performance of resonators and filters like any other MEMS device. In view of the recent advances and trends in device miniaturization, the fabrication and design compatibility among CMOS and MEMS components is imperative. Material selection for the devices considered has been optimized by using Ashby approach. For example the appropriate fabrication process for the devices depends on the type of materials and availability of material deposition and etching process etc. Following Ashby chart poly-$Si_{0.35}Ge_{0.65}$ is found to one of the best materials for MEMS resonator that can be used for CMOS compatible high Q applications. The close-match between theoretical and simulation results validates the proposed study. Thesis further presents design of third-order Chebyshev filter with novel V-shaped coupled beams. The vibrational frequencies, modal shapes, and bandwidth for the BPF have been calculated and verified with commercially available finite-element tools. From the results it is concluded that Lame filter with V-shaped coupled beams provide superior performance in terms of passband ripple, shape factor, and bandwidth in comparison to Lame filter with straight coupling beams.

Chapter - 1

Introduction

This chapter introduces various wireless transceiver architectures, followed by architecture based on RF MEMS resonator. Various types of existing resonators and their features are explained briefly. A brief introduction to MEMS resonators such as beam, comb, and bulk mode and their limitations are also provided. MEMS resonator key design parameters and its effect on performance are also described.

1.1 Background of wireless transceiver architecture

A transceiver is a device that consists of both a transmitter and a receiver sharing the same electronic circuitry. A transmitter modulates the baseband data and up-converts it into a carrier frequency with sufficient power amplification. The main function of a receiver is to demodulate the desired signal from the presence of undesired interference and noise. Therefore, comparing to a transmitter, receiver is much more challenging because of the requirement of high dynamic range and high out-of-band attenuation.

1.1.1 Direct conversion architecture

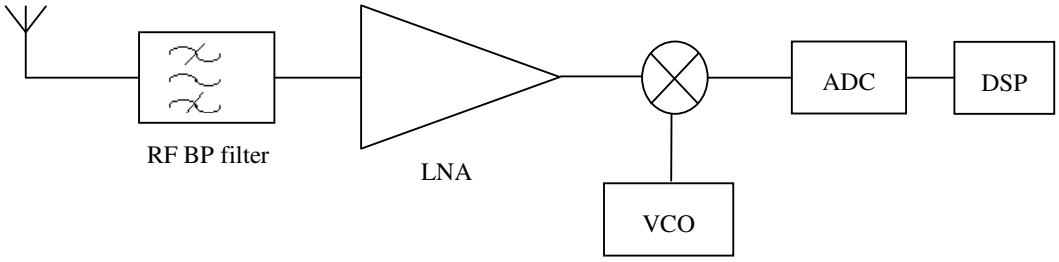

Figure 1.1: Simplified architecture of direct conversion receiver

Figure 1.1 shows a simplified architecture of direct conversion receiver. As the local oscillator frequency in a direct conversion receiver is set equal to the RF frequency, the IF frequency becomes zero and the image frequency could be successfully eliminated. In super heterodyne architecture image frequency eliminated with reject filter that adds more complexity and enables a number of off-chip components. [1-2]

1.1.2 Super heterodyne architecture

Since invented by Edwin Armstrong in 1917, super heterodyne architecture has still been used within a majority of wireless systems. As illustrated in Figure 1.2, the desired signal received by an antenna passes through a pre-select bandpass filter, a low noise amplifier (LNA), and then an image-reject filter to remove the out-of-band interference as well as the image frequency. The selected RF signal is then converted to an intermediate frequency (IF) signal by mixing with a local oscillator (LO) signal generated by a voltage controlled oscillator (VCO). A channel-select filter is used to assign the desired channel and reject all the in-band interference.

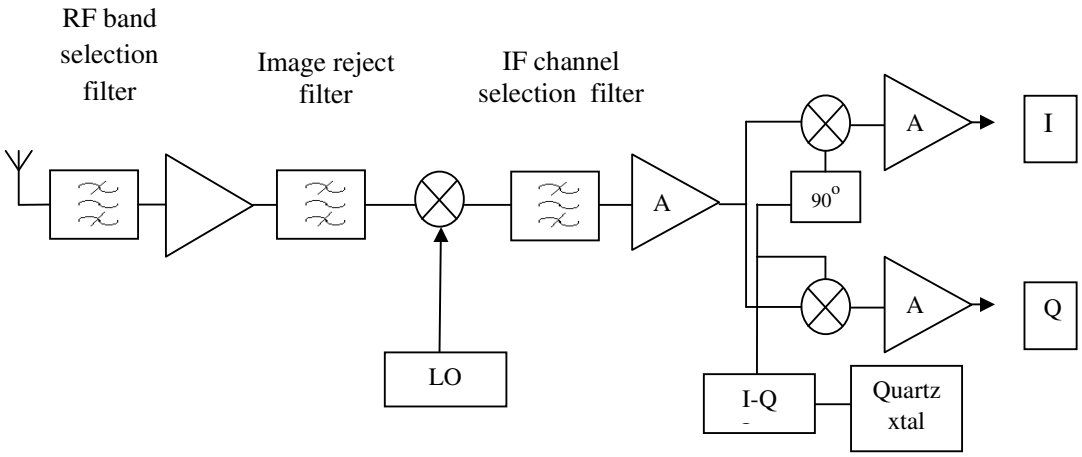

Figure 1.2: Super-heterodyne receiver

As shown in Figure 1.2 high *Q* vibrating mechanical components, such as ceramics, quartz crystal, and surface acoustic wave (SAW) resonator are used to integrate with band pass filters and oscillators. Filters utilizing such technologies successfully extinguish themselves by outstanding quality factor, low insertion loss, high percent bandwidth, and high out-of-band rejection Oscillators also benefit from high *Q* because the phase noise decreases as *Q* increases. However, as the demand for high- selectivity devices keeps on increasing, quartz and SAW devices have gradually failed to satisfy the stringent high *Q* requirement. More importantly, current high *Q* devices are bulky, where off-chip components make the ultimate miniaturization of the wireless communication systems difficult.

1.1.3 Architecture based on RF MEMS resonator

Figure 1.3 presents the system block diagram for a newly-invented RF channel select receiver that takes full advantages of achievable complexity utilizing MEMS elements. CMOS-compatible micromechanical devices with high Q (>10,000) and high frequencies (>1 GHz) have been reported recently[3] providing the potential of integration of wireless communication system. In addition to miniaturization, if channel selection is possible at RF carrier frequencies, succeeding electronic components such as LNA and mixer are no longer needed to handle the power of alternate channel interference. Therefore, dynamic range can be greatly relaxed, allowing significant reduction in power consumption as well as the cost.

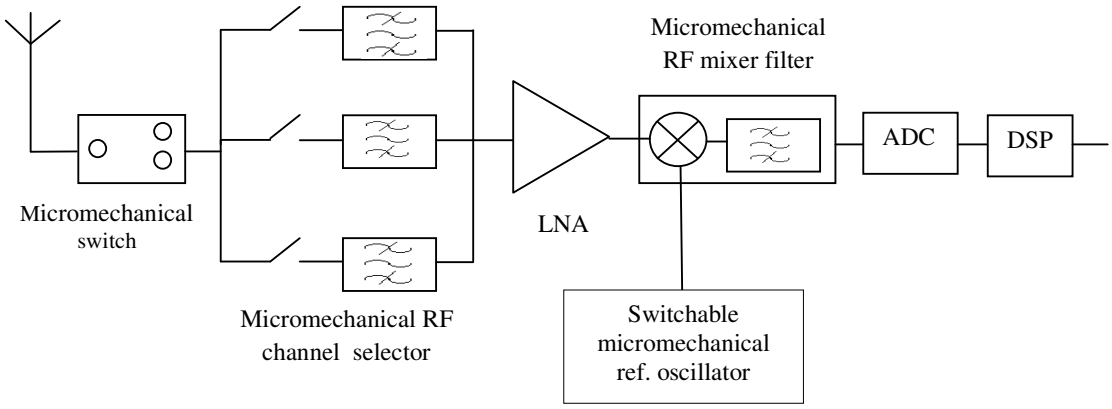

Figure 1.3: Simplified architecture of RF MEMS resonator-based channel select receiver

Silicon MEMS resonator has the potential to replace quartz crystal for timing and frequency reference application[4-12]. Beyond frequency references, MEMS resonators can also be used as a sensor[13-22], RF filters and mixers [23-24], and atomic force microscopy. Sensors for mass (vapor, chemicals, protein, etc.) are well reported in the literature. Almost all electronic instruments and communication system use some kind of timer or frequency reference; and this multi-billion dollar oscillator market is currently dominated by quartz crystal. Silicon micromechanical resonator has several advantages over quartz resonator. Some of its advantages are related to its fabrication technology which leverages the IC fabrication technology allowing it to be CMOS compatible [25], resulting into lower cost, smaller form factors, increased reliability and manufacturability, and single chip solutions. Previous research work has shown that the silicon micromechanical resonator has excellent long term stability of better than 1 ppm

[26-31]. One of the biggest advantages of MEMS resonator, not mentioned above, is its low power consumption and a good dynamic thermal response.

1.2 Overview of off-chip components

This section briefly introduces the currently employed off-chip components in today's front-end of wireless communication systems for filtering and frequency generation functions. Moreover, the feasibility for above-IC integration of these components on top of CMOS for reduced size and improved performance is discussed.

1.2.1 Quartz crystal resonators

A quartz crystal resonator uses the piezoelectric properties of quartz. A thin slice of quartz, cut at an appropriate orientation with respect to the crystallographic axis, is placed between two electrodes. An alternating voltage applied to these electrodes causes the quartz crystal to vibrate in a particular mode. These vibrational modes depend on the specific cut with respect to the crystal orientation. Quartz crystal resonators have a very stable resonance frequency over a large span of frequencies and the best long-term stability in comparison with other resonators. The quartz crystal is widely used for accurate frequency control [32], timing and filtering[33]. Also, quartz cut along specific directions shows almost zero temperature drift. This results in highly accurate resonators over a typical temperature range of 100ºC[34]. As quartz is monocrystalline material, it cannot be fabricated by thin-film depositions on top of a microelectronic chip. In other words, quartz crystal resonators cannot be integrated on top of CMOS.

1.2.2 Ceramic resonators

Ceramic resonators are similar to quartz crystal resonators, except the material. These resonators mostly use polycrystalline Lead-Zirconate-Titanate (PZT) as a base material instead of quartz. The high dielectric constant, good piezoelectric response and good temperature stability of this material have enabled practical filter applications over the past decades[35-38]. The use of high permittivity material significantly reduces the filter volume, almost half compared to quartz crystal, for low loss band pass filters. Commercially available ceramic filters can work up to 7 GHz with Q ranging from 1000 to 2000. They find usage in Bluetooth systems and other short range wireless applications targeting higher frequencies. They are not easily fabricated on top of CMOS circuitry because of their large dimensions and high processing temperature (> 450°C) for PZT.

1.2.3 Surface acoustic wave resonators

Surface acoustic wave (SAW) resonators are a class of MEMS which utilize standing waves generated on the surface of a piezoelectric material. A basic SAW resonator consists of two Inter Digital Transducers (IDTs) on a piezoelectric substrate. One of them acts as the device input and converts signal voltage variations into mechanical surface acoustic waves. The other IDT is employed as the output receiver to convert the mechanical SAW vibrations back into output voltages. These IDTs are reciprocal in nature therefore the signal voltage can be applied to either of the IDTs. The most commonly used piezoelectric materials for SAW resonators are $LiTaO_3$ and $LiNbO_3$. Moreover, zinc oxide (ZnO) and aluminum nitride (AlN) can also be used. They exhibit sharp cut-off characteristics and small size, highly suitable for RF and IF filtering for wireless applications[39]. The above-IC integration of SAW devices is almost impossible due to the stringent requirements on the acoustic properties and tight tolerances of the piezoelectric material[40].

1.2.4 Bulk acoustic wave resonators

Bulk Acoustic Wave (BAW) resonators are the most recent category of piezoelectric resonators employed for band pass RF filtering in the frequency range from 800 MHz to 12 GHz[41-43]. They generally consist of a parallel plate capacitor with a piezoelectric layer used as dielectric. By applying an ac electric signal to the electrodes, a longitudinal acoustic wave is excited in the bulk of the piezoelectric film. This wave is trapped by the reflecting electrode surfaces, thus forming an acoustic resonator. In order to attain a high Q, the acoustic losses into the supporting substrate must be made as small as possible. One way is to isolate the structure from the substrate by removing the substrate underneath the electrode. The other common approach is to create reflector layers between the resonator and the substrate. In BAW resonators thin films of aluminum nitride or zinc oxide are commonly employed as the piezoelectric layer. For these materials, resonances in the low GHz regime require piezoelectric layer thicknesses in the order of 1 μm (half the wavelength of the designed frequency) and are thus well within reach for thin-film technologies. The resonators are made as small as a few tens to a few hundreds of micrometers on a side, typical for a MEMS design. Solidly mounted and MEMS brane-supported film bulk acoustic resonators (FBARs) using AlN film have been

demonstrated to operate at resonant frequencies of 8 GHz and 1.36 GHz, with quality factors of 2000 and 210 and insertion loss of 5.5dB and 3.5dB respectively[44-45].

The above-IC integration of these devices seems quite attractive as the most commonly used piezoelectric materials ZnO and AlN can be deposited by sputtering. However, the piezoelectric properties of these materials are not good enough to meet the high performance and yield requirements for device fabrication. Moreover, piezoelectric material with multiple thicknesses would be required for filtering different frequencies, thereby increasing the process complexity.

The off-chip components, described above, play a pivotal role in the currently employed wireless communication systems for filtering and frequency generation functions despite of their large size and reduced power efficiency. The size, power consumption, and limitation for above-IC integration of these components have intrigued the researchers to find a viable solution in the form of micro scale high Q passive components. The use of high Q passives will eventually lead to low cost, miniaturized, and energy efficient wireless communication systems with an improved performance due to the elimination of board-level interconnect parasitics.

In this context, high Q on-chip MEMS resonators have emerged as the key element due to their high quality factor, low power consumption and possibility for above-IC integration.

1.3 Microelectromechanical resonators

Microelectromechanical (MEMS) resonators, as the name implies, are mechanical structure that has dimensions ranging from a few micrometers to hundreds of micrometers and can vibrate with an increased amplitude of vibration once a periodic force, applied electrically, whose frequency is equal or very close to the resonance frequency of the mechanical system. A classical example of a mechanical resonator at macro scale is a guitar string that can resonate in the audio frequency range (20 Hz-20 kHz), depending on the length of the string. The smaller sizes of the micromechanical resonators therefore allow them to operate at frequencies suitable for a variety of applications in electronic circuits and systems. In the following subsections a brief overview of micromechanical resonators is presented.

1.3.1 Beam resonators

Beam resonators are of very simple geometry and the easiest to fabricate using surface micromachining techniques. Three types of beam resonators, categorized by their clamping approach, are widely reported in the literature: clamped-free beam resonators (cantilevers) [46], clamped-clamped beam resonators [47], and free-free beam resonators [48]. They are generally available solution for application at lower frequencies. The clamped-free beam and free-free beam resonators exhibit low Q due to the viscous damping when operated under atmospheric conditions. In contrast, relatively high Q can be achieved for clamped-clamped beam resonators[49] compared to other beam resonators due to their high stiffness. The power handling capability limits the use of these resonators for communication applications. These resonators can be easily processed on top of CMOS due to their relatively easy design and wide choice of materials.

1.3.2 Comb drive resonators

The comb-drive resonators are amongst the earliest designed surface-micromachined resonators. They consist of two inter-digitated combs, one being fixed while the other is movable connected to a compliant suspension. A voltage difference applied between the two combs results in deflection of the movable comb by electrostatic forces. Comb-drive devices resonate at a few kHz due to their mass [50] and therefore are of little practical value for RF communication systems [51]. The response of these devices to a narrow range of frequencies makes them suitable for frequency-reference circuits [52]. The above-IC integration of these resonators is quite straightforward. As the structural layer for these resonators is relatively thick compared to beam resonators, the residual stress in this layer should be well suppressed.

1.3.3 Bulk mode resonators

In bulk mode resonators the acoustic waves propagate through the bulk of a material rather than over the surface. With high stiffness materials, these can resonate at high frequencies (MHz-GHz). They exhibit very high Q values, exceeding 10,000 compared to other resonators. A large number of bulk mode resonator designs have been investigated, showing exceptionally high quality factors at frequencies reaching into the GHz range [53]. The most commonly employed designs include longitudinal beam resonators [54], square [55], disk [56] and ring shape resonators [57].

The commonly investigated modes of vibration for the square and circular shape geometries are Lame mode (for square resonators), name after the French mathematician Gabriel Lame who first discussed it in 1817, wineglass mode (for disk resonators) and extensional modes (for square and disk resonators). In many articles both Lame and wineglass mode are used as synonyms and no difference between these two modes are made. In theses modes the motion preserves the volume of the resonator. Whereas, in extensional mode the volume of the resonator is not conserved due to the longitudinal motion of the resonant structure about its center.

A major issues with these resonators are their high motional resistance leading to high insertion loss, as described in the following section, and high bias voltage, in spite of their exceptionally high Q values, that appear as bottlenecks for integration in RF front-end architectures. Typically, an impedance of 50 Ω is required to match with the antenna and the battery voltage level for mobile applications is below 3.3 V [58]. Both of these issues can be dealt through the scaling of the resonator's transduction gap to a few tens of nanometer. As to generate a voltage level greater than the battery voltage level inside a microchip requires additional circuitry that consumes additional power and adds noise to the system [59]. The above-IC integration of bulk mode resonator requires a high-stiffness material that can be deposited at a temperature sufficiently low to avoid any deleterious effect on the CMOS circuitry.

From the above mentioned overview it is clear that the beam resonators and comb-drive resonators can be easily integrated on top of CMOS circuitry. The low resonance frequencies and low Q attributed to these geometries hinder their use in wireless communication front-ends. The bulk mode acoustic resonators appear to be the most suitable candidate for the above-IC integration (with a careful choice of material) due to their small size, extremely high Q values, and low power consumption. The following section therefore outlines the key parameters required to use these bulk mode MEMS resonators for wireless communication systems.

1.4 Key parameters of MEMS resonator

The mechanical resonator must meet some generalized performance measuring parameters for receiver applications, as described in the following subsections.

Figure 1.4 shows the sketch of the main parameters describing a resonator around its resonance frequency. In this figure, frequency is plotted versus transmission in decibels (dB).

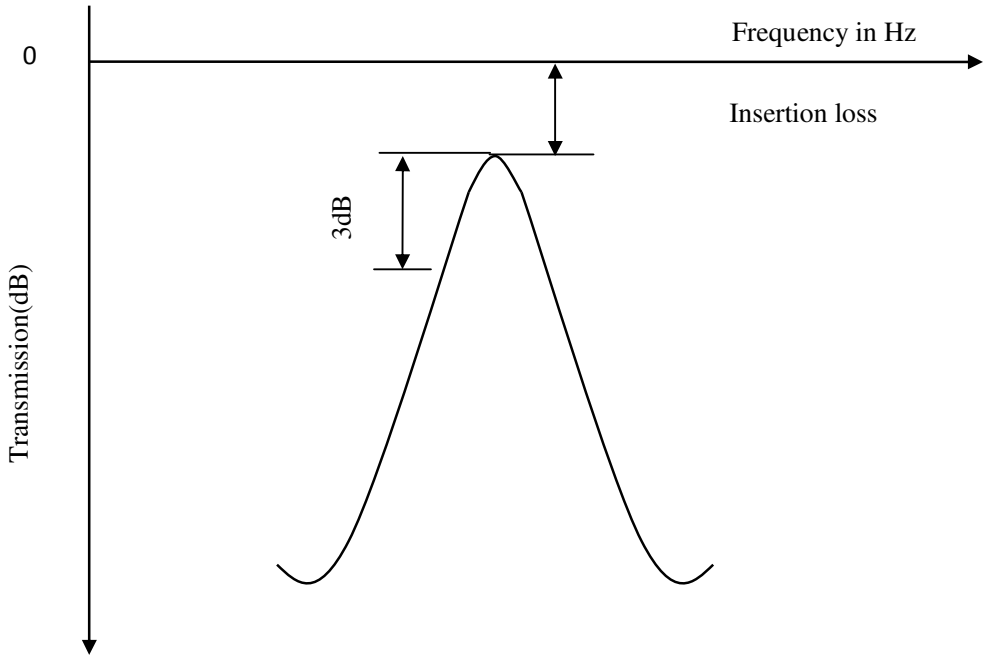

Figure 1.4: Description of resonator parameters

1.4.1 Central frequency

The central frequency (f_0) corresponds to the peak transmission in the measured response of a resonator, as represented in Figure 1.4. It is the nominal frequency of operation and it varies with the communication standard. For example in cellular and cordless applications RF filters, including image reject filters, have center frequencies from 0.8 GHz to 2.5 GHz, whereas intermediate frequency filters range from 455 kHz to 254 MHz [60].

1.4.2 Quality factor

The quality factor (Q) is an important descriptive parameter for the resonator's frequency selectivity, stability and motional resistance. It can be measured as the ratio between the center frequency to the bandwidth where the oscillations die out to the half of their maximum amplitude, as in eq.(1.1)

$$Q = \frac{f_0}{BW_{3dB}} \tag{1.1}$$

For intermediate frequency filtering resonators having Q value exceeding 5000 are generally required. The radio frequency (RF) pre-select or image reject filters can be implemented using resonators with Q's on the order of 500-1000.

1.4.3 Bandwidth

Bandwidth is generally the difference between the upper and lower frequency of a filter at which its transmission is 3dB below the pass band transmission. It is expressed in units of hertz or as a fraction of the central frequency. Like the central frequency, the band width requirements also vary from application to application. For example, for IF filtering a band width of 0.3% and 3% for RF filtering is typically required. A bandwidth of 100 kHz to 200 kHz is typical for GSM applications [61].

1.4.4 Insertion loss

Insertion loss (IL) is a measure of the reduction in the signal amplitude as the signal passes through the filter. Ideally, a passive filter is lossless; the higher the losses, the more power must be spent on (re)amplification in a subsequent stage. For high Q passive resonators in RF receivers, insertion losses up to 3.5dB-13.6dB are considered acceptable. In the specific case of capacitively transduced MEMSS resonators, the insertion loss is dominated by motional resistance (R_m). In other words, R_m gives the measure of dissipation of input signal as it passes through the resonator.

The motional resistance can be calculated from the measured response of the MEMS resonator by its transmission parameter (S_{21}), as in eq.(1.2) [62].

$$R_x = 2.\mathrm{R}_{\mathrm{port}}\left(10^{\frac{\mathrm{S}_{21}(\mathrm{dB})}{20}} - 1\right) \tag{1.2}$$

In this equation R_{port} is the port resistance of the vector network analyzer, typically 50 Ω.

1.4.5 Out of band rejection

The out of band rejection is measured from the resonance peak till the point where a certain frequency or a range of frequencies are lost in the measured spectrum. Ideally, it

should be very high in order to prevent the undesired frequency signal into the filtered frequency spectrum. For example, an out of band rejection of about 20dB is sufficient for IF and RF filter applications.

1.4.6 Thermal stability

The thermal stability of the resonance frequency of a resonator is an important parameter for its use in filtering applications, as the ambient and internal temperature of wireless systems may vary over time. A thermal stability of about 25 ppm/^{o}C is sufficient for front-end RF pre-select and image-reject filter applications. However the temperature coefficient should be much smaller for reference frequency generation in oscillators [63].

1.5 Motivation

Recent development in the radio frequency micro-electro-mechanical systems (RF MEMS) technology has attracted a great deal of attention from both academia and industries, which holds great promises to potentially revolutionize the entire regime of the wireless technology by bringing together microelectronics and micromechanical elements. As such, the implementation of complete wireless transceivers on a single chip could lead to a viable solution to many current issues and challenges in present-day wireless communications. Particularly, due to their orders-of-magnitude smaller size as compared to traditional off-chip passives (e.g., quartz crystal, ceramics, etc.), the next generation of wireless transceivers equipped with RF MEMS components can be realized with greatly enhanced performance. A CMOS-compatible MEMS technology has been demonstrated lately that enables alternative communication architecture by facilitating the integration of high-Q passive devices with active transistor electronics, allowing greater size reduction, lower power consumption and enhanced performance. Batch fabrication of these devices enables cost efficiency. The MEMS is a promising field to replace discrete frequency selective components Oscillators, resonators and clocks are frequency selective devices that generate a desired reference signal for the systems[64-65]. Electronic systems require at least one reference signal to enable system synchronization. The reference signals are defined by characteristics such as target signal frequency, frequency stability and bandwidth. All of these characteristics are set to standard values for the different fields of applications. Frequency stability of an RF transceiver reference signal is required to be better than 2.5 ppm where it is

approximately 1ppm for GPS applications [66]. Mechanically vibrating devices (ceramics, quartz crystals, etc.) have been used in reference frequency applications. Quartz crystals are unique devices by virtue of their high quality factor (Q) and high frequency stability, especially for applications where high accuracy is required. Accurate and stable electronics have been manufactured with these devices. However, their relatively large package conflicts with latest technology requirements where multiple resonators may be required. Prevalent portable applications and small size electronics lead to micro-size on-chip adaptable components.

MEMS frequency selective devices offer alternative solutions for mechanically vibrating devices. MEMS are suitable for vibration applications by their rugged structure. In the recent decade, significant demand for MEMS frequency clock generators has been growing in RF applications, especially in wireless and communication systems. Research has been conducted by many groups and some commercial products have been introduced by companies in the timing industry such as Discera (MRO-100, in 2003) and Bosch (SiT8002). Meanwhile, noteworthy progress in MEMS frequency selective devices has been achieved. Today, MEMS resonators, oscillators and filters are capable of covering a wide frequency range from a few kHz up to several GHz, which is simply known as radio frequency (RF) operation band. Additionally, established high selectivity, good stability, on chip integration and promising linear characteristics promotes further incentives for investments in this technology. Their low power consumption makes them appropriate candidates for portable applications, where battery life plays an important role.

1.6 Objectives and organization of thesis

The objectives of this thesis are as follows: (1) To select CMOS post–processing compatible material to fabricate MEMS resonators for oscillator and filtering functions in wireless front end architectures. (2) To design a novel MEMS High frequency band pass filter. This thesis is organized in six chapters. A brief outline of the thesis is presented below. Chapter 1 introduces various wireless transceiver architectures, followed by architecture based on RF MEMS resonator. Various types of existing resonators and its future's explained briefly also need of MEMS resonator is pointed out. Chapter 2 presents an electromechanical modeling of two-port MEMS resonators, nonlinear effects, quality factor and various loss mechanisms in MEMS resonator.

Details about various shapes of capacitive transduced micromechanical resonators, its fabrication materials and importance of material selection for high quality factor is outlined. In chapter 3 electromechanical model for disk and lame resonator discussed in detail this simplifies the resonator design used further chapter. Chapter 4 discuss about basic requirements for material selection in MEMS resonator. How material is selected based an important parameters such as high Q, high resonant frequency, and low process temperature using Ashby approach explained in detail, it was found that poly$Si_{0.35}Ge_{0.65}$ is the best possible material for MEMS resonator that can be used for CMOS compatible high Q applications. The close match between theoretical and simulation findings validate our proposed study. Chapter 5 presents novel design of low ripple V-shaped coupling beam MEMS High frequency bandpass filters for a bandwidth of 1 MHz. The theoretical design is validated by simulation. The V-shaped coupling beam Lame filter provides 22dB pass band ripple, but for the same design Lame filter with straight coupling beam provides 46dB pass band ripple. Another performance parameter 40dB shape factor of these filters are 1.990, 2.498 respectively. The V-shaped coupling beam provides 3dB bandwidth of 0.901MHz near to the design value 1MHz. Chapter 6 briefly summarizes this research and its outcome also gives recommendations for future work.

References:

[1] S.-J. Chen and Y.-H. Hsieh, *IQ Calibration Techniques for Cmos Radio Transceivers*. Springer Netherlands, 2006.

[2] M. Brandolini, P. Rossi, D. Manstretta, and F. Svelto, "Toward multistandard mobile terminals - Fully integrated receivers requirements and architectures," *IEEE Transactions on Microwave Theory and Techniques*, vol. 53, no. 3, pp. 1026-1038, 2005.

[3] J. E. Butler, T. Feygelson, C. T. Nguyen, G. Surface, D. Section, and F. Washington, "1.51-GHz Nanocrystalline diamond micromechanical disk resonator with material mismatched isolating support," *The seventeenth IEEE International Conference on Micro Electro Mechanical Systems*,pp. 641-644, 2004.

[4] C. T. Nguyen, "MEMSS technology for timing and frequency control.," *IEEE transactions on ultrasonics, ferroelectrics, and frequency control* , vol. 54, no. 2, pp. 251-270, 2007.

[5] V. Kaajakari, J. Kiihamaki, A. Oja, S. Pietikainen, V. Kokkala, and H. Kuisma "Stability of wafer level vacuum encapsulated single-crystal silicon resonators," *Sensors and Actuators a-Physical*, vol. 130, pp. 42-47, 2006.

[6] C. T. C. Nguyen and R. T. Howe, "Integrated CMOS micromechanical resonator high-Q oscillator," *IEEE J. Solid-State Circuits*, vol. 34, no. 4, pp. 440-455, 1999.

[7] D. R. Sparks, S. Massoud-Ansari, and N. Najafi, "Chip-Level Vacuum Packaging of Micromachines Using Nanogetters," *IEEE Trans. Adv. Packag.*, vol. 26, no. 3, pp. 277-282, 2003.

[8] H. Wan-Thai and C. T. C. Nguyen, "Stiffness-compensated temperature-insensitive micromechanical resonators," *The Fifteenth IEEE International Conference on Micro Electro Mechanical Systems*, 2002. vol. 2, pp. 731-734, 2002.

[9] E. Quevy and R. Howe, "Redundant MEMSS resonators for precise reference oscillators," *Radio Frequency integrated Circuits (RFIC) Symposium, 2005. IEEE*, pp. 113-116, 2005.

[10] M. A. Hopcroft, M. Agarwal, K. K. Park, B. Kim, C. M. Jha, R. N. Candler, G. Yama, B. Murmann, T. W. Kenny, "Temperature compensation of a MEMSS

resonator using quality factor as a thermometer," *19th IEEE International Conference on Micro Electro Mechanical Systems, Technical Digest*, pp. 222-225, 2006.

[11] C. T. C. Nguyen, "Frequency-selective MEMSS for miniaturized low-power communication devices," *IEEE Trans. Microw. Theory Tech.*, vol. 47, no. 8, pp. 1486-1503, 1999.

[12] J. W. Weigold, a. C. Wong, C. T. C. Nguyen, and S. W. Pang, "Merged process for thick single-crystal Si resonators and BiCMOS circuitry," *J. Microelectromechanical Syst.*, vol. 8, no. 3, pp. 221-228, 1999.

[13] R.A. Buser, N. F. de Rooij. "Resonant silicon structures," *Sensors and Actuators*,vol. 17, no. 1-2, pp. 145-154, 1989.

[14] G. Stemme, "Resonant silicon sensors," *J. Micromechanics Microengineering*, vol. 1, pp. 113-125, 1999.

[15] R. N. Kleiman, G. K. Kaminsky, J. D. Reppy, R. Pindak, and D. J. Bishop, "Single-crystal silicon high-Q torsional oscillators," *Review of Scientific Instruments*, vol. 56, no. 11. pp. 2088-2091, 1985.

[16] R. T. Howe and R. S. Muller, "Resonant-microbridge vapor sensor," *IEEE Transactions on Electron Devices*, vol. 33, no. 4, pp. 499-506, 1986.

[17] T. P. Burg, A. R. Mirza, N. Milovic, C. H. Tsau, G. a. Popescu, J. S. Foster, and S. R. Manalis, "Vacuum-packaged suspended microchannel resonant mass sensor for biomolecular detection," *Journal Microelectromechanical Systems*, vol. 15, no. 6, pp. 1466-1476, 2006.

[18] P. Parsons, a. Glendinning, and D. Angelidis, "Resonant sensors for high accuracy pressure measurement using silicon technology," *Proc. IEEE 1992 Natl. Aerosp. Electron. Conf. 1992*, pp. 349-355, 1992.

[19] E. Stemme and G. Stemme, "A balanced resonant pressure sensor," *Sensors Actuators A Phys.*, vol. 21, no. 1-3, pp. 336-341, 1990.

[20] V. Kaajakari, T. Mattila, A. Lipsanen, and A. Oja, "Nonlinear mechanical effects in silicon longitudinal mode beam resonators," *Sensors Actuators A Phys.*, vol. 120, no. 1, pp. 64-70, Apr. 2005.

[21] J.C. Greenwood, "Silicon in mechanical sensors," *J. Phys. E.*, vol. 21, pp. 1114-1128, 1988.

[22] W. Yun, R.T. Howe and P.R. Gray, "Surface micromachined, digitally force-balanced accelerometer with integrated CMOS detection circuitry," presented at Hilton Head, the *IEEE Solid-State Sensor and Actuator Workshop*, Hilton Head, SC USA, 22-25,June,1992

[23] L. Lin, C. T.-C. Nguyen, R. T. Howe, and a. P. Pisano, "Microelectromechanical filters for signal processing," *Proceedings IEEE Micro Electro Mechanical Systems*, vol. 7, no. 3, pp. 226-231, 1992.

[24] C.T.-C.Nguyen, "Microelectromechanical devices for wireless communications," *Proceedings MEMS 98. IEEE. Eleventh Annual International Workshop on Micro Electro Mechanical Systems. An Investigation of Micro Structures, Sensors, Actuators, Machines and Systems (Cat. No.98CH36176)*, pp. 1-7, 1998.

[25] B. Kim, M. Hopcroft, C. M. Jha, R. Melamud, S. Chandorkar, M. Agarwal, K. L. Chen, W. T. Park, R. Candler, G. Yama, a. Partridge, M. Lutz, and T. W. Kenny, "Using MEMSS to build the device and the package," *TRANSDUCERS EUROSENSORS '07 - 4th Int. Conf. Solid-State Sensors, Actuators Microsystems*, pp. 331-334, 2007.

[26] B. Kim, R. N. Candler, M. A. Hopcroft, M. Agarwal, W. T. Park, and T. W. Kenny, "Frequency stability of wafer-scale film encapsulated silicon based MEMSS resonators," *Sensors Actuators, A Phys.*, vol. 136, pp. 125-131, 2007.

[27] B. Kim and R.N. Candler, "Frequency stability of wafer-scale encapsulated MEMSS resonators," *Solid-State Sensors, Actuators, Microsystems Work.*, vol. 2, pp. 1965-1968, 2005.

[28] B. Kim, R.N. Candler, M. Hopcroft, M. Agarwal, W. Park, J. T. Li, and T. Kenny, "Investigation of MEMS Resonators Characteristics for Long-Term Operation and Wide Temperature Variation Condition," in *ASME International Mechanical Engineering Congress and RD&D Expo*, pp. 1-4, 2004.

[29] M. A Hopcroft, H. K. Lee, B. Kim, R. Melamud, S. Chandorkar, M. Agarwal, C. M. Jha, J. Salvia, G. Bahl, H. Mehta, and T. W. Kenny, "A High-Stability MEMSS Frequency Reference," TRANSDUCERS '07 / Eurosensors XXI, *14th*

International Conference on Solid-State Sensors, Actuators and Microsystems Lyon, France, 10-14 June 2007 .

[30] M. Xiong, "Development of UHF micromechanical resonators and arrays based on silicon-on-insulator (SOI) technology," Graduate Theses and Dissertations, University of South Florida, 2010.

[31] M. A Hopcroft, "Temperature-Stabilized Silicon Resonators for Frequency References," Ph.D. thesis in Mechanical Engineering, Stanford University, 2007.

[32] J. Viennet, M. Jardino, R. Barillet, and M. Desaintfuscien, "Frequency Control Loop with Digital Integrator," *IEEE Trans. Instrum. Meas.*, vol. 32, no. 2, pp. 322-326, 1983.

[33] W. P. Mason, "Electrical Wave Filters Employing Quartz Crystals as Elements," Bell System Technical Journal, vol. 13, pp. 405-452, 1934.

[34] J. Jacques and M. Bontemps, "Design of a MEMSS-based 52 MHz oscillator," Ph.D. thesis in Eindhoven University of Technology ,2009.

[35] S. B. Cohn, "Microwave Bandpass Filters Containing High-Q Dielectric Resonators," *IEEE Trans. Microw. Theory Tech.*, vol. 16, pp. 218-227, 1968.

[36] S. J. Fiedziuszko, I. C. Hunter, S. MEMSber, T. Itoh, Y. Kobayashi, T. Nishikawa, and S. N. Stitzer, "Dielectric Materials , Devices , and Circuits," *IEEE Trans. Microw. Theory Tech.*, vol. 50, no. 3, pp. 706-720, 2002.

[37] J. K. Plourde and Chung-Li Ren, "Application of Dielectric Resonators in Microwave Components," *IEEE Trans. Microw. Theory Tech.*, vol. 29, no. 8, pp. 754-770, 1981.

[38] R. D. Richtmyer, "Dielectric resonators and filters," *J. Appl. Phys.*, vol. 10, pp. 391-398, 1939.

[39] Y. Satoh, O. Ikata, and T. Miyashita, "RF SAW Filters," *Power*, vol. 1, pp. 1-8, 1992.

[40] R. Aigner, "Volume manufacturing of BAW-filters in a CMOS fab," in *Proceedings of IEEE International Ultrasonics Symposium*, 2008, pp. 582-589.

[41] A. Müller, D. Neculoiu, G. Konstantinidis, A. Stavrinidis, D. Vasilache, A. Cismaru, M. Danila, M. Dragoman, G. Deligeorgis, K. Tsagaraki, a Muller, D.

Neculoiu, G. Konstantinidis, A. Stavrinidis, D. Vasilache, A. Cismaru, M. Danila, M. Dragoman, G. Deligeorgis, and K. Tsagaraki, "6.3-GHz Film Bulk Acoustic Resonator Structures Based on a Gallium Nitride/Silicon Thin MEMS brane," *IEEE Electron Device Lett.*, vol. 30, no. 8, pp. 799-801, 2009.

[42] H. Yu, W. Pang, H. Zhung, and E. S. Kim, "Film Bulk Acoustic Resonator at 4.4 GHz with Ultra Low Temperature Coefficient of Resonant Frequenc," in *18th IEEE International Conference on MEMSS*, 2005, pp. 28-31.

[43] K. M. Lakin, J. Belsick, J. F. McDonald, and K. T. McCarron, "Improved bulk wave resonator coupling coefficient for wide bandwidth filters," *2001 IEEE Ultrasonics Symposium. Proceedings. An International Symposium (Cat. No.01CH37263)*, vol. 1, pp. 827-831, 2001.

[44] R. Lanz and P. Muralt, "Bandpass filters for 8 GHz using solidly mounted bulk acoustic wave resonators.," *IEEE Trans. Ultrason. Ferroelectr. Freq. Control*, vol. 52, no. 6, pp. 936-46, 2005.

[45] J. J. Lutsky, R. S. Naik, R. Reif, and C. G. Sodini, "A sealed cavity TFR process for RF bandpass filters," proc. IEDM1996, San Francisco,CA, USA, Dec. 8-11, pp. 95-98, 1996.

[46] T. T. Mon, M. S. M. Sani, R. A. Baker and N. M. Z. N. Mohamed, "Design Analysis of Silicon Cantilever for Label-less Sensing using Finite Element Method," *IEEE Mechatronic and Embedded Systems and Applications*, *Proceedings.* pp. 89-93, 2008.

[47] Y. W. Lin, S. Lee, S. S. Li, Y. Xie, Z. Ren, and C. T. C. Nguyen, "Series-resonant VHF micromechanical resonator reference oscillators," *IEEE J. Solid-State Circuits*, vol. 39, no. 12, pp. 2477-2491, 2004.

[48] K. Wang, A. Wong, S. MEMSber, and C. T. Nguyen, "VHF Free - Free Beam High- Q Micromechanical Resonators," *J. Microelectromechanical Syst.,*vol. 9, no. 3, pp. 347-360, 2000.

[49] a. N. Cleland and M. L. Roukes, "Fabrication of high frequency nanometer scale mechanical resonators from bulk Si crystals," *Appl. Phys. Lett.*, vol. 69, no. 18, pp. 2653-2655, 1996.

[50] N. and R. T. H. Willium C. Tang, Tu-Chong H, "W. C. Tang, T.-C. H. Nguyen, and R. T. Howe, 'Laterally driven polysilicon resonant microstructures,'" *Sensors Actuators A Phys.*, vol. 20,pp. 25-32, 1989.

[51] T. Hirano, T. Furuhata, K. J. Gabriel, and H. Fujita, "Design, fabrication, and operation of submicron gap comb-drive microactuators," *J. Microelectromechanical Syst.*, vol. 1, no. 1, pp. 52-59, 1992.

[52] C. T. Nguyen and R. T. Howe, "CMOS Micromechanical Resonator Oscillator," in *IEEE International Electron Devices Meeting*,Washington, DC, USA, Dec. 8-11, pp. 199-202,1993.

[53] J. Wang, S. MEMSber, Z. Ren, C. T. Nguyen, and S. MEMSber, "1.156-GHz Self-Aligned Vibrating Micromechanical Disk Resonator," vol. 51, no. 12, pp. 1607-1628, 2004.

[54] T. Mattila, J. Kiihamäki, T. Lamminmäki, O. Jaakkola, P. Rantakari, a. Oja, H. Seppä, H. Kattelus, and I. Tittonen, "A 12 MHz micromechanical bulk acoustic mode oscillator," *Sensors Actuators, A Phys.*, vol. 101, pp. 1-9, 2002.

[55] V. Kaajakari, T. Mattila, A. Oja, J. Kiihamäki, and H. Seppä, "Square-extensional mode single-crystal silicon micromechanical resonator for low-phase-noise oscillator applications," *IEEE Electron Device Lett.*, vol. 25, no. 4, pp. 173-175, 2004.

[56] W. L. Huang, Z. Ren, and C. T. C. Nguyen, "Nickel vibrating micromechanical disk resonator with solid dielectric capacitive-transducer gap," *Proc. IEEE Int. Freq. Control Symp. Expo.*,Miami,FL, pp. 839-847, 2006.

[57] Y. Xie, S. Li, Y. Lin, S. MEMSber, Z. Ren, and C. T. Nguyen, "1.52-GHz micromechanical extensional wine-glass mode ring resonators.," *IEEE Trans. Ultrason. Ferroelectr. Freq. Control.*, vol. 55, no. 4, pp. 890-907, 2008.

[58] M. Nawaz, "Low Impedance Wheel Resonators for Low Voltage and Low Power Applications," PhD dissertation,Universität Erlangen-Nürnberg, 2009.

[59] C. T. C. Nguyen, "Series-resonant micromechanical resonator oscillator," *IEEE Int. Electron Devices Meet. 2003*, Washington, DC, Dec. 8-10, pp. 961-964, 2003.

[60] C. T. C. Nguyen, L. P. B. Katehi, and G. M. Rebeiz, "Micromachined devices for wireless communications," *Proc. IEEE*, vol. 86, no. 8, pp. 1756-1767, 1998.

[61] J. L. Lopez, J. Verd, J. Giner, a Uranga, G. Murillo, E. Marigo, F. Torres, G. Abadal, and N. Barniol, "High Q CMOS-MEMS Resonators and Its Applications As RF Tunable Band-Pass Filters," *Solid-State Sensors,Actuators and Microsystems Conference*, Denver, Colorado, June 21-25, pp. 557-560, 2009.

[62] N. Ciressan, "Nanogap MEMS Resonators on SOI, Ph.D. thesis in ÉCOLE POLYTECHNIQUE FÉDÉRALE DE LAUSANNE," 2009.

[63] J. Wang, L. Yang, S. Pietrangelo, Z. Ren, and C. T. C. Nguyen, "RF MEMS resonators: Getting the right frequency and Q," *Tech. Dig. - IEEE Compd. Semicond. Integr. Circuit Symp*, Oregon, USA, pp. 170-173, 2007.

[64] C. T.-C. Nguyen, "Transceiver front-end architectures using vibrating micromechanical signal processors(invited)," *Dig.of.Papers.* Topical Meeting on Silicon Monolithic Integrated Circuits in RF Systems, Sept. 12-14, pp. 23-32, 2001.

[65] H. Wan-Thai, "Resonator miniaturization for oscillators," 2008 *IEEE Frequency Control Symposium*, May.19-21, pp. 392-395, 2008.

[66] C.S. Lam, "An Assessment of the Recent Development of MEMS Oscillators as Compared with Crystal Oscillators," *2nd Symposium on Piezoelectricity, Acoustic Waves, and Device Applications*, Zhejiang university, China,pp. 308-315, 2006.

This chapter is devoted to theoretical modeling and recent advancement of (MEMS) resonators. The first section presents the resonator model, the electrical equivalent circuit based on linear conditions. The relation between the mechanical parameters such as force, velocity, and displacement etc. to that of electrical parameters such as voltage, current, charge etc established. A brief explanation about the resonator quality factor, different loss mechanisms which can affect its performance, and list of some reported resonator is also covered. From this concluded that to obtain high Q proper anchor design, also systematic material selection approach needed.

2.1 Modeling of bulk-mode resonators

Any bulk mode resonator disk, lame can be represented by a mechanical lumped element model of mass- spring-damper system. This mechanical equivalent model can be used to describe the dynamic behavior of the resonator.

2.1.1 Mechanical model using linear conditions

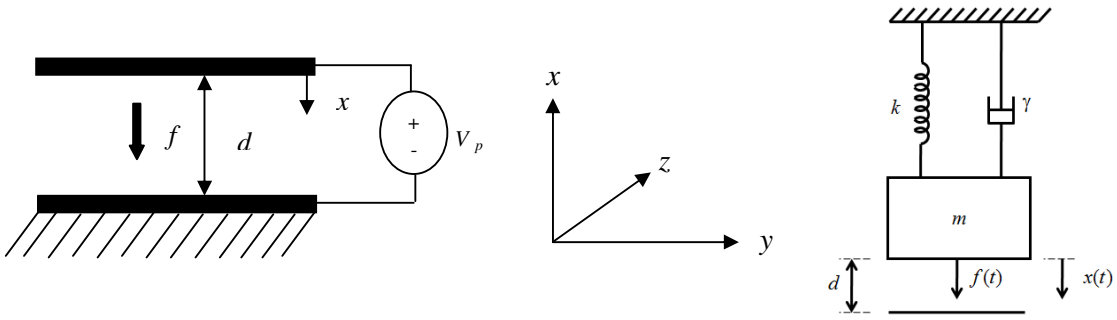

Figure 2.1: (a) Variable parallel plates capacitor and (b) mechanical lumped model

Figure 2.1 shows the static actuation of a parallel plate capacitor and the mechanical lumped model for the MEMS resonator. The equation of motion for forced oscillations of this system is:

$$m\ddot{x} + y\dot{x} + kx = f = F\sin\omega t \qquad (2.1)$$

where m is the mass, γ is the damping, k is the linear spring constant of the resonator and f is the force with the magnitude F. We also define the quality factor as $Q=\sqrt{\frac{km}{\gamma}}$ and the resonance frequency $\omega_{res}=\sqrt{\frac{k}{m}}$.

The solution of this equation gives the sinusoidal displacement of the resonator, caused by the forcing term[1- 2].

$$x(t)=\frac{f/k}{1-\frac{\omega^2}{\omega_{res}^2}+j\frac{1}{Q}\frac{\omega}{\omega_{res}}} \tag{2.2}$$

The amplitude of vibration, $|x|$, is given by

$$|x|=\frac{f/m}{\sqrt{\left(\omega_{res}^2-\omega^2\right)^2+\frac{\omega_{res}^2\omega^2}{Q}}} \tag{2.3}$$

At resonance, $\omega = \omega_{res,}$ and the amplitude becomes

$$|x|=Q\frac{f}{k} \tag{2.4}$$

The MEMS resonator is actuated by using an electrostatic force, f_e. The coupling is provided by capacitive transduction over a narrow gap, d, which separates the resonator from the electrode. Knowing that:

$$f_e=\frac{\partial E}{\partial x} \tag{2.5}$$

$$E=\frac{1}{2}Cv^2 \tag{2.6}$$

$$v=V_p+v_i=V_p+V_{AC}\sin\omega t \tag{2.7}$$

where E is the energy of the system, C is the transducer working capacitance, V_p is the bias voltage and v_i is the alternating excitation voltage, the electrostatic force can be calculated as

$$f_e = \frac{\partial E}{\partial x} = \frac{\partial \frac{1}{2} C v^2}{\partial x} = \frac{1}{2}\frac{\partial C}{\partial x} v^2 = \frac{1}{2}\frac{\varepsilon_0 A}{d^2} v^2 = \frac{1}{2}\frac{\varepsilon_0 A}{d^2}\left(V_p^2 + 2V_p V_{AC}\sin\omega t + V_{AC}^2 \sin^2 \omega t\right) \quad (2.8)$$

where ε_0 is the vacuum permittivity and A is the overlap area between the resonator and the input electrode.

The first term in the bracket represents the constant component of the force, caused by the DC bias. In normal operation, the high order terms are very small, and can be neglected. The second term is the signal component of the force:

$$f = F\sin\omega t \cong \frac{\varepsilon_0 A}{d^2} V_p V_{AC} \sin\omega t \quad (2.9)$$

This force excites the resonator to vibrate, creating a DC-biased, time-varying capacitor between the movable structure and the electrode, which sources an output current given by:

$$i = V_p \frac{\partial C}{\partial t} = V_p \frac{\partial C}{\partial x}\frac{\partial x}{\partial t} = \eta \dot{x} \quad (2.10)$$

where we identify

$$\eta = V_p \frac{\partial C}{\partial x} \cong V_p \frac{\varepsilon_0 A}{d^2} \quad (2.11)$$

as the electromechanical coupling coefficient which establishes the connection between the mechanical and electrical domains (velocity and current).

2.1.2 Small signal electrical equivalent circuit

Force-Voltage equivalence has been used to constitute the electromechanical analogy. Table 2.1 lists the equivalent terms in the electrical and the mechanical domain.

Table 2.1: Electro-mechanical analog components

Mechanical domain	Electrical domain
Force	Voltage
Velocity	Current
Mass	Inductor
Compliance	Capacitor
Damping	Resistor

Figure 2.2 presents the equivalent series RLC circuit which can be used to model the operation of a MEMS resonator. The equivalent circuit models only the first mode of the resonator. The intrinsic resonator behavior is modeled using a motional inductance L_x, a motional capacitance C_x, and a motional resistance R_x, which are physical representations of the resonator mechanical properties: effective mass (m_{re}), and effective stiffness (k_{re}) and damping (γ) respectively. C_s is the feed through capacitance between port 1 and 2 and C_p are the capacitances coupling the pads to the substrat.

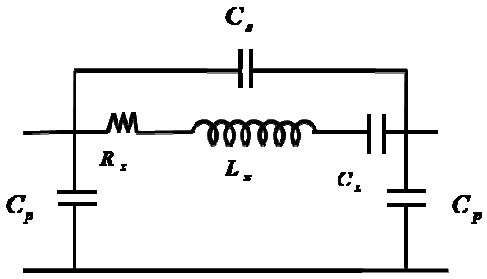

Figure 2.2: Small signal equivalent circuit

Using the electromechanical coupling coefficient eq.(2.11), the lumped elements can be calculated as shown below, by eq.(2.12) - (2.14).

$$L_x = \frac{m_{re}}{\eta} \tag{2.12}$$

$$C_x = \frac{\eta^2}{k_{re}} \tag{2.13}$$

$$R_x = \frac{\gamma}{\eta^2} = \frac{\sqrt{m_{re}k_{re}}}{Q}.\frac{1}{\eta^2} \tag{2.14}$$

At resonance $\omega_{res}L_x = \dfrac{1}{\omega_{res}C_x}$

thus the equivalent inductance and capacitance cancel each other, and the resonator admittance becomes equal to:

$$Y_{res} = \frac{1}{R_x} + j\omega_{res}C_s \tag{2.15}$$

Two types of currents are possible: from the feed through capacitance and from the resonator motion, the later dominates. Consequently, in order to maximize the desired current, R_x should be as small as possible, by building structures with small mass, stiffness, and high electromechanical coupling.

Knowing that $\omega_{res} = \sqrt{k_{re} / m_{re}}$ we can detail the motional resistance formula, as follows:

$$R_x = \frac{k_{re}}{\omega_{res} Q} \cdot \frac{d^4}{V_p^2 \varepsilon_0^2 A^2} \tag{2.16}$$

It becomes clear that in order to minimize R_x, while keeping reasonable DC bias levels, the most important design parameter is the gap d. The overlap area between the electrode and the resonator and the quality factor should also be maximized.

2.1.3 Nonlinear effects in MEMS resonators

The linear model previously presented is only usable when small-displacement characteristics of the device are required. However, MEMS structures can present strong nonlinearities due to large signal related phenomena, which limit the power handling of the device and hence the maximum signal-to-noise ratio which can be achieved.

Nonlinearities in electrostatically actuated MEMS resonators, also called amplitude-frequency (A-F) effects, that create Duffing bifurcation instabilities, and excess phase noise[3]. The nonlinear effects can have mechanical and capacitive origin. Even though single crystal silicon is considered to be a quasi-linear material until the fracture point, in micromechanical structures with very high Q even small material nonlinearities can become significant. Another source of mechanical nonlinearity is the geometrical deformation of the structure under large force. The capacitive nonlinearity is inherent to the electrostatic coupling mechanism, due to inverse relationship between displacement and parallel plate capacitance[4].

Figure 2.3(a) and Figure 2.3(b) presents nonlinearity effect of the resonator response[5]. At the bifurcation point, x_b, the A-F curve has an infinite slope. Above bifurcation, the curve is no longer a single-valued function, but it shows a hysteretic behavior. Thus, the response becomes dependent on the frequency sweep direction: if increased, the resulting response will follow the first curve Figure 2.3(a); if decreased, it will follow the second one Figure 2.3(b). As indicated in the nonlinearity graphs, the greatest vibration amplitude before hysteresis, called the critical vibration amplitude, x_c, is higher than the vibration amplitude at the bifurcation point. This parameter can be used to estimate the limit for linear operation.

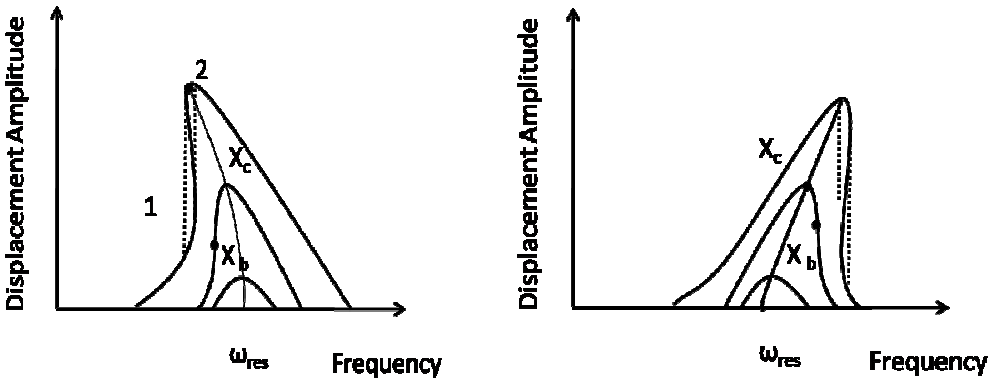

Figure 2.3: Nonlinearity effect on the resonator

In order to take into account the nonlinear effects, the linear spring constant, k, has to be replaced in the equation of motion for forced oscillations eq.(2.1) with the nonlinear spring, $k(x) = k_0(1+ k_1x+ k_2x^2+\ldots)$. Thus, if we take into consideration only the first three nonlinear terms, the equation of motion becomes:

$$m\ddot{x}+\gamma\dot{x}+k_0x+k_1x^2+k_2x^3=f \tag{2.17}$$

From eq.(2.17), the critical drive level can be calculated for any specific type of resonator.

2.1.4 Quality factor and loss mechanisms in MEMS resonators

In mechanical resonators, operating in linear regime, The quality factor is the ratio between the maximum stored energy and the dissipated energy per oscillation cycle:

$$Q = 2\pi\frac{\text{Energy stored per cycle}}{\text{Energy dissipated per cycle}} \tag{2.18}$$

From eq.(2.1) ,By normalizing it to the resonator mass, m, we obtain:

$$\ddot{x}+\frac{\gamma}{m}\dot{x}+\frac{k}{m}x=\frac{f}{m} \tag{2.19}$$

or we can rewrite it as:

$$\ddot{x}+2\zeta\omega_{res}\dot{x}+\omega_{res}^2x=\frac{f}{m} \tag{2.20}$$

where we define the damping factor ζ, as

$$\zeta = \frac{\gamma}{2m\omega_{res}} \tag{2.21}$$

ζ =1, the system is critically-damped, and the system converges to zero, than in any other case, without oscillating. When ζ>1, the over-damped system will still not oscillate, but it will take longer to converge to zero.

when ζ <1, the system is under-damped, and it oscillates at a natural frequency ω_{res}. In this case, the quality factor is defined in relationship to the damping factor and the resonance peak will have higher amplitude with higher *Q*:

$$Q = \frac{1}{\zeta} \tag{2.22}$$

The quality factor of a resonator is experimentally approximated from the 3dB bandwidth (BW_{3dB}):

$$Q = \frac{\omega_{res}}{2\pi.BW_{3dB}} \tag{2.23}$$

According to eq.(2.18), in order to increase the quality factor of a resonator which oscillates at a given frequency ω_{res}, it is possible to either maximize the stored energy by increasing the mass, or to reduce the energy losses.

There are several different loss mechanisms which decrease the total quality factor of a device and that should be minimized:

1. Air damping (Q_{air}) [6-7]: When oscillating, the resonator has to overcome the resistance of air trapped in the actuation gaps (squeeze-film damping) and those generated by friction with air for the sides parallel to the vibration displacement (slide-film damping). The energy loss caused by squeeze- film damping dominates when it exists. This source of energy loss is dominant at low and medium frequencies, and it can be avoided by packaging the resonator under vacuum.
2. Thermoelastic damping ($Q_{thermoelastic}$)[8]: TED is a design-dependent type of loss, caused by the cyclic temperature gradient generated in the resonator's body by opposing volume changes due to vibration. The resonator will dissipate heat to return to the equilibrium state, thus loosing energy.

3. Internal friction($Q_{material}$) [9]: This effect is generated by material imperfections like meta stable defects (impurities, dangling or broken bonds), which cause energy dissipation in the form of heat. The contribution of these losses to the system depends on both the material and fabrication technology used.

4. Acoustic anchor losses (Q_{anchor}) [10-11]: MEMS resonators are freestanding structures, anchored to the substrate with suspension tethers or pillars. In all cases, the suspensions create paths of energy dissipation, which can be minimized by placement in the nodal points of the resonating structure, by choosing small widths, and by carefully designing their shape/ dimensions for low motion of the suspensions.

5. Energy transfer to other vibration modes: If the desired mode is in the close vicinity of other spurious modes, they can couple, generating energy loss of the main mode. The separation between these modes can be enlarged by carefully designing the resonator.

All the above mentioned loss mechanisms add up directly for total energy loss, and the overall quality factor can be expressed as:

$$\frac{1}{Q_{total}} = \frac{1}{Q_{air}} + \frac{1}{Q_{material}} + \frac{1}{Q_{thermoelastic}} + \frac{1}{Q_{anchor}} + \frac{1}{Q_{energy\ \text{transfer}}} \tag{2.24}$$

If the resonator is operated under vacuum, the losses due to air damping are very small. Therefore, the most important phenomena affecting the quality factor are the acoustic anchor losses, loss due to material imperfections, loss due thermoelastic damping and energy transfer through coupling to other vibration modes. i.e.

$$\frac{1}{Q_{total}} = \frac{1}{Q_{material}} + \frac{1}{Q_{thermoelastic}} + \frac{1}{Q_{anchor}} + \frac{1}{Q_{energy\ \text{transfer}}} \tag{2.25}$$

2.1.5 Capacitively transduced MEMS resonator structures

Various shapes of capacitive micromechanical resonators have been reported till date, operating in different vibration modes, and fabricated with different materials. Table 2.2 provides an expansive list of such devices[12].

Table 2.2: Some reported capacitively transduced MEMS resonators

Type & references	Material	Frequency	Quality factor
Clamped-clamped beam (flexural mode)	Poly silicon (2 µm thick)	9.34 MHz	3,100
Clamped-clamped beam (flexural mode)	Single crystal silicon (20 µm thick)	80 kHz	74,000
Free-free beam (flexural mode)	Poly silicon (2.05 µm thick)	92 MHz	7,450
Comb drive (flexural mode)	Single crystal silicon (30 µm thick)	32 kHz	50,000
Square plate extensional (bulk acoustic mode)	Single crystal silicon (25 µm thick)	2.18 MHz	1,160,000
Square plate lame (bulk acoustic)	Poly silicon carbide (2 µm thick)	173 MHz	9,300
Wine-glass disk (bulk acoustic mode)	Poly silicon (3 µm thick)	60 MHz	48,000
Radial-contour disk (bulk acoustic)	Poly silicon (2 µm thick)	156 MHz	9,290
Circular disk (flexural mode)	Nickel (3 µm thick)	11.6 MHz	1,651
Square plate (flexural mode)	Poly silicon (2.2 µm thick)	68 MHz	15,000
Ring (contour mode)	Poly silicon (2 µm thick)	1.2 GHz	15,000
Square (flexural mode)	Single crystal silicon	5.1 MHz	80,000
Triangular beam (torsional mode)	Single crystal silicon	20 MHz	220,000

All such a MEMS resonators essentially consists of the following three components: (i) an input- transducer which converts the input electrical signal into a mechanical signal i.e. an electrostatic force (alternatively piezoelectric, magneto static etc.). (ii) A mechanical resonant structure which can vibrate in one or more modes due to the produced electrostatic force, and(iii) an output-transducer that senses the motion of the vibrating structure, hence converting the mechanical signal back to an output electrical signal.

Micromechanical resonators can have different shapes like beams, square plates, circular disks, annular rings, comb etc., and can again be classified according to their modes of operation, namely flexural, torsional, and bulk mode devices .

Flexural mode of vibration is representative of transverse standing waves. In such devices, the displacement of the structures is orthogonal to the bending stress in the structure. In resonators vibrating in the torsional mode, the dominant stress is shear-stress and the displacement produced is rotational in nature. Bulk mode operation can be described in terms of standing longitudinal waves.

The most common transduction type used in MEMS resonators is electrostatic actuation and sensing, as it can produce small components that are robust, relatively simple to fabricate with materials compatible with integrated transistor circuits, have better thermal stability, and are tolerant to environmental changes. Capacitively transduced devices, in general offer the best frequency-Q products, since the signal transduction occurs without the need for direct physical contact between the electrodes and the resonating body, and thus suffer less from material-interface losses and quality factor degradation that can impede other transducer types.

2.2 Conclusion

In this chapter, MEMS resonator modeling is explained in detail. This also includes nonlinear effects in MEME resonators. It was explained that the most important phenomena affecting the quality factor are the acoustic anchor losses, loss due to material imperfections, loss due thermoelastic damping and energy transfer through coupling to other vibration modes. For obtaining high Q from eq.(2.25) concluded that anchor loss should be minimum. It is possible obtain high Q with proper anchor design. Also from Table 2.2, it is observed that different resonator structure material gives different quality factor, so for improving the quality factor systematic material selection method is needed. In Chapter 4 this issue is addressed in detail.

References:

[1] R. A Wickstrom and J. R. Davis, "Gate Transistor," *IEEE Trans. Electron Devices*, vol. 14, no. 3, pp. 117–133, 1967.

[2] V. Kaajakari, J. K. Koskinen, and T. Mattila, "Phase noise in capacitively coupled micromechanical oscillators.," *IEEE Trans. Ultrason. Ferroelectr. Freq. Control*, vol. 52, no. 12, pp. 2322–2331, 2005.

[3] M. Agarwal, S.A. Chandorkar, R. N. Candler, B. Kim, M.A. Hopcroft, R. Melamud, C. M. Jha, T. W. Kenny, and B. Murmann, "Optimal drive condition for nonlinearity reduction in electrostatic microresonators," *Appl. Phys. Lett.*, vol. 89, no. 21, p. 214105, 2006.

[4] V. Kaajakari, T. Mattila, A. Oja, and H. Seppä, "Nonlinear limits for single-crystal silicon microresonators," *J. Microelectromechanical Syst.*, vol. 13, no. 5, pp. 715–724, 2004.

[5] V. Kaajakari, "MEMS Tutorial: Nonlinearity in Micromechanical Resonators," http://www.kaajakari.net

[6] F. R. Blom, "Dependence of the quality factor of micromachined silicon beam resonators on pressure and geometry," *J. Vac. Sci. Technol. B Microelectron. Nanom. Struct.*, vol. 10, no. 1, p. 19, 1992.

[7] T. Corman, P. Enoksson, G. Stemme, and Corman, Thierry and Enoksson, Peter and Stemme, Goran, "Gas damping of electrostatically excited resonators," *Sensors Actuators A Phys.*, vol. 61, no. 1–3, pp. 249–255, 1997.

[8] A. Duwel, R. N. Candler, T. W. Kenny, and M. Varghese, "Engineering MEMS resonators with low thermoelastic damping," *J. Microelectromechanical Syst.*, vol. 15, no. 6, pp. 1437–1445, 2006.

[9] P. Mohanty, D. a. Harrington, K. L. Ekinci, Y. T. Yang, M. J. Murphy, and M. L. Roukes, "Intrinsic dissipation in high-frequency micromechanical resonators," *Phys. Rev. B*, vol. 66, no. 8, p. 085416, 2002.

[10] Y. H. Park and K. C. Park, "High-fidelity modeling of MEMS resonators - Part I: Anchor loss mechanisms through substrate," *J. Microelectromechanical Syst.*, vol. 13, no. 2, pp. 238–247, 2004.

[11] F. D. Bannon, S. Member, J. R. Clark, and C. T. Nguyen, "High- Q HF Microelectromechanical Filters," vol. 35, no. 4, pp. 512–526, 2000.

[12] J. Basu, S. Chakraborty, and T. K. Bhattacharyya, "Micromechanical radial-contour mode disk resonator for a CMOS-MEMS oscillator," *Proc. 2010 Annu. IEEE India Conf. Green Energy, Comput. Commun. INDICON 2010*, pp. 5–8, 2010.

The first section presents the disk resonator model, important design parameters of the circular disk resonator, and the electrical equivalent circuit of the resonator. The second section presents the Lame resonator model, important design parameters of the Lame resonator, and the electrical equivalent circuit of the resonator.

3.1 Introduction

Figure 3.1 shows the perspective-view schematic of a self aligned disk resonator. The resonator consists of a disk suspended above the substrate by an anchor of height '*h*'. The disk radius is *R*. The disk is surround by actuation electrodes with precious gap 'd', gap between the actuation electrode and disk constitutes electromechanical transducer.

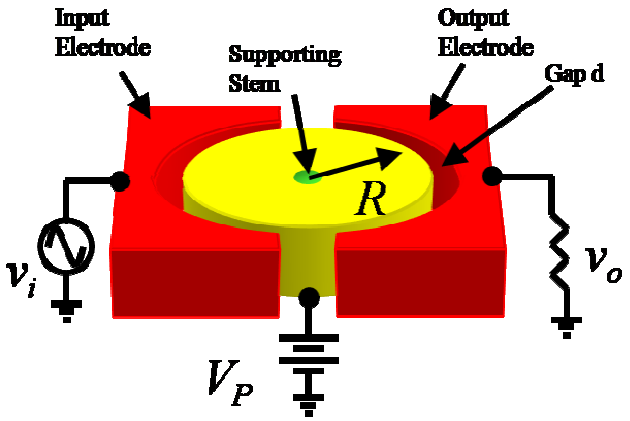

Figure 3.1: The disk resonator

3.1.1 Resonator operation

To excite the device of Figure 3.1 in its two-port configuration, a (DC)-bias voltage V_P is applied to the disk and an alternating current (AC) signal v_i to its input electrode. The DC-bias voltage V_P serves only to charge the electrode-to-disk capacitance, and thereby, does not incur power consumption. From eq.(2.8) electrostatic input force F_i in a radial direction (pointing outward from the disk) given by

$$F_i = \frac{1}{2}\left(\frac{\partial C_1}{\partial r}\right)\left(V_p - v_i\right)^2 \cong -Vp\left(\frac{\partial C_1}{\partial r}\right)v_i \qquad (3.1)$$

where only the dominant term at resonance has been retained (i.e., components at DC and at frequencies different from v_i have been neglected), where $\partial C_1/\partial r$ is the change in electrode-to-resonator overlap capacitance per unit radial displacement at the input port (i.e., port 1).

Since the capacitance at input port 1 is varying with distance r, so the input port capacitance is given by

$$C_1(r) = \frac{\varepsilon_0 A}{d-r} = \frac{\varepsilon_0 A}{d\left(1-\frac{r}{d}\right)} = C_0\left(1-\frac{r}{d}\right)^{-1}$$

where C_o is the static drive electrode-to-disk capacitance.

An expression for $\partial C_1/\partial r$ can be obtained from the differentiating the above expression

$$\frac{\partial C_1}{\partial r} = \frac{C_0}{d}\left(1-\frac{r}{d}\right)^{-2} = \frac{C_0}{d}\left(1+\left(-\frac{r}{d}\right)\right)^{-2} \tag{3.2}$$

If displacements are small, eq.(3.2) can be expanded to obtain the more useful form.

Using Binomial expansion theorem given below, we can expand the above equation

$$(1+x)^n = 1+nx+n(n-1)\frac{x^2}{2!}+n(n-1)(n-2)\frac{x^3}{3!}+.....$$

$$\frac{\partial C_1}{\partial r} = \frac{C_0}{d}\left[1+(-2)\left(\frac{-r}{d}\right)+(-2)(-3)\frac{\left(-r/d\right)^2}{2}+(-2)(-3)(-4)\frac{\left(-r/d\right)^3}{6}+.....\right]$$

$$\frac{\partial C_1}{\partial r} = \frac{C_0}{d}\left[1+\frac{2}{d}(r)+\frac{3}{d^2}(r^2)+\frac{4}{d^3}(r^3)+.....\right]$$

$$\frac{\partial C_1}{\partial r} = \left(\frac{C_0}{d}\right)\left(1+A_1 r+A_2 r^2+A_3 r^3+....\right), \tag{3.3}$$

where $A_1 = \frac{2}{d}, A_2 = \frac{3}{d^2}, A_3 = \frac{4}{d^3}$

For the present purpose of obtaining a linear model for the disk resonator, $\partial C_1/\partial r$ can be approximated by the first term in eq.(3.3) means

$$\frac{\partial C_1}{\partial r} = \left(\frac{C_0}{d}\right)$$

which then can be expanded into:

$$\frac{\partial C_1}{\partial r} = \left(\frac{C_0}{d}\right) = \frac{\left(\frac{\varepsilon_0 A}{d}\right)}{d} = \frac{\varepsilon_0 A}{d^2} = \frac{\varepsilon_0 (arc \times thickness)}{d^2} = \frac{\varepsilon_0 (\varphi_1 R \times t)}{d^2} \tag{3.4}$$

$$\frac{\partial C_1}{\partial r} \approx \frac{\varepsilon_0 \varphi_1 R t}{d^2}, \tag{3.5}$$

where R and t are the radius and thickness, respectively, of the disk; ε_o is the permittivity in vacuum; d is the electrode-to-resonator gap spacing; and φ_1 is the angle defined by the edges of the input electrode (i.e., electrode 1). When the signal frequency v_i matches to the radial-contour mode resonance frequency of the disk, the resulting force drives the disk into a vibration mode shape in which it expands and contracts radial around its perimeter, in a fashion reminiscent of breathing, with a zero-to-peak radial displacement amplitude at any point of the disk (r, θ) given by

$$\Re(r,\theta) = A\mathrm{h}J_1(\mathrm{h}r) \tag{3.6}$$

$$\Re(R,\theta) = \frac{QF_i}{jk_{re}} \tag{3.7}$$

where k_{re} is the effective stiffness at a location on the perimeter. J_n(y) is the Bessel function of the first kind of order n, A is a drive force-dependent ratio [1], and h is a constant defined as

$$\mathrm{h} = \sqrt{\frac{\omega_0^2 \rho}{\left(\frac{2E}{2+2\sigma}\right) + \frac{E\sigma}{1-\sigma^2}}} \tag{3.8}$$

where ρ, σ, and E are the density, Poisson ratio, and Young's modulus, respectively of the structural material.

The radial vibration of the disk creates a DC-biased (by V_P) time-varying capacitance between the disk and output electrode that then sources an output motional current i_o proportional to the amplitude of vibration (radial displacement) given by

$$i_o = \frac{dQ}{dt} = \frac{d(C_2 V_P)}{dt} = \frac{V_P(dC_2)}{dt}$$

$$= \frac{V_P\left(dC_2\right)}{dt}$$
$$= V_P\left(\frac{\partial C_2}{\partial r}\right)\left(\frac{\partial r}{\partial t}\right)$$
$$= V_P\left(\frac{\partial C_2}{\partial r}\right)\left(\frac{\partial R_{(R,\theta)}}{\partial t}\right)$$
$$= V_P\left(\frac{\partial C_2}{\partial r}\right)\left(-j\omega_o\right)\ \ R_{(R,\theta)}$$
$$= V_P\left(\frac{\partial C_2}{\partial r}\right)\left(-j\omega_o\right)\left(\frac{QF_i}{jk_{re}}\right)$$
$$= V_P\left(\frac{\partial C_2}{\partial r}\right)\left(-j\omega_o\right)\left(\frac{Q}{jk_{re}}\right)\left(-Vp\left(\frac{\partial C_1}{\partial r}\right)v_i\right)$$

$$i_0 = \omega_0 \frac{Q}{k_{re}}\left(\frac{\partial C_1}{\partial r}\right)\left(\frac{\partial C_2}{\partial r}\right)V_p^2 v_i \tag{3.9}$$

where $\partial C_2/\partial x$ is the change in electrode-to-resonator overlap capacitance per unit radial displacement at the output port (i.e., port 2), which takes on a form similar to that of eq.(3.5), but with φ_1 replaced by φ_2. This device operates by first converting the input electrical signal v_i to a mechanical force F_i, which is filtered by the high Q mechanical response of the resonator, allowing only components at the disk resonance frequency to be converted to a disk displacement (r, θ) [or velocity $v(r, \theta)$]. This mechanical domain displacement then is converted back to the electrical domain into the output current i_o by action of the output electrode capacitive transducer. It should be noted that output current is only generated if the DC-bias voltage V_P is finite. If the DC voltage between the output electrode and disk is set to zero, then no current flows, and the device is effectively "off" Thus, V_P provides an on/off switchability for this device.

3.1.2 Resonance frequency design

The dimensions needed to attain a specified nominal resonance frequency f_{onom} for a radial-contour mode disk can be obtained by solving the mode frequency equation given by [1]

$$\delta \times \frac{J_0(\delta)}{J_1(\delta)} = 1 - \sigma \tag{3.10}$$

where ω_{onom} is the nominal radian resonance frequency for a purely mechanical system (i.e., with no applied electrical signals, hence no electrical stiffness.

$$\delta = \omega_{onom} R \sqrt{\frac{\rho\left(1-\sigma^2\right)}{E}} \tag{3.11}$$

Above relations can be simplified to obtain the following expression for the resonant frequency [2]

$$\omega_{onom} = \frac{\delta}{R\sqrt{\frac{\rho\left(1-\sigma^2\right)}{E}}}$$

$$f_{onom} = \frac{\delta}{(2\pi) R\left(\sqrt{\left(1-\sigma^2\right)}\right)\sqrt{\frac{\rho}{E}}}$$

$$f_{onom} = \frac{\delta}{(2\pi)\left(\sqrt{\left(1-\sigma^2\right)}\right) R}\sqrt{\frac{E}{\rho}}$$

$$f_{onom} = \frac{\alpha k}{R}\sqrt{\frac{E}{\rho}}$$

where $\alpha k = \dfrac{\delta}{(2\pi)\left(\sqrt{\left(1-\sigma^2\right)}\right)}$ and value of αk is calculated by using eq.(3.10).

So, final equation for Resonant frequency is given by

$$f_{onom} = \frac{\alpha k}{R}\sqrt{\frac{E}{\rho}} \tag{3.12}$$

where k is a parameter dependent upon Poisson's ratio (k = 0.342 MHz/μm for polysilicon), and α is a mode dependent scaling factor that accounts for higher order modes. As seen in eq.(3.10), eq.(3.11), or eq.(3.12), the frequency of resonance is a strong function of structural material properties and of geometry, in particular, of the disk radius a lateral dimension. For the given parameters thickness of the disk is t = 2μm, gap distance d = 1um, for Poly-Si, E = 160GPa, σ = 0.22, ρ = 2.33e^{-15} Kg/μm^3 and bias voltage V_p = 50V, keeping R as variable parameter resonant frequency calculated for fist three mode using MATLAB code, and the graph is plotted in Figure 3.2.From the graph it is observed that for a fixed frequency the first mode requires a small diameter, while compare to the second and third modes.

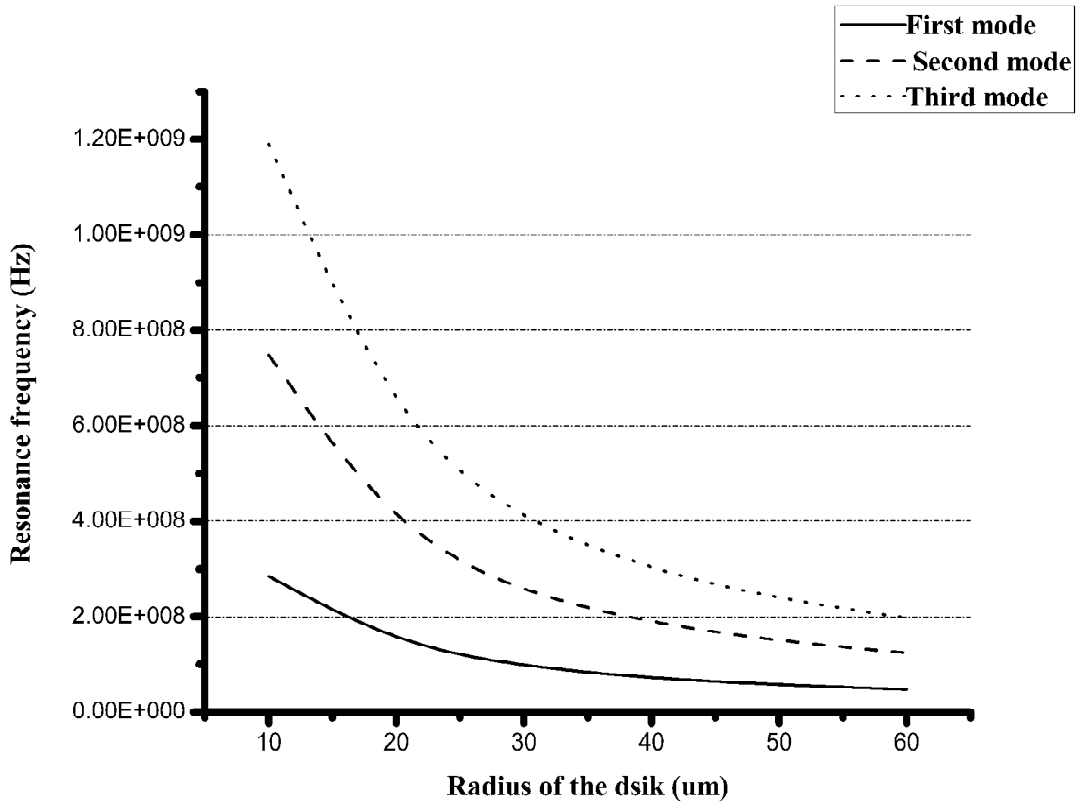

Figure 3.2: Design curve of radial-contour mode resonance frequency with radius of the resonator disk

3.1.3 Frequency pulling via electrical stiffness

Because the electrode-to-resonator capacitance is a non-linear function of the disk radial displacement, there are many force components generated than represented in eq.(3.1). In particular, expanding eq.(3.1) further and inserting the first two terms of eq.(3.3) yields:

$$\begin{aligned} F_i &= \frac{1}{2}\frac{C_0}{d}\left(V_p^2 - 2V_p v_i + v_i^2 + A_1 V_p^2 r - 2A_1 v_i V_p r + A_1 v_i^2 r\right) \\ &= \frac{1}{2}\left(....-2V_p v_i + A_1 V_p^2 r + A_1 v_i^2 r + ...\right) \end{aligned} \tag{3.13}$$

where the last form includes only terms that can generate components at resonance.

Expanding the last form of eq.(3.13), inserting the eq.(3.4) in eq.(3.1), and inserting

$$v_i = V_i \cos \omega t \qquad r = \Re \sin \omega_0 t$$

$$F_i = -\left[Vp\frac{C_0}{d} V_i \cos \omega t - \left(V_p^2 + \frac{V_i^2}{2}\right)\left(\frac{C_0}{d^2}\right)\Re \sin \omega_0 t \right] \tag{3.14}$$

where the second term is at the resonance frequency, but in quadrature with the input force (i.e., the first term)and proportional to the displacement amplitude $\Re$ both qualities also exhibited by the mechanical spring restoring force of the resonator. However, although the mechanical spring restoring force generally acts to oppose an input force, this force acts to increase the input force. In effect, the second term in eq.(3.14) can be interpreted as an electrical spring constant of the form:

$$k_{en} = \left(V_p^2 + \frac{V_i^2}{2} \right) \frac{\varepsilon_0 \varphi_n R\, t}{d^3}, n = 1, 2... \tag{3.15}$$

The electrical stiffness of all electrodes regardless of their position subtract from the mechanical spring constant of the beam k_m, changing its resonant frequency to

$$f_o = \left(\frac{k_{re}}{m_{re}} \right)^{\frac{1}{2}} = \left(\frac{k_m - k_{e1} - k_{e2}}{m_{re}} \right)^{\frac{1}{2}}$$

$$f_o = f_{norm} \left[1 - \frac{\left(k_{e1} + k_{e2} \right)}{k_m} \right]^{\frac{1}{2}}$$

$$f_o \cong f_{norm} \left[1 - \frac{1}{2} \frac{\left(k_{e1} + k_{e2} \right)}{k_m} \right] \tag{3.16}$$

where m_{re} is the effective stiffness of the disk at any point on its perimeter; k_{re} is the effective stiffness at that same location with all voltages applied; k_m is the mechanical stiffness of the disk at the same location.

Using eq.(3.16) the fractional frequency change due to electrical stiffness related parameter, for common case where $V_P >> V_i$:

$$f_o = f_{norm} - f_{norm} \frac{1}{2} \frac{\left(k_{e1} + k_{e2} \right)}{k_m}$$

$$f_o - f_{norm} = -f_{norm} \frac{1}{2} \frac{\left(k_{e1} + k_{e2} \right)}{k_m}$$

$$\frac{f_o - f_{norm}}{f_0} = -\frac{1}{2} \frac{\left(k_{e1} + k_{e2} \right)}{k_m}$$

$$\frac{\Delta f}{f_0} = -\frac{1}{2} \frac{\left(k_{e1} + k_{e2} \right)}{k_m}$$

Substituting the value of k_{e1} and k_{e2} from eq.(3.15) , we get

$$\frac{\Delta f}{f_o} = -\frac{1}{2}\frac{(k_{e1}+k_{e2})}{k_m} = -\frac{1}{2}\frac{V_p^2}{k_m}\frac{\varepsilon_0 Rt}{d^3}(\varphi_1+\varphi_2) \tag{3.17}$$

For high frequency (HF) and very high frequency (VHF) resonators, the value of k_m ranges from 500 N/m to 100,000 N/m, respectively, which are generally much larger than that of their k_e's but still of a size that allows fractional frequency shifts ranging from 0.1% – 10%. For the case where the high stiffness of disk resonators precludes tunability by the DC-bias V_P often used by HF and VHF resonators, it also suppresses mechanisms for instability (e.g., temperature dependence of the electrode to resonator gap spacing d [3], microphonics, etc.), perhaps making for an overall zero sum gain from a design perspective.

3.1.4 Temperature dependence of the resonance frequency

The HF and VHF micromechanical resonators are govern by a combination of temperature dependent parameters like., electrical stiffness, Young's Modulus '*E*' and resonator dimensions.

In the case under consideration as the mechanical stiffness is high, it reduce the influence of electrical stiffness To verify this, the fractional frequency change with temperature due to a change in electrode to resonator gap spacing d is obtained.

For general case (not $V_P >> V_i$)

$$\frac{\Delta f}{f_o} = -\frac{1}{2}\frac{\left(V_p^2+0.5V_i^2\right)}{k_m}\frac{\varepsilon_0 Rt}{d^3}(\varphi_1+\varphi_2) \tag{3.18}$$

Differentiating above equation with respect to '*d*'

$$\frac{\partial\left(\frac{\Delta f}{f_0}\right)}{\partial d} = -\frac{1}{2}\frac{\left(V_p^2+0.5V_i^2\right)}{k_m}\frac{\varepsilon_0 R\ t}{d^3}(\varphi_1+\varphi_2)$$

$$= \frac{3}{2}\frac{\left(V_p^2+0.5V_i^2\right)}{k_m}\frac{\varepsilon_0 R\ t}{d^4}(\varphi_1+\varphi_2)$$

To find temperature dependence of resonance frequency differentiate eq.(3.18) with respect to T

$$\frac{\partial\left(\frac{\Delta f}{f_0}\right)}{\partial T} = \frac{\partial\left(\frac{\Delta f}{f_0}\right)}{\partial d}\frac{\partial d}{\partial T}$$

$$\frac{\partial\left(\frac{\Delta f}{f_0}\right)}{\partial T} = \frac{3}{2}\frac{\left(V_p^2 + 0.5V_i^2\right)}{k_m}\frac{\varepsilon_0 R\ t}{d^4}\left(\varphi_1 + \varphi_2\right)\left[\frac{\partial d}{\partial T}\right]$$

$$\frac{\partial\left(\frac{\Delta f}{f_0}\right)}{\partial T} = \frac{3}{2}\frac{\left(V_p^2 + 0.5V_i^2\right)}{k_m}\frac{\varepsilon_0 R t}{d^4}\left(\varphi_1 + \varphi_2\right)\left[\alpha_{si} d + \left(\alpha_{si} - \alpha_e\right) L_e\right] \tag{3.19}$$

where α_{si} = thermal expansion coefficient of silicon; α_e = thermal expansion coefficient of surrounding electrode; L_e= suspended electrode length

For a gap spacing (> 20 nm), the temperature coefficient of the resonance frequency for a disk resonator is mainly govern by temperature dependencies of the Young's Modulus of its structural material and its own dimensions [4].

$$TC_f = \frac{1}{f_o}\frac{\partial f}{\partial T} \tag{3.20}$$

From eq.(3.12)

$$f_{onom} = \frac{\alpha k}{R}\left(\frac{E}{\rho}\right)^{\frac{1}{2}}$$

Differentiating above equation w. r. to T

$$\frac{\partial f_{onom}}{\partial T} = \frac{\alpha k}{1}\left[-\frac{1}{R^2}\frac{\partial R}{\partial T}\left(\frac{E}{\rho}\right)^{1/2} + \frac{1}{R}\frac{1}{2}\left(E\rho\right)^{\left(-1/2\right)}\frac{\partial E}{\partial T}\right]$$

$$\frac{\partial f_{onom}}{\partial T} = \frac{\alpha k}{R}\left(\frac{E}{\rho}\right)^{\frac{1}{2}}\left[-\frac{1}{R}\frac{\partial R}{\partial T} + \frac{1}{2}\left(E\right)^{(-1)}\frac{\partial E}{\partial T}\right]$$

$$\frac{\partial f_{onom}}{\partial T} = f_{onom}\left[-\frac{1}{R}\frac{\partial R}{\partial T} + \frac{1}{2}\frac{1}{E}\frac{\partial E}{\partial T}\right]$$

Substituting the above value in eq.(3.20), we get

$$TC_f = \frac{1}{f_{onom}} \frac{f}{T}$$

$$TC_f = \frac{1}{f_{onom}} f_{onom} \left[-\frac{1}{R}\frac{R}{T} + \frac{1}{2}\frac{1}{E}\frac{E}{T} \right]$$

$$TC_f = \left[-\frac{1}{R}\frac{R}{T} + \frac{1}{2}\frac{1}{E}\frac{E}{T} \right]$$

$$TC_f = -\alpha_{poly} + \frac{1}{2} TC_E \tag{3.21}$$

where α_{poly} = thermal expansion coefficient.

3.1.5 Mechanical equivalent model

To conveniently model and simulate the impedance behavior of this mechanical resonator when used in an electromechanical circuit, an electrical equivalent circuit is needed. Despite its mechanical nature, the disk resonator of Figure 3.1 still looks like an electrical device when looking into its ports, and so can be modeled by either of the electrical inductor-capacitor-resistor (LCR) equivalent circuits shown in Figure 3.4. The values of elements in the equivalent circuits are governed by the total integrated kinetic energy in the resonator, its mode shape, and the parameters associated with its transducer ports[5]. The total kinetic energy in a vibrating disk can be obtained by integrating the kinetic energies of all infinitesimal mass elements *dm* in the disk, and can be expressed as

For a small element (with mass dm) on circular disk, the kinetic energy is given by

$$KE_{dm} = \frac{1}{2} \times dm \times v^2(r, \theta)$$

And the total *KE* of circular disk is given by

$$KE_{tot} = \frac{1}{2} \int_0^{2\pi} \int_0^R dm \times v^2(r, \theta) \tag{3.22}$$

where $v(r, \theta)$ is the velocity magnitude at location (r, θ) is given by

$$v(r, \theta) = \omega \Re(r, \theta) = \omega A h J_1(hr) \tag{3.23}$$

and mass is given by

$$\text{Mass} = \text{Density} \times \text{Volume}$$

$$dm = \rho \times Volume$$

$$dm = \rho \times Area \times dr$$

$$dm = \rho \times t \times rd\theta \times dr \tag{3.24}$$

Substituting the value of eq.(3.23) and (3.24) in eq.(3.22) to get

$$KE_{tot} = A^2\omega^2 h^2 \pi\rho t \int_0^R rJ_1^2(hr)\,dr \tag{3.25}$$

To find equivalent mass at a location (r, θ), divide the total *KE* by one half the square of the velocity at that location i.e.

$$m_{re} = \frac{KE_{tot}}{\frac{1}{2}v^2(R,\theta)} = \frac{2\pi\rho t \int_0^R rJ_1^2(hr)\,dr}{J_1^2(hR)} \tag{3.26}$$

The expression for equivalent stiffness and damping at a location on the disk perimeter can be obtain using standard equations shown below

$$k_{re} = \omega_0^2 m_{re} \tag{3.27}$$

$$c_{re} = \frac{w_0 m_{re}}{Q} = \sqrt{\frac{k_{re} m_{re}}{Q}} \tag{3.28}$$

The corresponding equivalent mechanical model shown in Figure 3.3.

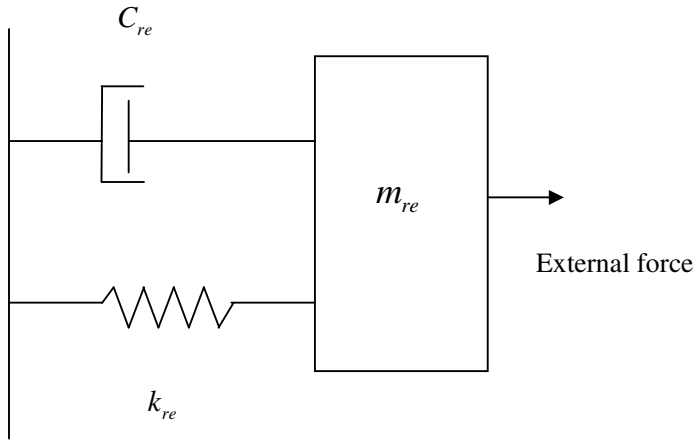

Figure 3.3: Mechanical equivalent model

The electromechanical coupling factor at port *n* is given by

$$\eta_{en} = \frac{F_i}{v_{in}} = \frac{V_p\left(\frac{\partial C_n}{\partial x}\right)v_{in}}{v_{in}}$$

$$\eta_{en} = V_p\left(\frac{\partial C_n}{\partial x}\right) \tag{3.29}$$

where n = 1 and 2 corresponds to input and output port respectively.

3.1.6 Small signal electrical equivalent circuit

The electrical equivalent circuit for the radial-contour mode disk resonator configured as a two-port is shown in Figure 3.4. The elements of the electrical circuit are obtained from mechanical lumped element values[6]. The C_o represents capacitance from an I/O electrode to AC ground, and as such, is primarily composed of a combination of electrode-to-resonator overlap capacitance and electrode-to-substrate capacitance. The exact capacitance is combination of parallel plate and parasitic capacitance

The value of capacitor C_x is given by

$$C_x = \frac{\eta_{e1}\eta_{e2}}{k_{re}}$$

and for R_x and L_x we use following derivation.

For R_x

Since

$$Q = \frac{1}{\omega_0 C_x R_x}$$

or

$$R_x = \frac{1}{\omega_0 C_x Q} = \frac{1}{\omega_0\left(\frac{\eta_{e1}\eta_{e2}}{k_{re}}\right)\left(\frac{\omega_0 m_{re}}{c_{re}}\right)} = \frac{c_{re}}{\eta_{e1}\eta_{e2}} \tag{3.30}$$

For L_x

Since

$$Q = \frac{\omega_0 L_x}{R_x}$$

or

$$L_x = Q\frac{R_x}{\omega_0} = \frac{\left(\frac{\omega_0 m_{re}}{c_{re}}\right)\left(\frac{c_{re}}{\eta_{e1}\eta_{e2}}\right)}{\omega_0} = \frac{m_{re}}{\eta_{e1}\eta_{e2}} \tag{3.31}$$

Substituting the value of η_{e1} and η_{e2} from eq.(3.29) into R_x of eq.(3.30)

$$R_x = \frac{c_{re}}{\eta_{e1}\eta_{e2}} = \frac{c_{re}}{V_p\left(\frac{\partial C_1}{\partial r}\right)V_p\left(\frac{\partial C_2}{\partial r}\right)}$$

Substituting the value of $\frac{\partial C_1}{\partial r}$ and $\frac{\partial C_2}{\partial r}$ from eq.(3.5)

we get

$$R_x = \left(\frac{\omega_0 m_{re}}{Q}\right)\left(\frac{1}{V_P^2}\right)\left(\frac{d^4}{\varphi_1\varphi_2(\in_0 R\, t)^2}\right) \tag{3.32}$$

Equation (3.32) implies that R_x can be reduced by increasing the DC-bias voltage V_P, increasing the disk thickness t, or decreasing the electrode-to-disk gap. The bias voltage V_P can sometimes be constrained by the system power supply voltage, or by the pull-in voltage of the resonator [6].

Figure 3.4 presents the equivalent series RLC circuit which can be used to model the operation of a MEMS resonator. The intrinsic resonator behavior is modeled using a motional inductance L_x, a motional capacitance C_x, and a motional resistance R_x, The C_o represents capacitance from an I/O electrode to AC ground, and as such, is primarily composed of a combination of electrode-to-resonator overlap capacitance and electrode-to- substrate capacitance. The exact capacitance is combination of parallel plate and parasitic capacitance.

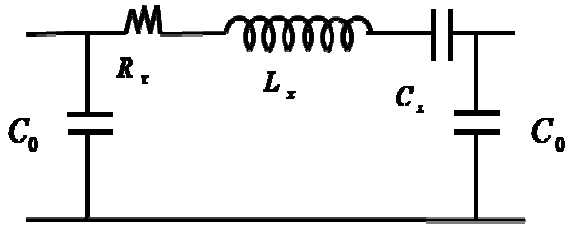

Figure 3.4: Small signal equivalent circuit

$$C_o = C_{pp} + C_{par}$$

For precise model

$$C_{pp} = \frac{\varepsilon_0 \varepsilon_r \frac{2\pi Rt}{360} A_{ec}}{d} \tag{3.33}$$

R is the radius of the disk, t is the thickness of the disk and A_{ec} is the angle covered with one electrode, d is the gap-distance, ε_0 is 8.85418×10^{-12} F/m and ε_r is 1 for air. For simple model

$$C_{pp} = \frac{\varepsilon_0 \varepsilon_r \pi Rt}{d}$$

πR is the effective width at the coupling area, t is the thickness.

For the given parameters thickness of the disk is t = 2µm, gap distance d = 1um, For Poly-Si, E = 160GPa, σ = 0.22, ρ = $2.33e^{-15}$ Kg/µm^3 and bias voltage V_p=50V, keeping R = 10 µm. Small signal equivalent circuit parameters calculated using MATLAB code.

Table 3.1: Small signal equivalent circuit parameters

Parameters	L_x(*Henry*)	C_x(*Farad*)	R_x(*Ohm*)	C_o(*Farad*)
Precise model	1.9242	2.7549e-019	2.8115e+005	2.7803e-015
Simple model	2.3406	1.3300e-019	4.4628e+005	2.7803e-015

From Table 3.1 it is observed that there is considerable amount of difference in R_x, but C_o value is same for both simple as well as precise model .

3.2 Lame-mode resonator

Figure 3.5 presents lame-mode vibration structure with side support . If material of the proof mass is isotropic and the length is much larger than its thickness the resonance frequency can be approximated using [7- 8].

$$f_0 = \sqrt{\frac{G}{\rho}} . \frac{1}{\sqrt{2}L} \tag{3.34}$$

$$G = \frac{E}{2(1+v)} \tag{3.35}$$

where ρ = Material density, L = Length of the square plate, E = Young's modulus, v = Poisson's coefficient.

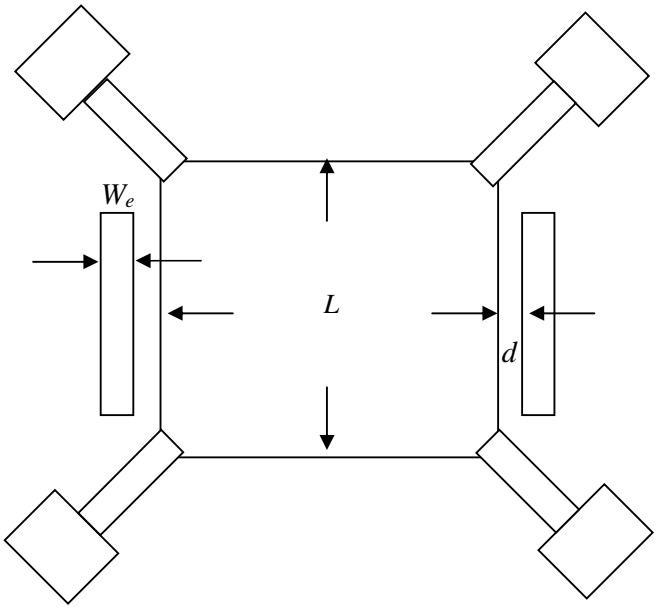

Figure 3.5: Lame-mode vibration structure

3.2.1 Equivalent mechanical model

The resonator can be represented by a mechanical lumped-element model of a mass-spring-damper system as shown in Figure 3.6. For a square plate of side length L and thickness h, its effective mass may be approximated to the mass of the square, given by[9]. Total kinetic energy m_{re} of the vibrating plate is given by.

$$m_{re} = \rho h L^2 \tag{3.36}$$

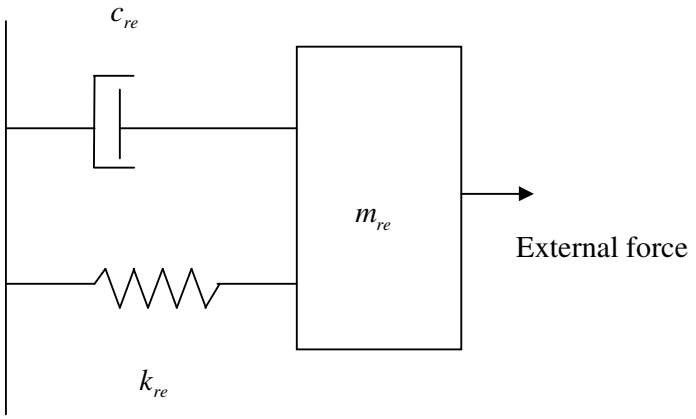

Figure 3.6: Equivalent mechanical model of MEMS resonator

And the effective stiffness is given by

$$k_{re} = \pi^2 Eh \tag{3.37}$$

$$c_{re} = \frac{\omega_0 m_{re}}{Q} = \sqrt{\frac{k_{re} m_{re}}{Q}} \tag{3.38}$$

3.2.2 Equivalent electrical model

Figure 3.7 presents the equivalent series RLC circuit which can be used to model the operation of a MEMS lame resonator[9-11]. The elements of the electrical circuit can be related to those of the mechanical model by using the 'force-voltage analogy' as follows:

$$R_x = \frac{c_{re}}{\eta_{e1}\eta_{e2}}, L_x = \frac{m_{re}}{\eta_{e1}\eta_{e2}}, C_x = \frac{\eta_{e1}\eta_{e2}}{k_{re}}, C_0 = \frac{\varepsilon_0 h W_e}{d_0} \tag{3.39}$$

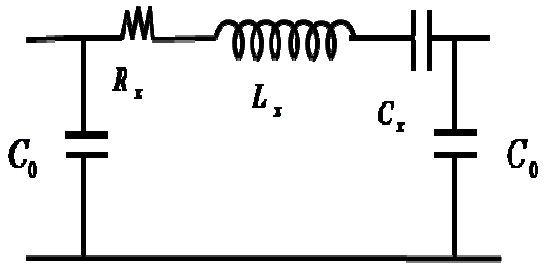

Figure 3.7: Equivalent electrical models of a MEMS resonator

where W_e is the width of the input/output electrode. the transduction ratio η_{e1} and η_{e2} can be calculated with [9], where *Vp* is the DC bias voltage applied to the resonance square.

$$\eta_{e1} = \eta_{e2} = V_p \frac{C_0}{d}$$

all these parameters are used while designing filter based on Lame structure in Chapter 6,corresponding MATLAB code is given in Appendix-I

3.3 Conclusion

This chapter explained the electro-mechanical modeling of Disk and Lame MEMS resonator. An analytical model for resonator and resonant frequency is presented in this chapter. The factors that affect resonance frequency are also explained.

References:

[1] M. Onoe, "Contour vibrations of isotropic circular plates," *J. Acoust. Soc. Amer*, vol. 28, pp. 1158-1162, 1956.

[2] Robert A.Johnson, *Mechanical Filters in Electronics*. Wiley Series on Filters, John Willey & Sons,Canada, 1983.

[3] W. Hsu, J. R. Clark, C. T. Nguyen, and A. Arbor, "A Resonant Temperature Sensor Based on Electrical Spring Softening Center for Wireless Integrated Microsystems Department of Electrical Engineering and Computer Science," in *in Tech. Dig., 11th Int. Conf. on Solid-State Sensors Actuators*, 2001, pp. 1484-1487.

[4] T. Remtema and L. W. Lin, "Active frequency tuning for micro resonators by localized thermal stressing effects," *Sensors and Actuators a-Physical*, vol. 91, no. 3, pp. 326-332, 2001.

[5] F. D. Bannon, J. R. Clark, and C. T.-C. Nguyen, "High-Q Hf microelectromechanical filters,'" *IEEE J. Solid-State Circuits*, vol. 35, no. 10, pp. 1517-1517, 2000.

[6] H. C. Nathanson, W. E. Newell, R. A. Wickstrom and J. R.Davis, "The Resonant Gate Transistor," *IEEE Trans. Electron Devices*, vol. 14, no. 3, pp. 117–133, 1967.

[7] S. A. Bhave, D. Gao, R. Maboudian, R. T. Howe, B. Sensor, and C. Hall, "Fully differential poly-SiC Lamé-mode resonator and checkerboard filter," *18th IEEE International Conference on Microelectromechanical systems,* 30 Jan - 03 Feb, FL, USA, pp. 223–226, 2005.

[8] L.Khine, M.Palaniapan and W.K. Wong, "12.9MHz Lame-Mode differential SOI bulk resonators," *Solid-State Sensors, Actuators and Microsystems Conference*,10-14, June, Lyon, France, pp. 1753–1756, 2007.

[9] V. Kaajakari, T. Mattila, A. Oja, J. Kiihamäki, and H. Seppä, "Square-extensional mode single-crystal silicon micromechanical resonator for low-phase-noise oscillator applications," *IEEE Electron Device Lett.*, vol. 25, no. 4, pp. 173–175, 2004.

[10] M. Motiee, R. R. Mansour, and A. Khajepour, "Novel MEMS filters for on-chip transceiver architecture, modeling and experiments," *J. Micromechanics Microengineering*, vol. 16, no. 2, pp. 407-418, 2006.

[11] Y. Xu and J. E.-Y. Lee, "Single-device and on-chip feedthrough cancellation for hybrid MEMS resonators," *IEEE Trans. Ind. Electron.*, vol. 59, no. 12, pp. 4930–4937, 2012.

Chapter - 4

Material Selection Methodology

4.1 Introduction

Resonator is a key component in the transceiver system, which are often utilized for frequency selection in the radio-frequency (RF) and intermediate-frequency (IF) stages. Microelectromechanical (MEMS) resonators are the prime candidates for being used as frequency selection and generation components due to their ability to resonate at GHz frequencies and their exceptionally high *Q*. Moreover these resonators provide frequency stability, thermal stability, and CMOS compatibility[1-2] Many approaches to obtain high frequency are being investigated to render MEMS resonators compatible with the CMOS circuitry. However, according to the best knowledge of the authors, the material selection approach is hardly used to enhance the performance of the MEMS resonators[3].

With the development of fabrication techniques, the numbers of materials that can be used for MEMS resonator have been increased. Three basic requirements for material selection in MEMS resonator are high *Q*, high resonant frequency, and low process temperature which in turn depends on suitable material to be used for the disk and supporting beam. Through several material selection strategies have been developed in the past, the methodology for selecting the material for disk and supporting beam in high *Q*-MEMS resonator had never been proposed. Ashby provides a comprehensive material selection strategy with less computation[4]. For MEMS based design, the Ashby approach is widely accepted . So the Ashby approach is used to choose suitable material for a center-supported disk resonator. This chapter present a detailed analysis of material selection for the high *Q*-disk MEMS resonator based on the electro-static actuation model compatible with Ashby approach.

4.1.1 MEMS disk resonator structure and its operation

Figure 4.1 shows a center-supported disk resonator of radius '*R*' and thickness '*t*', supporting beam of diameter ' *a*' and height' *h*'. The electrodes are positioned around the

circumference of the disk with a specific gap spacing, '*d*'. This narrow air (or vacuum) gap defines the capacitive, electromechanical transducer of the device. To excite vibrations, a dc bias voltage 'V_P' is applied to the disk structure, and an ac input signal 'v_i' to oppositely located input electrodes. These voltages result in a force proportional to the product 'V_P 'and 'v_i ' that drives the resonator into its vibration. For radial-contour mode disk expands equally in all the lateral directions.

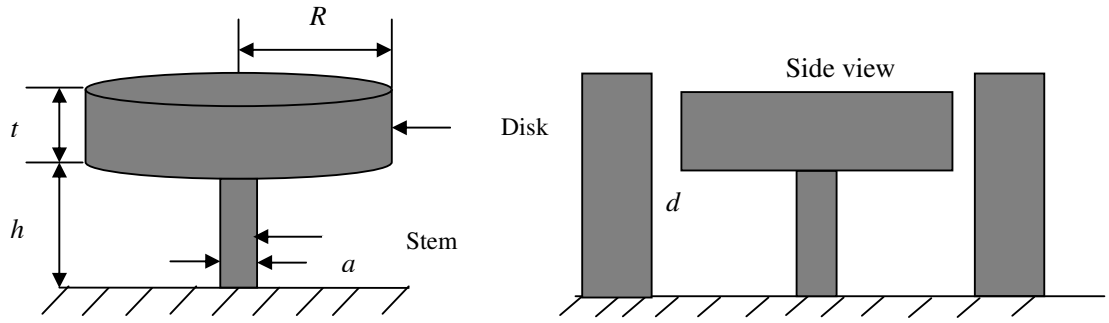

Figure 4.1: Schematic view of MEMS disk resonator

4.1.2 Materials for MEMS resonator

There is a wide variety of materials available for MEMS, however only few materials can be qualified as structural materials for MEMS devices due to difficulties in micro fabrication technologies. These materials are traditionally grouped under four classes: metals and alloys, glasses and ceramics, polymers and elastomers, and composites. The properties of materials commonly studied while designing are Young's modulus (E), Poisson's ratio (σ), fracture strength (σ_F), yield strength, fracture toughness, coefficient of thermal expansion and residual stress (σ_R)[5]. Using Ashby approach, the designer considers all the materials and studies their properties to optimize the design performance and reliability. Certain other properties like electrical resistivity and conductivity are also considered while dealing with the electrical aspects. The properties of materials with different deposition techniques and length scale changes drastically from its bulk values however the properties whose physical origins lie at the atomic scale (size and weight of atoms, nature of bonding and bond density, etc.) are expected to be the same in micromechanical and bulk structures [6]. Sharpe has tabulated initial design values based on an extensive survey of such measurements whose values are listed in Table 4.1 along with the nominal bulk values tabulated by Ashby and Jones.

Table 4.1: Recommended initial design values of material properties

Property	Recommendation
Density, ρ (kg/ m^3)	$\rho_\mu \approx \rho_{bulk}$
Young's Modulus, E(GPa)	$0.8\ E_{bulk} \leq E_\mu \leq E_{bulk}$
Poisson's ratio σ	0.25
Fracture strength, σ_F (Mpa)	$\sigma_{F,\mu} \approx \sigma_{F,bulk}$
Linear expansion coefficient, α (K^{-1})	$\alpha_\mu \approx \alpha_{bulk}$
Specific heat, Cp (J $kg^{-1}1K^{-1}$)	$C_{p,\mu} = C_{p,bulk}$
Intrinsic loss coefficient, η_i	$10^{-2} < \eta_i$ (Polymers) $10^{-5} < \eta_i < 10^{-2}$ (Metals) $10^{-7} < \eta_i < 10^{-4}$ (Ceramics)
Residual stress σ_R	$-1\ GPa \leq \sigma_R \leq 1\ GPa$

μ indicates micro scales.

The following three properties identified by MacDonald et al [7] are of extreme importance for MEMS devices; Compatibility with semiconductor technology, good electrical and mechanical properties, intrinsic properties that retard development of high stress during processing. It is already know that 0.35 μm technology can withstand at 525°C for 90 min [8]. Therefore we are interested to find such materials that can be deposited at temperatures lower than 450°C and exhibit mechanical properties suitable for vibrating micromechanical disk resonator. Through literature review [4-10] it has been observed that the possible materials used for MEMS disk resonator for CMOS technology are Nickel(Ni), poly$Si_{0.35}Ge_{0.65}$,bulk metallic glass materials [11-14],which include $Pt_{57.5}Cu_{14.7}Ni_{5.3}P_{22.5,}$ $Zr_{44}Ti_{11}Cu_{10}Ni_{10}Be_{25,}$ and $Au_{49}Ag_{5.5}Pd_{2.3}Cu_{26.9}Si_{16.3}$.

Table 4.2: Material performance indices for high *Q* resonators[4-10]

Material	Modulus, *E* (GPa)	Density, ρ (kg/m^3)	Process temperature Tp[^{o}C]
Nickel	195	8900	380
$polySi_{0.35}Ge_{0.65}$	146	4280	450
$Pt_{57.5}Cu_{14.7}Ni_{5.3}P_{22.5}$[8]	94.8	15300	250-280
$Zr_{44}Ti_{11}Cu_{10}Ni_{10}Be_{25}$	96.7	6100	380-450
$Au_{49}Ag_{5.5}Pd_{2.3}Cu_{26.9}Si_{16.3}$	66.38	11000	150-190

4.1.3 Material selection – the Ashby method

Ashby material selection strategy is used to characterize the appropriate material for desired performance depending upon its attributes (mechanical, electrical and thermal properties of the material). Once the need of the application is decided, the performance indices are discovered, all the materials are considered and their material properties are studied. After that material selection charts are plotted and analyzed. The materials that meet the need are then taken into consideration and thus subset of the originally considered materials is obtained[14].

Three things specify the design of structural elements: the functional requirements, the geometry, and the properties of the material. The performance of an element is described by an equation of the form as[14]

$$p = f(F, G, M) \tag{4.1}$$

where p describes some performance aspects of the component: its mass or volume, or cost, or life for example. Optimal design is the selection of the material and geometry, maximizing or minimizing p according to its desirability. The optimization is subject to constraints, some of which are imposed by the material properties M.

The three groups of parameters in eq.(4.1) are said to be 'separable' when the equation can be written as

$$p = f_1(F).f_2(G).f_3(M) \tag{4.2}$$

the performance can be optimized by optimizing the appropriate material indices. This optimization can conveniently be performed using graphs with axes corresponding to different material properties [14].

4.1.4 Performance indices

4.1.4.1 *Quality factor*

The mechanical quality factor (Q) of a disk resonator is defined as

$$Q = 2\pi \frac{W}{\Delta W}$$

where ΔW denotes the energy dissipated per cycle of vibration and W denotes the maximum vibration energy stored per cycle ,which is expressed as[15]

$$W = \frac{1}{2}\frac{E_d}{\left(1-\sigma_d^2\right)}\pi t[\gamma_p B J_2(\gamma_p)]^2 \tag{4.3}$$

where ρ is the density, E_d is the Young's modulus of the disk material σ is the Poisson's ratio of the disk material, J_2 is Bessel function, B is the vibration amplitude, t is the thickness, γ_p is frequency parameter for the p^{th} mode. which is given by

$$\gamma_p = \alpha k \tag{4.4}$$

where k is a parameter dependent upon Poisson's ratio, and α is a mode-dependent scaling factor that accounts for higher order.

The amount of energy loss per cycle through the enter support beam is further expressed as[15]

$$\Delta W = \pi \sigma_{zz}^2 \pi a^2 u_z \tag{4.5}$$

where σ_{zz} is the normal stress on the substrate, u_z is the displacement in the substrate due to the normal stress which is given by [15]

$$u_z = \frac{8a(1-v_{sub}^2)}{E_{sub}(1-2v_{sub})}\psi\sigma_{zz} \tag{4.6}$$

where,

$$\sigma_{zz} = \frac{E_s \sigma_s}{1-\sigma_z} \frac{2B}{a\cos\left(\frac{2\pi}{\lambda}h\right)} J_1\left(\gamma_p \frac{a}{R}\right) \tag{4.7}$$

where h is the height of the stem, R is the radius of the disk and a is the diameter of supporting beam. For increasing the Q-factor , the value of W should be high, and ΔW should be low. Therefore, for high Q, the value of E_d should be high and E_s should be as low as possible. Hence by using eq.(4.3) and eq.(4.7) we can say that material index related to the Quality factor is E_d. Therefore first material index is: $IM_1=E_d$.

Therefore, the performance index related to quality factor in the disk is $PI_1 = f(E_d)$.

4.1.4.2 *Resonant frequency*

The mechanical resonant frequency for the radial contour mode of a disk is governed mainly by its material properties and its radius. Neglecting second order effects due to thickness and finite anchor dimensions, the resonant frequency may be determined by finding a numerical solution for the system of equations[16-17].

$$\delta \times \frac{J_0(\delta)}{J_1(\delta)} = 1-\sigma \tag{4.8}$$

where

$$\delta = \omega_{onom} R \sqrt{\frac{\rho\left(1-\sigma^2\right)}{E}} \tag{4.9}$$

where R is the radius of the disk, and E, ρ and σ are the Young's modulus of elasticity, mass density and Poisson's ratio of the material of the disk respectively. Simplification of eq.(4.8) and eq.(4.9) can yield the following expression for the resonant frequency for the i^{th} breathing mode:

$$f_{onom} = \frac{\alpha k}{R}\sqrt{\frac{E}{\rho}} \tag{4.10}$$

where k is a parameter dependent upon Poisson's ratio (k = 0.342 MHz/μm for polysilicon), and α is a mode dependent scaling factor that accounts for higher order modes. Therefore an infinite number of resonant frequencies are possible for a disk of a certain shape and material; however, the fundamental mode is typically the frequency of primary interest for this resonator. Both the resonator material and its dimensions have

an effect on the natural frequency. Poisson's ratio for the most of the MEMS material is 0.25 so it is neglected. Therefore, the second material index related to the resonant is defined as: $IM_2 = \sqrt{\frac{E}{\rho}}$

Therefore, the performance indices related to the resonant frequency is $PI_2 = f(E, \rho)$.

4.1.5 Results

Figure 4.2 shows the plot of density versus Young's modulus (E) for all possible disk resonator materials. From eq.(4.3) and eq.(4.9) it is clear that material with a high value of Young's modulus (E) and low value of density provides high Q and high resonant frequency. It is observed from the plot that poly $Si_{0.35}Ge_{0.65}$ followed by $Zr_{44}Ti_{11}Cu_{10}Ni_{10}Be_{25}$ and Ni are the possible material that provide high Q and high resonant frequency. However for the next generation CMOS technology, the requirements for the thermal budget is less than 450°C [5]. Figure 4.3 shows the plot of Young's modulus (E) versus process temperature for all possible disk materials that are compatible with CMOS technology.

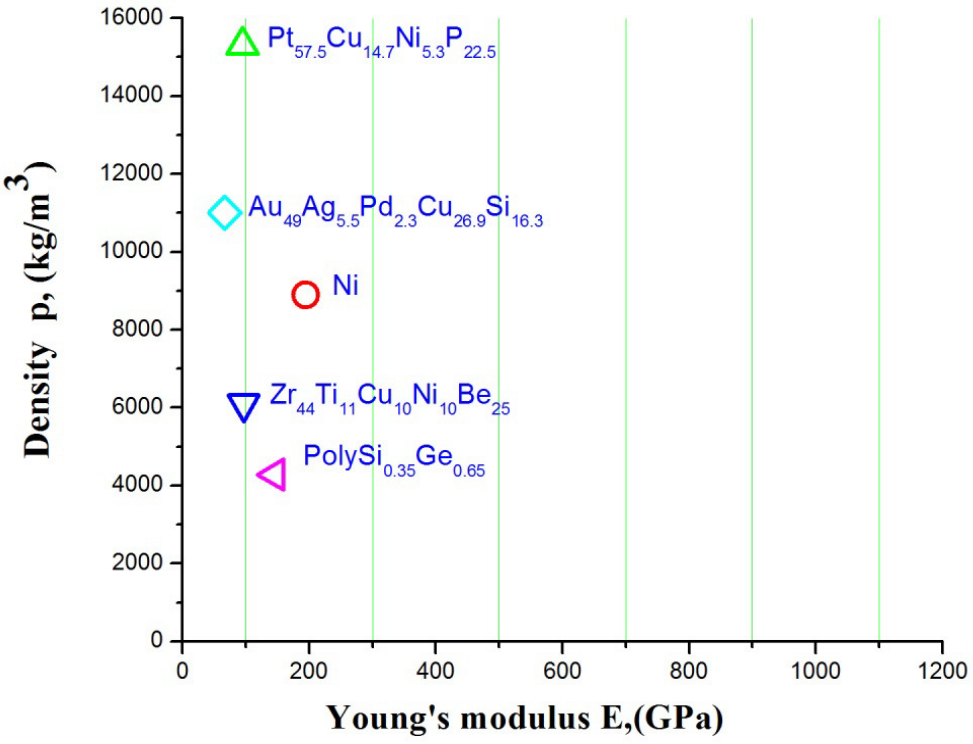

Figure 4.2: Variation of density versus Young's modulus for all possible materials

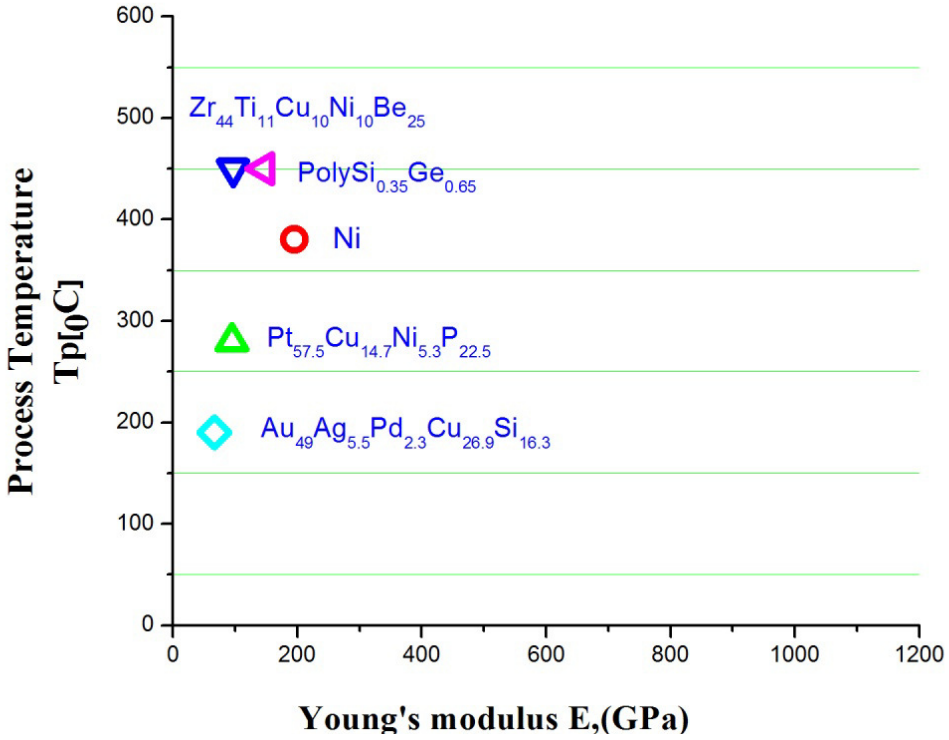

.

Figure 4.3: Variation of process temperature versus Young's modulus for all possible materials

From eq.(4.3), it is clear that the material should have high Young's modulus, therefore from Figure 4.3, it is clear that Ni followed by poly $Si_{0.35}Ge_{0.65}$ and $Zr_{44}Ti_{11}Cu_{10}Ni_{10}Be_{25}$ are the most suitable materials to be used as disk materials for MEMS resonators. Out of these three materials poly $Si_{0.35}Ge_{0.}65$ possess lowest value of density Hence it is concluded that poly $Si_{0.35}Ge_{0.65}$is the best possible material to be used for MEMS resonators. The outcome of this study is compared with the experimental founding's of Quevyeb[18]. According to them poly-SiGe disk resonator has been developed with *Q*'s of 15,300 at frequency up to 425 MHz. This validates our proposed study.

4.2 Disk resonator design and simulation

Based on the disk resonator model given in Chapter 4. Its resonant frequency calculated for the design parameter given in Table 4.3.

Table 4.3: Disk resonator design parameter

Design parameters	**Value**
Disk Radius *R*	10
Air gap *d*	1um
Supporting Stem diameter *a*	2um
Thickness of the disk	2um
Thickness of the stem	2um
Resonant frequency simple model	2.8525e+008

For polysilcon Young's modulus $E = 160\text{GPa}$, mass density $\rho = 2300\ kg/m^3$, and Poisson's ratio of the material $\sigma = 0.22$. The Poly MUMPs process parameters[19] have been used for design.

Figure 4.4 shows a snapshot of the mechanical response of a disk resonator vibrating in the first radial-contour mode simulated in CoventorWare to verify the analytical results for the structure.

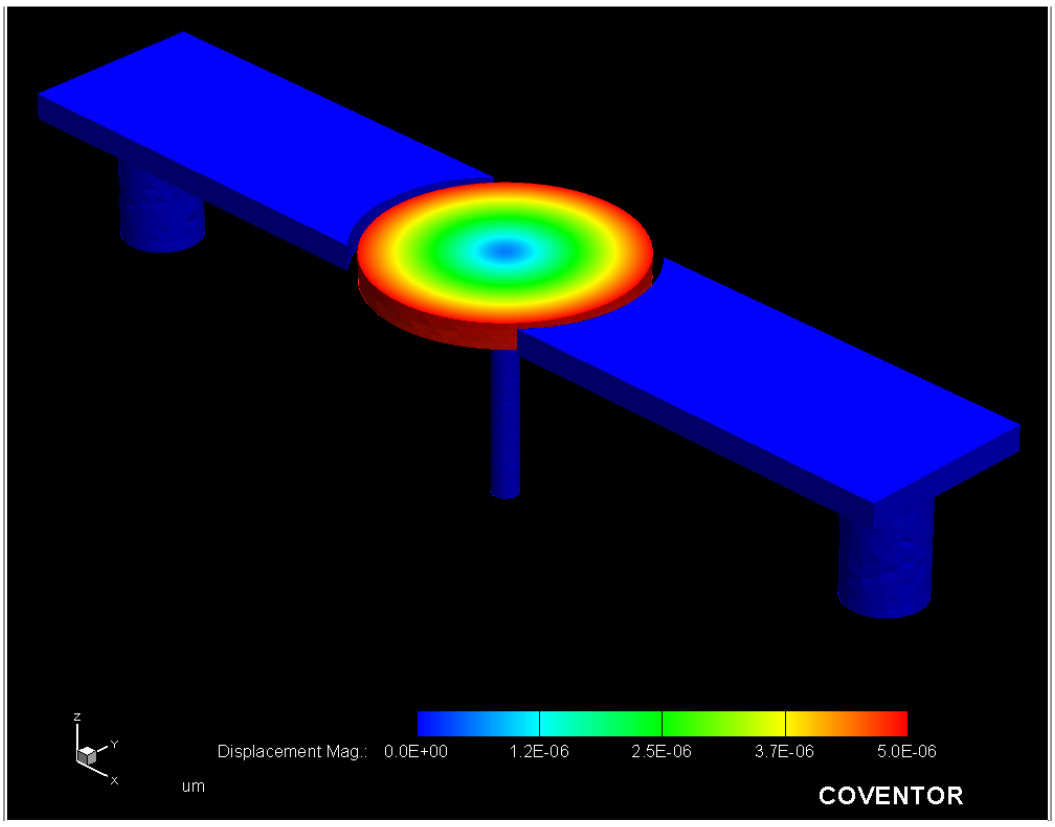

Figure 4.4: Fundamental radial-contour modal shape of the disk

Normally for finding mechanical harmonic resonant frequency designer and analyzer is used. To get the above result first force in x-direction find out through simulation. Force acting area is calculated through MATLAB coding. then the pressure is found out to be 0.000181MPa. The structural response of the disk resonator determined by applying a harmonic excitation, with a 0.000181MPa load applied to the side-surface of the disk and the frequency is swept from. 260-300MHz. The peak in the frequency response corresponds to the desirable frequency of the contour mode. The fundamental radial-contour mode resonance frequency obtained from modal analysis for this disk is 274.5382MHz.

4.2.1 S-parameter simulation

Figure 4.5 illustrates architect circuit simulation setup and the frequency response. The resonator is biased with $V_P = 5V$. Input electrode is driven with AC voltage of $1V$ peak-to-peak, and output voltage measured across the load resister.

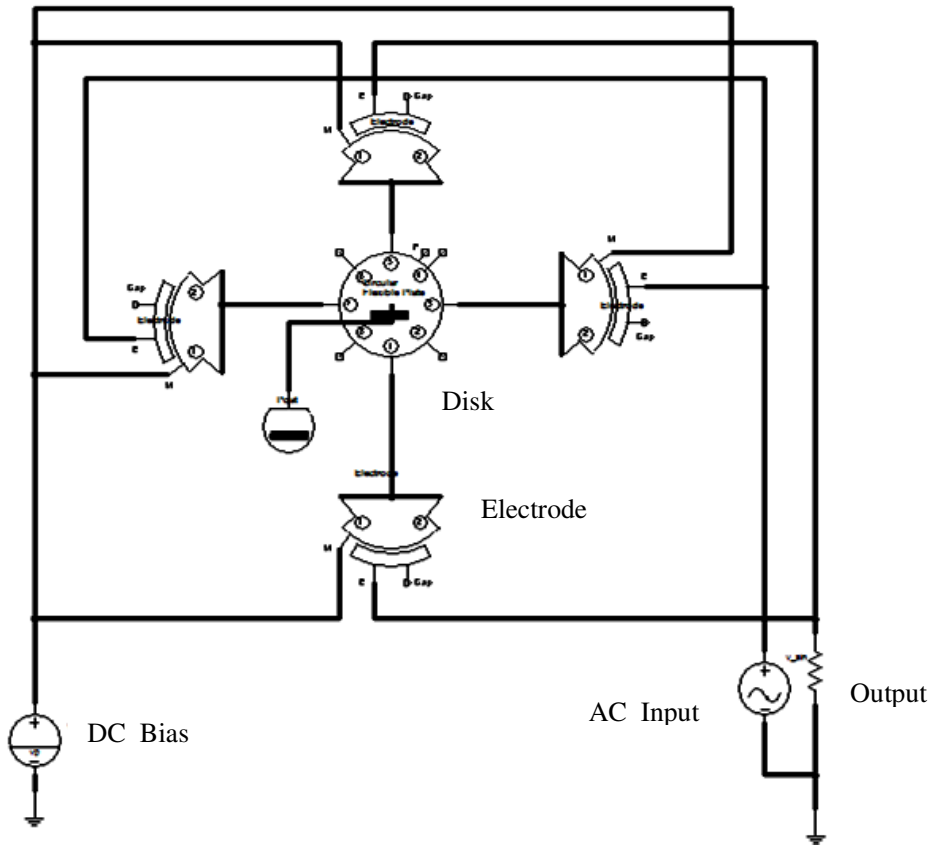

Figure 4.5: S-parameter simulation circuit setup

The frequency response plot of the disk resonator shown below Figure 4.6. The peak value insertion loss 185.38 dB. at f_o = 277.07MHz

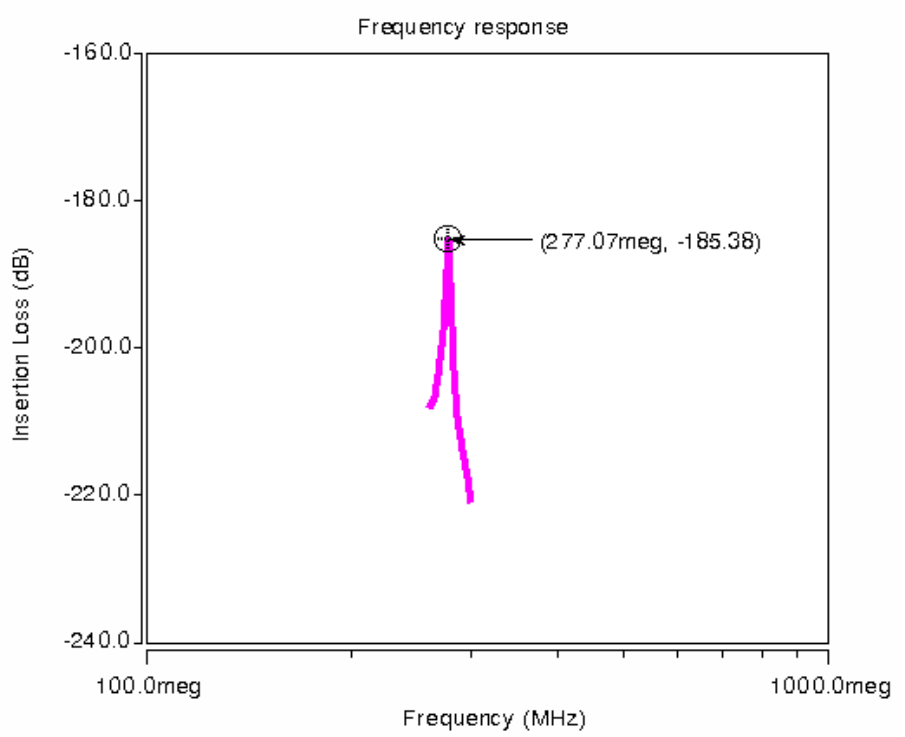

Figure 4.6: Frequency response of the disk

4.2.2 *Q* factor simulation

When determining the quality factor of a micromechanical resonator or filter, several energy dissipation mechanisms must be taken into account including air damping, material related losses, thermo elastic damping, and anchor losses. The overall resonator *Q* can be found as the sum of the inverses of the individual *Q*'s associated with all the contributing loss mechanisms

$$\frac{1}{Q_{total}} = \frac{1}{Q_{air}} + \frac{1}{Q_{material+thermal}} + \frac{1}{Q_{anchor}} \tag{4.11}$$

In eq.(4.11) $1/Q_{material+thermal}$ is attributed to intrinsic losses in the material and the thermoelastic dissipation, $1/Q_{anchor}$ represents energy loss through the anchor, $1/Q_{air}$ is the air damping depicts the loss of energy contained in a resonating structure to the surrounding atmospheric environment. $1/Q_{air}$ is not on issue at vacuum, nor for high

frequency resonators in air. $1/Q_{material+thermal}$ is also not dominant. so both $1/Q_{anchor}$ and $1/Q_{material+thermal}$ values are find out from simulation.

Disk design parameter is already given in Table 4.3. For this simulation we use the centre supported disk, the electrode around it, and the substrate to which they are anchored. energy "leaks" from the resonating disk into the substrate through the anchors at the centre of the disk. The quiet-boundary BC applies special elements that are essentially distributed dampers with properties defined to eliminate the reflection of the elastic wave impinging on the boundary. Energy that is lost to the substrate is lost forever. This loss mechanism is known as anchor loss or anchor damping.

The direct harmonic solver is used to find the harmonic response of the device to a sinusoidal load applied to the disk [20]. This is done to mimic the effect of an AC signal disturbing the disk at a certain frequency. For harmonic analysis settings for various boundary condition is given in Figure 4.7 and Figure 4.8 respectively.

For linkage BCs master slave concept is used (see Figure 4.7). The quiet boundary BCs are again applied in the surface BCs dialog, and the load patch BC with the value of the previously calculated electrostatic pressure is applied in the harmonic surface BC dialog (see Figure 4.8).

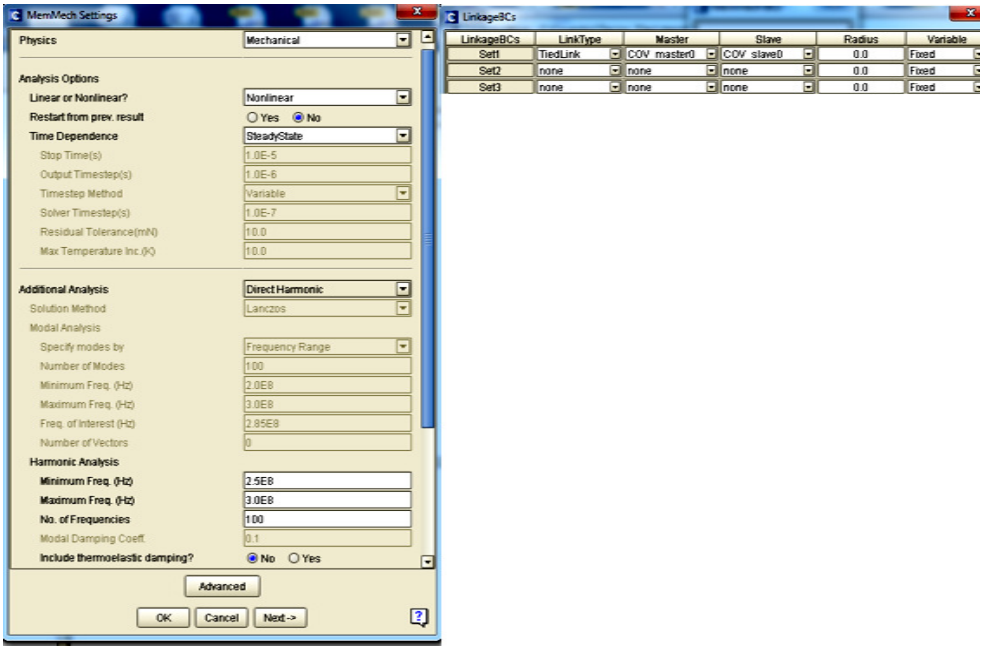

Figure 4.7: Linkage BCs setup

SurfaceBCs

SurfaceBCs	FixType	Patch1	and1	Patch2	and2	Patch3	LoadValue		Variable	Transi
Set1	none	bottom	and	none	and	none	Scalar	0.0	Fixed	Fixed
Set2	LoadPatch	force	and	none	and	none	Scalar	0.000...	Fixed	Fixed
Set3	QuietBoundary	back	or	front	and	none	Vector	Edit	Fixed	Fixed
Set4	QuietBoundary	left	or	right	and	none	Vector	Edit	Fixed	Fixed
Set5	QuietBoundary	bottom	and	none	and	none	Vector	Edit	Fixed	Fixed
Set6	none	none	and	none	and	none	Scalar	0.0	Fixed	Fixed
Set7	none	none	and	none	and	none	Scalar	0.0	Fixed	Fixed
Set8	none	none	and	none	and	none	Scalar	0.0	Fixed	Fixed

Figure 4.8: Surface BCs setup

For this simulation, note that to find the resonant mode frequency, load the simulation results in the visualizer, and cycle through the mode shapes until you see the step in which the distortion is only in the disk as shown in Figure 4.9.

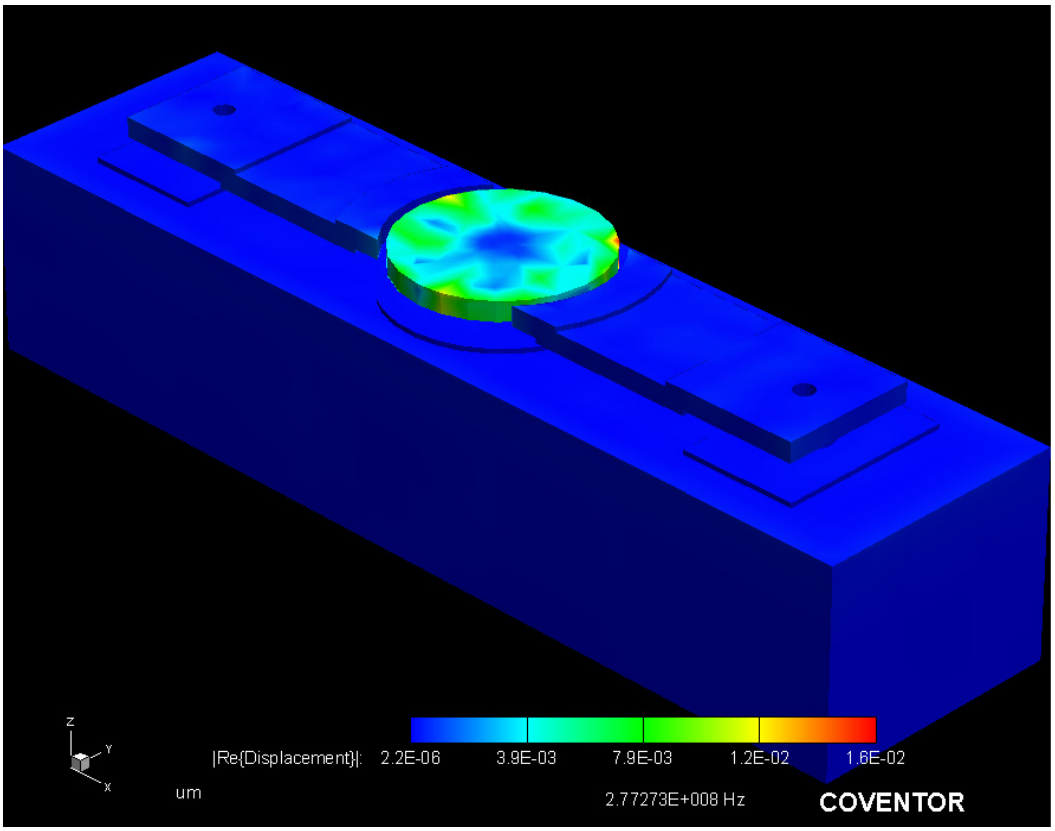

Figure 4.9: Resonant frequency mode

From the simulation anchor loss is found out. The value of $1/Q_{anchor}$ is = 5.21459E-02. Total loss not only depend on anchor loss but also material and thermo elastic losses. This thermo elastic damping occurs in vibrating solids. The oscillatory strain field has recoverable elastic energy associated with it, but there is also an irreversible conversion of elastic energy to thermal energy. The strain field induces local

temperatures proportional to the strain. The temperature gradients induce heat conduction, so that over the vibratory cycle the local thermal energy is no longer available and is lost. This process damps the motion.

For performing TED simulation the disk with an electrode model without the substrate is used in this simulation. From the simulation, material and thermo elastic losses is found out. The value of $1/Q_{material+thermal}$ =1.995819E-05 by using eq.(4.11) total value of Q found out to be 50124.

From Ashby approach it is clear that Ni followed by poly $Si_{0.35}Ge_{0.65}$ and $Zr_{44}Ti_{11}Cu_{10}Ni_{10}Be_{25}$ are the most suitable materials to be used as disk materials for MEMS resonators. So the quality factor for Ni followed by poly $Si_{0.35}Ge_{0.65}$ is simulated through CoventorWare. The results are given in the below Table 4.4.

Table 4.4: Energy losses in disk resonator

Material	**Resonant frequency**	$1/Q_{anchor}$	$1/Q_{(material+thermal)}$	Q_{total}
Nickel (Ni)	1.70303E08	3.003712E-02	8.869593E-06	112778.037
poly$Si_{0.35}Ge_{0.65}$	1.636364E0	3.078724E-02	4.02992E-07	2481470

4.3 Conclusion

Material selection for high Q disk MEMS resonator, using Ashby approach has been discussed in this chapter. In this work we have developed the performance and material indices for high Q disk MEMS resonator. Using the material selection chart, it was observed that for high Q, high resonant frequency and CMOS compatible process temperature, poly$Si_{0.35}Ge_{0.65}$ are the most suitable disk material.

From Table 4.4., it is confirmed that poly$Si_{0.35}Ge_{0.65}$ is the best material for MEMS disk resonator because of high Q compared to the Nickel (Ni). Ashby approach results are validated with simulation both are showing poly$Si_{0.35}Ge_{0.65}$ is the best material for the MEMS disk resonator.

References:

[1] C. T. Nguyen, "MEMS technology for timing and frequency control.," *IEEE Trans. Ultrason. Ferroelectr. Freq. Control*, vol. 54, no. 2, pp. 251–270, 2007.

[2] J. Basu, S. Chakraborty, and T. K. Bhattacharyya, "Micromechanical radial-contour mode disk resonator for a CMOS-MEMS oscillator," *Proc. 2010 Annu. IEEE India Conf. Green Energy, Comput. Commun. INDICON 2010*, pp. 5–8, 2010.

[3] Ashish K.Sharma and Navneet Gupta, "Material Selection of RF-MEMS Switch used for reconfigurable antenna using Ashby's methodology," *Prog. Electromagn. Res. Lett.*, vol. 31, pp. 147–157, 2012.

[4] M. F. Ashby, *Materials Selection in Mechanical Design*, Third Edition. ELSEVIER, Butterworth-Heinemann, 2005.

[5] S.D.Senturia, *Microsystem design*, vol. 1. Norwell (MA): Kluwer Academic Publishers, 2001.

[6] S. Spearing, "Materials issues in microelectromechanical systems (MEMS)," *Acta Mater.*, vol. 48, no. 1, pp. 179–196, 2000.

[7] L. Y. Chen, Z. L. Zhang, J. J. Yao, D. C. Thomas, and N. C. Macdonald, "Selective chemical vapor deposition of tungsten for micro electromechanical structures," *Sensors and Actuators,* vol. 20, no. 1–2, pp. 123–133.

[8] S. Sedky, "SiGe: An attractive material for post-CMOS processing of MEMS," *Microelectron. Eng.*, vol. 84, no. 11, pp. 2491–2500, 2007.

[9] V. T. Srikar and S. M. Spearing, "Materials selection in micromechanical design: An application of the Ashby approach," *J. Microelectromechanical Syst.*, vol. 12, no. 1, pp. 3–10, 2003.

[10] S. N. R. Kazmi, C. Salm, and J. Schmitz, "Materials selection for Low Temperature Processed High Q Resonators using Ashby,"*12 th Annual Workshop on semiconductor Advances for Future Electronics and Sensors*, 26-27 November, Veldhoven, The Netherlands, pp. 81–84.

[11] M. Gad-el-Hak, *The MEMS Handbook MEMS applications,* Taylor & Francis, Boca Raton ,FL, 2006.

[12] N. M. S. Wei Gao, *An Introduction to Electronic and Ionic Materials*, 7th ed, River Edge,New Jersey: World Scientific, 1999.

[13] J. Schroers, T. Nguyen, S. O'Keeffe, and A. Desai, "Thermoplastic forming of bulk metallic glass-Applications for MEMS and microstructure fabrication," *Mater. Sci. Eng. A*, vol. 449–451, no. 2, pp. 898–902, 2007.

[14] O. Parate and Navneet Gupta, "Material selection for electrostatic microactuators using Ashby approach," *Mater. Des.*, vol. 32, no. 3, pp. 1577–1581, 2011.

[15] F. A. Zhili Hao, "Support loss in micromechanical disk resonators," in *18th IEEE International Conference on Micro Electro Mechanical Systems*, 30 Jan - 03 Feb, FL, USA, pp. 137–141,2005.

[16] Y. W. Lin, S. Lee, S. S. Li, Y. Xie, Z. Ren, and C. T. C. Nguyen, "Series-resonant VHF micromechanical resonator reference oscillators," *IEEE J. Solid-State Circuits*, vol. 39, no. 12, pp. 2477–2491, 2004.

[17] J. Wang, J. E. Butler, D. S. Y. Hsu, and C. T. Nguyen, "High-Q Micromechanical Resonators in Ch_4 Reactant Optimized High Acoustic Velocity CVD Polydiamond,"*Solid-State Sensors, Actuator and Microsystems Workshop*, 02-07 June, Hilton Head, pp. 61–62,2002.

[18] E.P.Quevy, A .San Paulo, E .Basol, R.T.Howe, T.J. King, J.Bokor ,"Back-End-Of-Line Poly-Sige Disk Resonators,"*19th IEEE International Conference on Micro Electro Mechanical Systems*, 22-26 Jan,Istanbul,Turkey, pp. 234–23,2006.

[19] J. Carter, A. Cowen, B. Hardy, R. Mahadevan, M. Stonefield, and S. Wilcenski, *PolyMUMPs Design Handbook*. MEMSCAP Inc.

[20] Application Notes Physical and System-Level Design CoventorWare, 2012.

Chapter - 5

Novel V-shaped Coupled Beam MEMS Lame Filter

In this chapter, V-shaped coupled beam low pass band ripple Lame filter is designed. Important filter parameters such as insertion loss, shape factor and *Q* factor are find out based on simulation. This filter gives better pass band ripple compare to normal straight beam coupling lame filter. V-shaped coupled beam Lame filter provides 22dB reduction in bandpass ripple, also shape factor is improved from 2.498 to 1.990. V-shaped coupled beam provides 3 dB bandwidth of 0.901 MHz near to the design value 1 MHz.

5.1 Introduction

Filter is a key component in the transceiver system, which are often utilized for frequency selection in the radio-frequency (RF) and intermediate-frequency (IF) stages [1] .With the recent advancements in micro electromechanical system (MEMS) based IC processes targeted at RF designs, MEMS filters and oscillators have emerged as viable candidates having the capability of signal processing applications, where a very high Q is essential [2].

Micro electromechanical (MEMS) narrow pass band filters are the prime candidates for being used as frequency selection components due to their ability to select narrow band at MHz frequencies. This chapter presents three micromechanical lame resonators vibrating in the lame mode [3] and mechanically coupled using two extensional mode beams have been used to implement a third-order series resonator-based filter; with capacitive transducers used to interface this filter with electrical circuitry. This coupled system produces three mechanical resonance modes at closely spaced frequencies. Hence, the frequency response peaks due to these modes overlap producing the pass band characteristic of a BPF. The center frequency is set by the resonant frequency of the constituent resonators, while the bandwidth is determined by the stiffness and location of attachment of the beams[4]. Reports on this particular filter topology are not much common in present literature in comparison to filters based on other resonator geometries like beams or contour mode disks [5-7].

In filter design important issue is pass band ripple. Moreover V-shaped coupling beam Lame filters provide less pass band ripple. This chapter is organized as follows; introduction about filter and its performance parameters explained briefly in Section 1. Section 2 explains the design of various coupling beam for coupled Lame filter. Section 3 explains the design of Lame filter. Section 4 explains about mechanical mode simulation. Section 5 explains about S-parameter simulation. Section 6 gives the discussion about the result of the reported work.

5.1.1 Filter theory

An electric filter is a network that transforms an input signal in some specific way to yield a desired output signal. The signal may be considered in the time or frequency domain. A filter is often a frequency-selective device which passes signals of certain frequencies and blocks or attenuates signals of other frequencies.

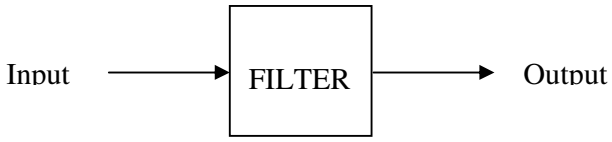

Figure 5.1: Symbolic representation of a filter

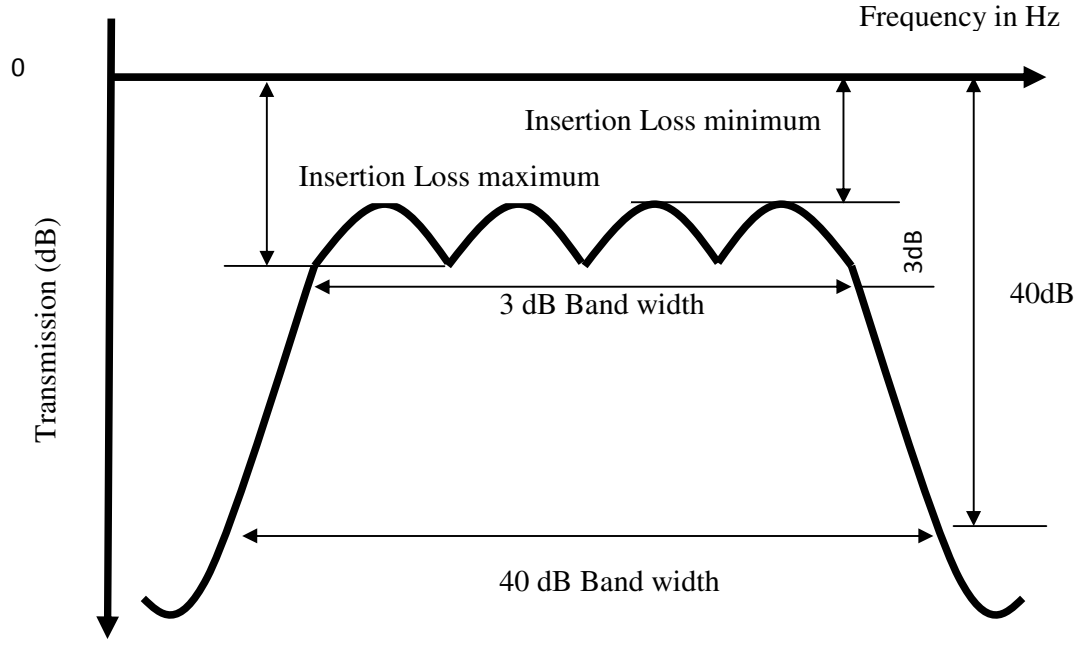

Figure 5.2: Parameters typically used for filter specification[6]

Figure 5.2 shows the frequency response of an ideal Bandpass filter. The deference between the two frequencies corresponding to 3 dB attenuation is the 3 dB bandwidth. The region outside the 40 dB points is the stop band. The deference between the two frequencies corresponding to 40 dB attenuation is the 40 dB bandwidth. A bandpass is a frequency band in which the attenuation of the filter transmission characteristic is small, where as in stop band the opposite is true. where 40 dB shape factor is the ratio between 40 dB bandwidth to3 dB band width.

5.2 Design of coupling beam

Since, a single resonator ideally has an infinite *Q* hence zero bandwidth, thus, two or more resonators should be coupled together to achieve the desired filter bandwidth as shown in Figure 5.3.

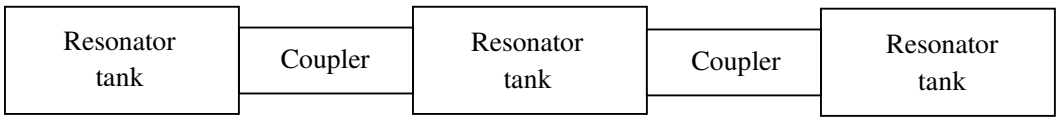

Figure 5.3: MEMS filter block diagram based on resonator

A. Extensional-mode coupling beams

The design of various type of coupling beam plays a vital role. In this thesis a lame mode plate act as resonator tank. It vibrates in the lateral direction, so the required coupler modes should be extensional in type. Figure 5.4 shows transmission line model of a coupling beam.

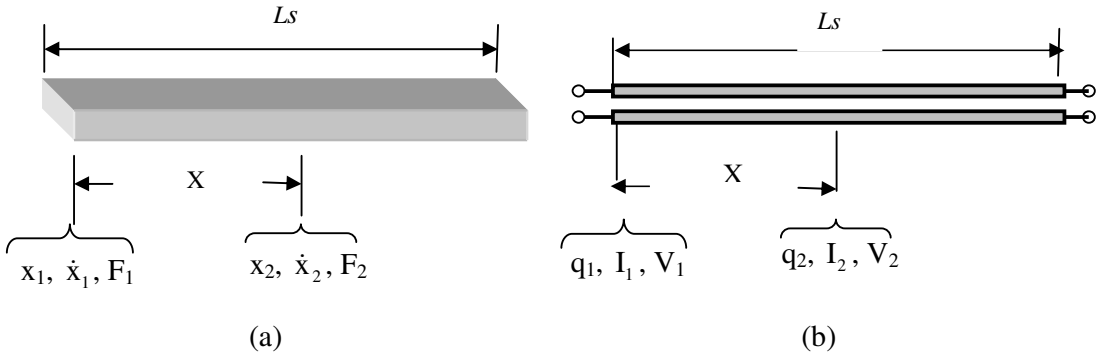

Figure 5.4: Transmission line models: (a) mechanical and (b) electrical

$$Z_0 = \frac{1}{A_c\sqrt{\rho E}}, \beta = \frac{\omega}{v_p}, v_p = \sqrt{\frac{E}{\rho}} \tag{5.1}$$

where L_s is length of the coupling beam, Z_0 is acoustic impedance, E Young's Modulus. To find the electrical equivalent of coupled beam ,following steps are used.

1) Write the transmission matrix(or) ABCD matrix expression for the coupled beam.

$$\begin{pmatrix} F_1 \\ \dot{x}_1 \end{pmatrix} = \begin{pmatrix} \cos\beta x & jZ_0 \sin\beta x \\ jZ_0 \sin\beta x / Z_0 & \cos\beta x \end{pmatrix} \begin{pmatrix} F_2 \\ \dot{x}_2 \end{pmatrix}$$

where, F and x denote force and displacement respectively.

2) Now, Z-parameters can be calculated from the ABCD- parameters, which can again yield the components of the T-network (Figure 5.5) as given in eq.(5.2)

$$Z_a = Z_b = \frac{A\text{-}1}{C} = -jZ_0 \frac{cos\beta L_s - 1}{sin\beta L_s} \tag{5.2}$$

$$Z_c = \frac{1}{C} = -jZ_0 \frac{1}{sin\beta L_s} \tag{5.3}$$

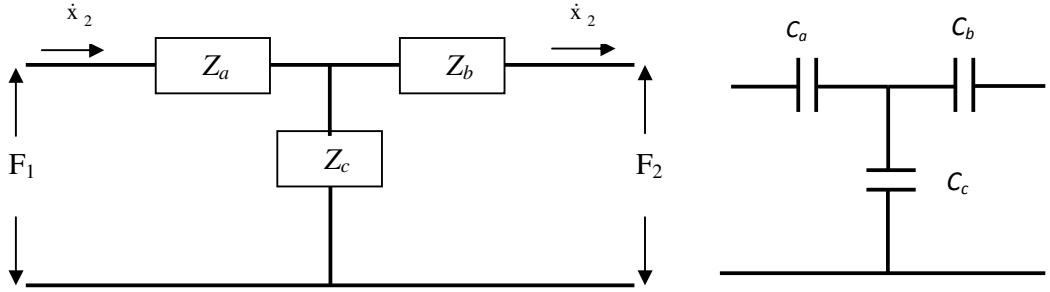

Figure 5.5: (a) General coupling beam model and (b) coupling wire equivalent

3) Condition $\beta L_s = \frac{\pi}{2}$, is applied to ABCD matrix, choose the condition such that the coupling becomes insensitive to changes in the wire-length. Thus, for a one-quarter wavelength long coupling beam, the matrix becomes:

$$\begin{pmatrix} A & B \\ C & D \end{pmatrix} = \begin{pmatrix} 0 & jZ_0 \\ j/Z_0 & 0 \end{pmatrix} = \begin{pmatrix} 0 & \frac{jK}{\omega} \\ \frac{j\omega}{K} & 0 \end{pmatrix} \tag{5.4}$$

4) Now in this modified ABCD matrix Z_0 replaced with K/ω ,where, K is a constant defined as ($K = \pi A_c E/2L_s$), A_c is coupling beam cross section.

The coupler length

$$L_s = \frac{\pi}{2\beta} = \frac{\pi}{2}\frac{1}{2\pi f_0}\sqrt{\frac{E}{\rho}} = \frac{1}{4f_0}\sqrt{\frac{E}{\rho}} \tag{5.5}$$

The bandwidth of the resulting filter is defined by the stiffness of the coupling beam and the resonator's stiffness.

Again, coupler-width depends on the desired coupling beam stiffness which controls the bandwidth B of the filter. The required coupling beam stiffness can be derived using [8].

$$B = \left(\frac{f_0}{k_{ij}}\right)\left(\frac{K_{sij}}{\sqrt{k_{ri}k_{rj}}}\right), \qquad K_{sij} = k_{ij}\left(\frac{B}{f_0}\right)\sqrt{k_{ri}k_{rj}} \tag{5.6}$$

where f_0 is the center frequency of the filter, k_{ri} and k_{rj} are the resonator equivalent stiffness at the coupling location, and K_{sij} is the required spring constant of the coupling beam between i^{th} and j^{th} resonators. Also, k_{ij} is the normalized coupling coefficient between two consecutive resonators (given in Table 5.1 where q denotes the normalized resonator quality factor). Using the impedance and the material properties, the width of the coupling beam can be calculated using:

$$K_{sij} = \frac{\pi A_c E}{2L_s} = \frac{\pi WtE}{2L_s}, \quad W = \frac{K_{sij}2L_s}{\pi tE} \tag{5.7}$$

From the required beam stiffness, the shunt-arm impedance found from eq.(5.3) is:

$$Z_c = \frac{1}{C} = -jZ_0 = -\frac{jK_{sij}}{\omega} = \frac{K_{sij}}{j\omega} \tag{5.8}$$

$$Z_c = \frac{1}{j\omega C_c} = \frac{K_{sij}}{j\omega}, \quad C_c = \frac{1}{K_{sij}} \tag{5.9}$$

B. ***V- shaped extensional-mode coupling beams***

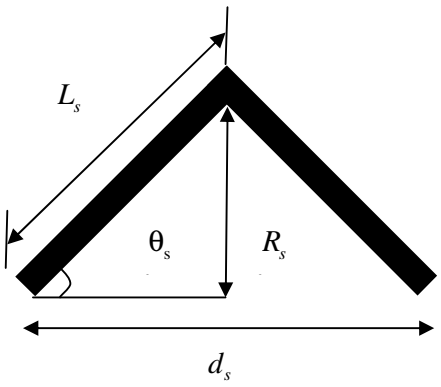

Figure 5.6: V-shaped coupling beam with less than λ/8 length

Assuming known distances $d_s = L/4$, From figure 5.6 the coupling beam length L_s. and height R_s is given by

$$L_s = \frac{d_s}{2\cos\theta_s}, R_s = L_s \sin\theta_s \tag{5.10}$$

T network equivalent of a coupling beam with less than λ/8 length shown in Figure 5.7.

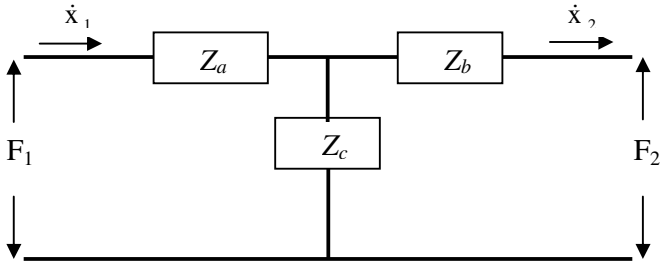

(a)

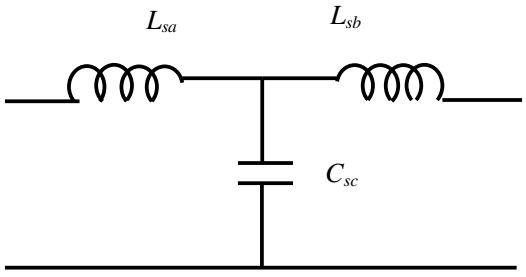

(b)

Figure 5.7: T-network equivalent of a V-shaped coupling beam with less than λ/8 length

Sub λ/8 designs are of interest because they lend easily to lumped models[9]. In this case, eq.(5.2) and eq.(5.3) reduce to

$$Z_a=Z_b=\frac{A\text{-}1}{C}=j\omega Ls_a=j\omega Ls_b=j\omega\left(\frac{M_{static}}{2}\right) \tag{5.11}$$

$$Z_c=\frac{1}{C}=\frac{1}{j\omega Cs_c}=\frac{K_{sc}}{j\omega} \tag{5.12}$$

$$M_{static}=2\rho A_c L_s, K_{sc}=12\frac{EI_s}{L_s^3} \tag{5.13}$$

where M_{static} is the static mass and K_{sc} is the lumped stiffness of the coupling element.

The bandwidth of the resulting filter is defined by the stiffness of the coupling beam and the resonator's stiffness. The coupled vibrating plates exhibit two resonance frequencies as in-phase and out-of-phase vibrating modes. These in-phase and out-of-phase vibrating modes spacing define the filter bandwidth (BW). Where f_o is the center frequency of the filter, also the resonance frequency of each resonator,

$$B=\left(\frac{f_0}{k_{ij}}\right)\left(\frac{K_{sc}}{k_r(c)}\right), \qquad K_{sc}=k_{ij}\left(\frac{B}{f_0}\right)k_r(c) \tag{5.14}$$

where $K_r(c)$ is the resonator stiffness at location c. c varies from 0 to L. k_{ij} is the normalized coupling coefficient between two consecutive resonators (given in Table 5.1 where q denotes the normalized resonator quality factor). Using the impedance and the material properties, the width of the coupling beam can be calculated using:

$$K_{sc}=12\frac{EI_s}{L_s^3}, \qquad I_s=\frac{Wt^3}{12}, \qquad W=\frac{K_{sc}L_s^3}{Et^3} \tag{5.15}$$

where I_s is moment of inertia. From the required beam stiffness, the shunt-arm impedance found considering that for an inductor $Z_L = j\omega L$ and for a capacitor $Z_c = 1/j\omega C$, the mass and stiffness in the form of inductor and capacitor are

$$Ls_a=Ls_b=\left(\frac{M_{static}}{2}\right)=\rho A_c L_s, \qquad Cs_c=\frac{L_s^3}{12EI_s} \tag{5.15}$$

5.3 Filter design

Three identical resonators physically connected by two mechanical couplers constitute a third order BPF, From the theory of vibrations, the number of resonance modes of a mechanical system is equal to the number of coupled resonators [10-12]. Third-order

Chebyshev filter topology has been chosen to approximate the desired frequency characteristics, due to its sharper roll-off than the Butterworth or Bessel's filters; and better phase response and lower component count than inverse Chebyshev or elliptic filters. Parameters of the BPF structure for achieving a center frequency of 12.9 MHz and bandwidth of 1 MHz are given in Table 5.1 and Table 5.2.

Table 5.1: Normalized coupler coefficients (*K-q*) for Chebyshev response with 0.1 dB Ripple (for 3 dB bandwidth) [12]

Order *N*	**Normalized quality factor q_1, q_N**	**Coupler coefficient k_{12}**	**Coupler coefficient k_{23}**	**Coupler coefficient k_{34}**
2	1.6382	0.711	-	-
3	1.4328	0.665	0.665	-
4	1.3451	0.690	0.542	0.690

The resonator is designed to operate in lame mode, in which the edges of square beam bend in anti-phase while the volume of the beam is unchanged. The vibration frequencies, modal shapes, bandwidth for the BPF has been verified using simulations in CoventorWare finite-element software [13]. These resonators were using SOIMUMPs process from MEMSCAP for design.

Table 5.2: Parameters of the MEMS bandpass filter

Parameters of the filter	**Straight beam (a)**	**V-shaped beam (b)**
Length of lame resonator Plate *L* (μm)	320	320
Beam *W* (μm)	24	24
Length of coupling beam L_s (μm)	160	31
Thickness of the coupling beam *t* (μm)	25	25
Gap between electrode and plate *d* (μm)	2	2
Resonator spring constant (k_r)	1.8552e+07	1.8552e+07

Case a: Figure 5.8 shows the layout of Lame filter with straight coupling beam of length λ/4 here wave length calculated from acoustic velocity.

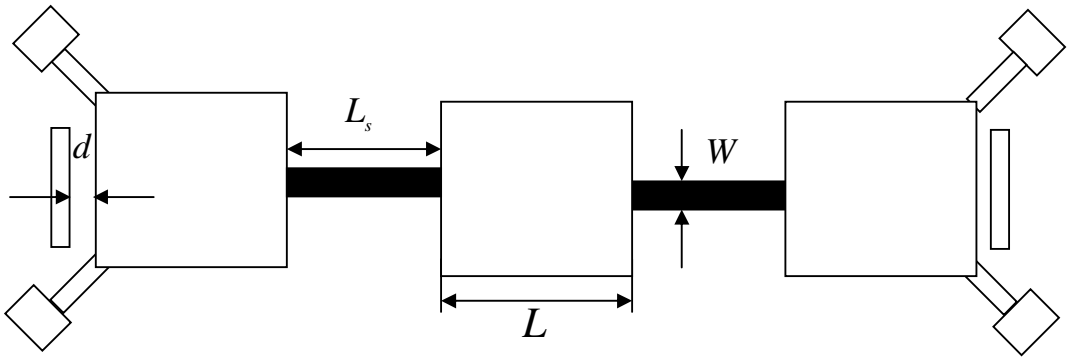

Figure 5.8: Lame filter straight coupling beam with λ/4 length

Case b: Figure 5.9 shows the layout of Lame filter with V-shaped coupled beam of length less than λ/8 is used.

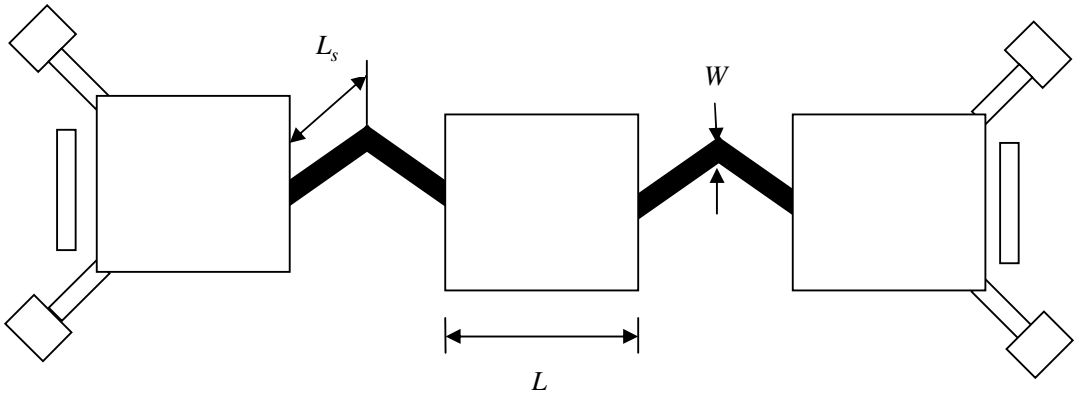

Figure 5.9: Lame filter V-shaped coupling beam with less than λ/8 length

5.4 Filter simulation

Lamer resonator design parameter is already given in Table 5.2. For this simulation we use Lame resonator that is anchored in four corner as shown in Figure5.8, the electrode are placed side by side, and the substrate to which they are anchored. Normally for finding mechanical harmonic and model resonant frequency designer and analyzer is used. The vibration frequencies, modal shapes, bandwidth etc. for the BPF has been verified using simulations in CoventorWare Finite Element software. The modal simulation results given in Figure 5.10 reveal that the predicted mode shapes can indeed be obtained for the filter geometry. The corresponding resonance frequency values are also provided.

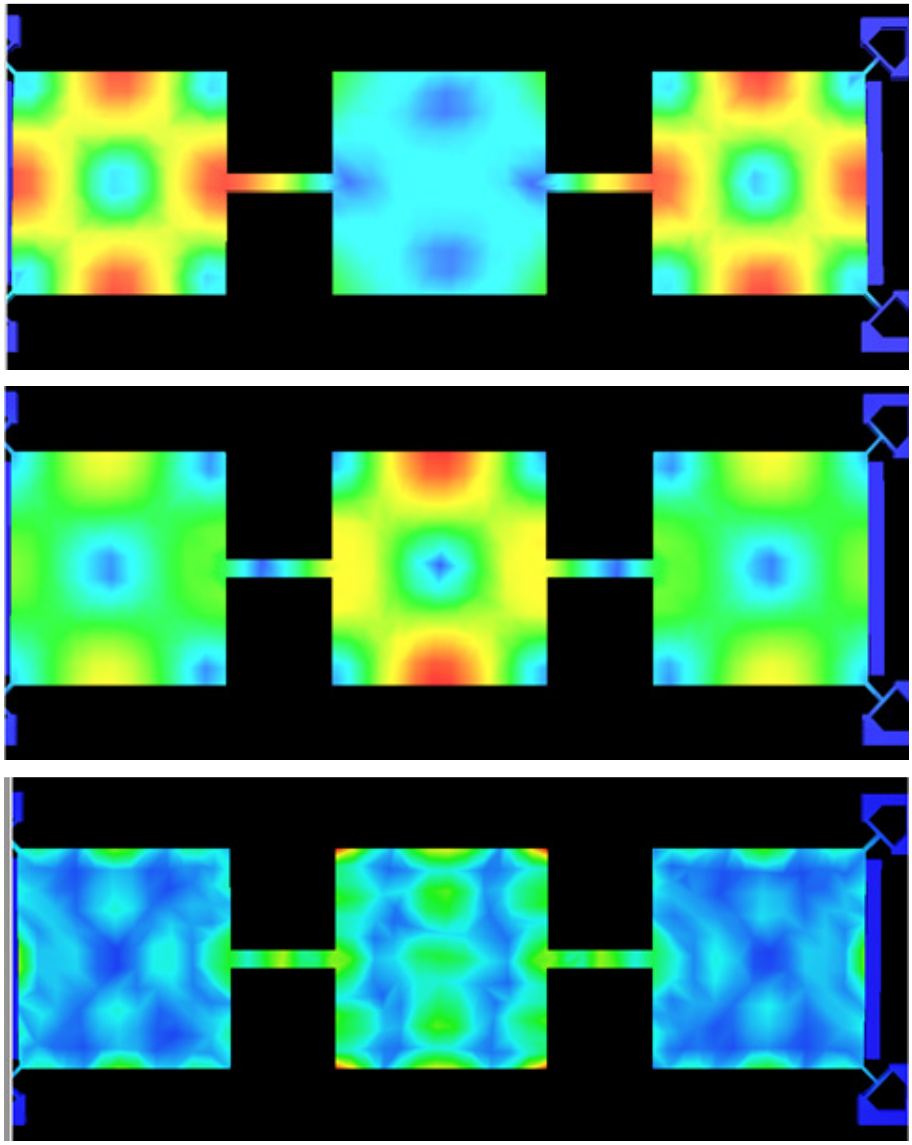

Figure 5.10: Lame mode shapes of the triple plate system with straight beam obtained using modal simulations: (a) 1st mode, (b) 2nd mode and (c) 3rd mode

Normally for finding mechanical harmonic resonant frequency Designer and analyzer is used. To get the above result first force in x-direction find out through simulation. Force acting area is calculated through MATLAB coding. then the pressure is found out to be 0.000001128MPa. The structural response of the plate resonator determined by applying a harmonic excitation, with a 0.000001128MPa load applied to the side-surface of the disk and the frequency is swept from. 10 MHz -13 MHz. The peak in the frequency response corresponds to the centre frequency of the lame mode filter.

Harmonic response has been found (Figure 5.11) by subjecting the lateral surface of a single plate of the system to a harmonic force. The unterminated frequency response shows distinct resonance peaks at the closely situated lame mode vibration frequencies. This also verifies the bandwidth (1 MHz here) of the designed filter.

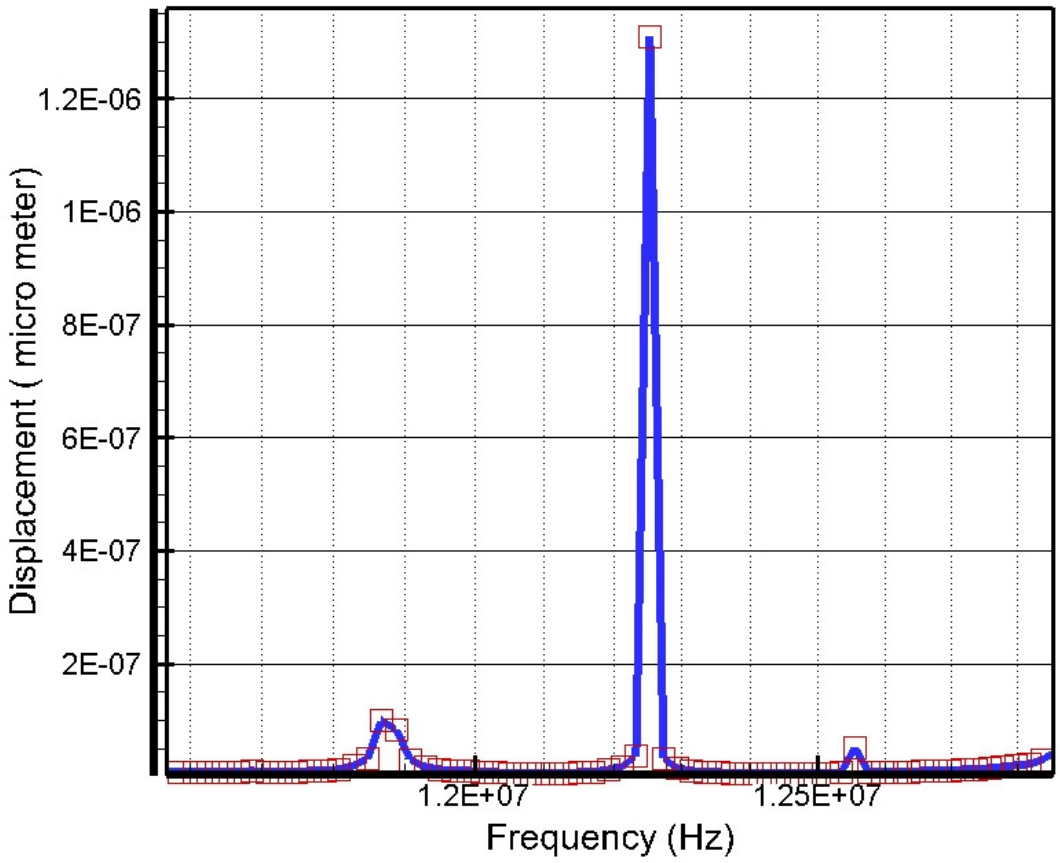

Figure 5.11: Un-terminated harmonic responses of triple plate bandpass filter owing distinct peaks at the closely spaced lame vibration modes

The Lame mode resonance frequency obtained from modal analysis for this plate is 11.74748 MHz, 12.23232 MHz and 12.71717 MHz. from this result over all bandwidth found out to be 1 MHz .

The modal simulation results for V-shaped coupled beam filter is given in Figure 5.12. The corresponding resonance frequency values are also provided.

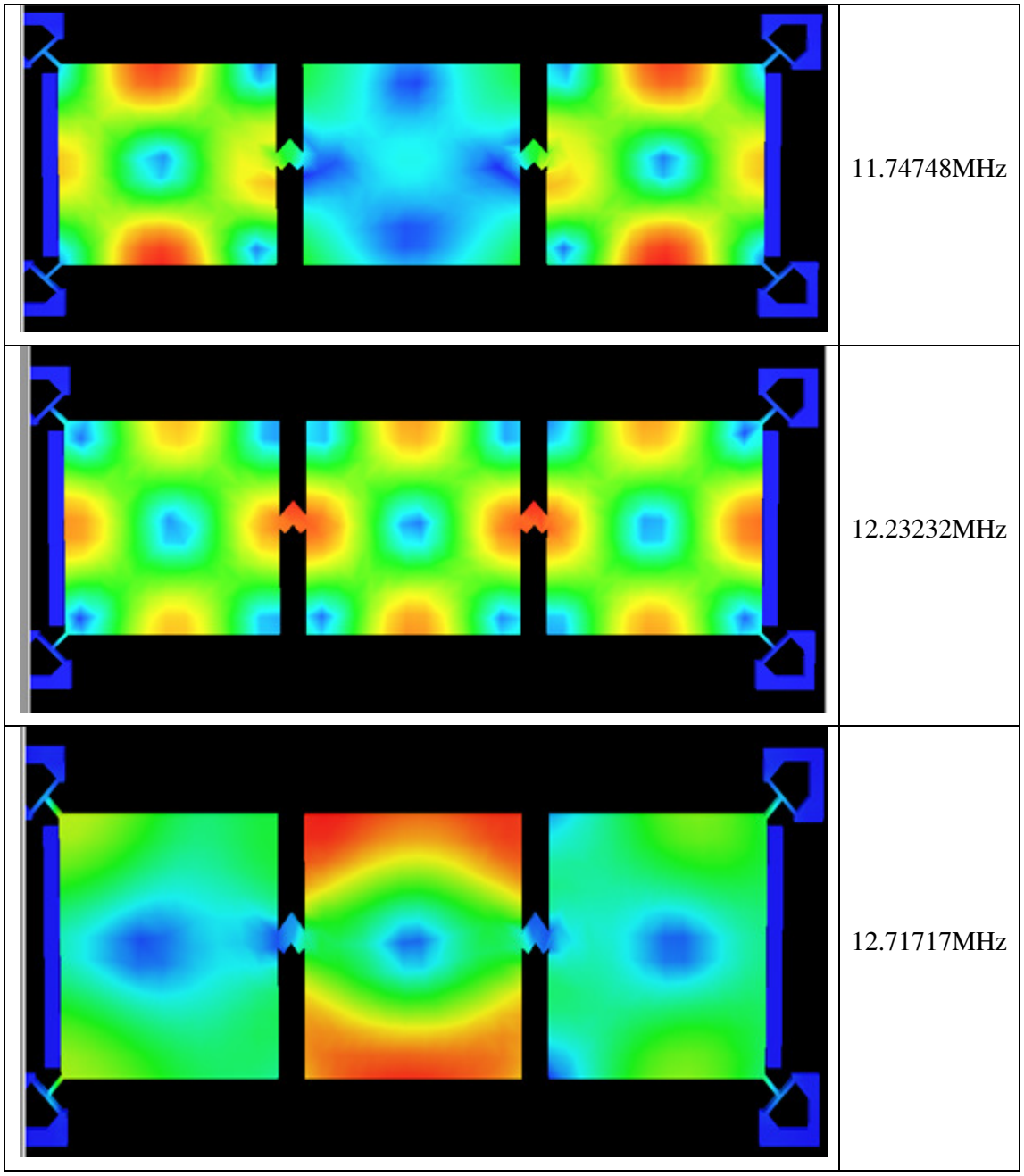

Figure 5.12: Lame mode shapes of the triple plate with V-shaped coupled beam system obtained using modal simulations: (a) 1st mode, (b) 2nd mode and (c) 3rd mode

Harmonic response has been found (Figure 5.13) by subjecting the lateral surface of a single plate of the system to a harmonic force.

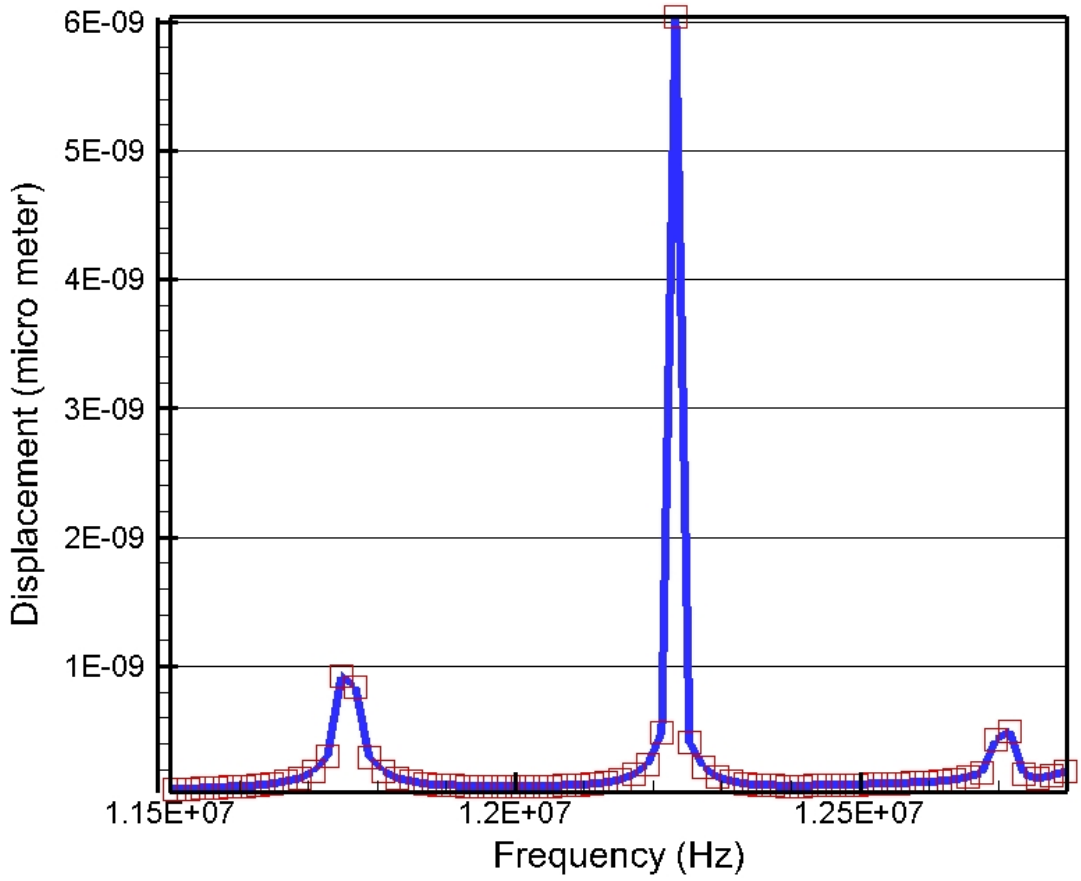

Figure 5.13: Un-terminated harmonic response of triple plate V-shaped coupled beam bandpass filter owing distinct peaks at the closely spaced lame vibration modes

The un-terminated frequency response shows distinct resonance peaks at the closely situated lame mode vibration frequencies. This also verifies the band width (1 MHz here) of the designed filter, but with less displacement compare to normal beam coupling case. This shows band pass ripple is reduced significantly.

5.5 S-parameter simulation

Figure 5.13 shows the circuit set up for S-parameter simulation. In this circuit design parameters such as length of the coupling beam, width of the coupling beam, and lame resonator length is given from Table 5.2. Pull in voltage is calculated from DC transfer sweep analysis. it comes around 900 V. To smooth the pass band and reduce the insertion loss, a termination resistance R_{port} is needed. The value of the termination resistance is given by [14].

$$R_{port}=R_x\left(\frac{Q_{res}}{q_i Q_{filter}}\text{-}1\right) \tag{5.17}$$

where R_x is resonator motional impedance. Q_{res} is the resonator unloaded quality factor. Q_{filter} is the filter unloaded quality factor these values are found out from simulation, and q_i is a normalized "q" value obtained from a filter design hand book. When determining the quality factor of a micromechanical resonator or filter, several energy dissipation mechanisms must be taken into account including air damping, material related losses, thermo elastic damping, and anchor losses. The overall resonator Q can be found as the sum of the inverses of the individual Q's associated with all the contributing loss mechanisms.

$$\frac{1}{Q_{total}}=\frac{1}{Q_{air}}+\frac{1}{Q_{material+thermal}}+\frac{1}{Q_{anchor}} \tag{5.18}$$

In eq.(5.18) $1/Q_{material+thermal}$ is attributed to intrinsic losses in the material [15] and the thermoelastic dissipation [16], $1/Q_{anchor}$ represents energy loss through the anchor[17], $1/Q_{air}$ is the air damping depicts the loss of energy contained in a resonating structure to the surrounding atmospheric environment. $1/Q_{air}$ is not on issue at vacuum, nor for high frequency resonators in air. $1/Q_{material+thermal}$ is also not dominant. so both $1/Q_{anchor}$ and $1/Q_{material+thermal}$ values are find out from simulation.

From eq.(5.17) calculated value of R_{port} is1.2375 MΩ and 2.2079 MΩ for normal coupling beam filter and V-shaped coupling beam filter respectively. The circuit set up for Lame filter straight coupling beam is given in Figure 5.14. Input ac voltage is taken a 130 milli volt.

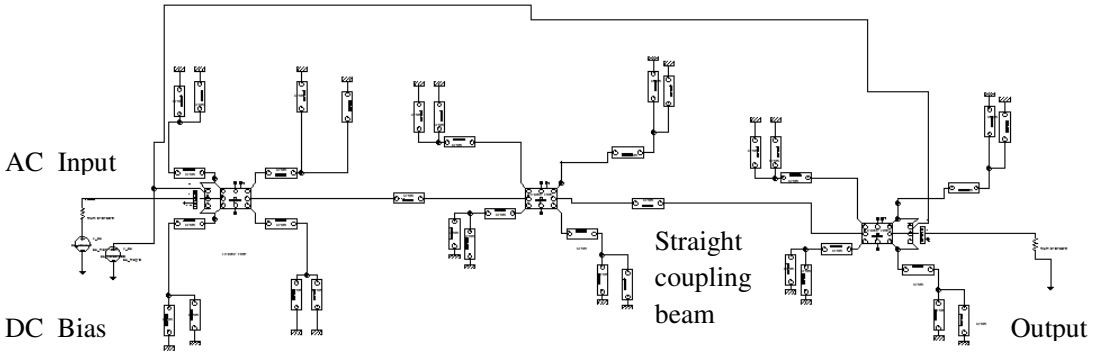

Figure 5.14: Circuit set up for Lame filter straight coupling beam with λ/4 length

The circuit set up for Lame filter V-shaped coupling beam with less than λ/8 length is given in Figure 5.15.for input ac voltage is taken as 130 milli volt also coupling beam shape, width and length are changed according to design given in Table 5.2.

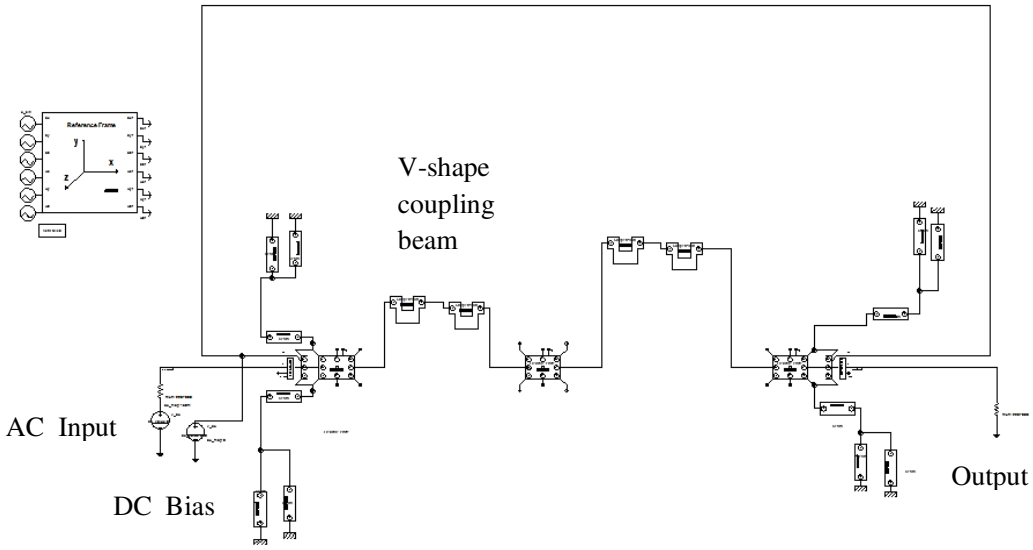

Figure 5.15: Circuit set up for Lame Filter V-shaped coupling beam with less than λ/8 length

From the Figure 5.16 all the filter parameter are observed and tabulated in Table 5.3 it is observed that lame filter with V-shaped coupling beam provides better pass band ripple compare to normal straight coupling beam filter.

Figure 5.16 shows the frequency response of both filter for unmatched condition.

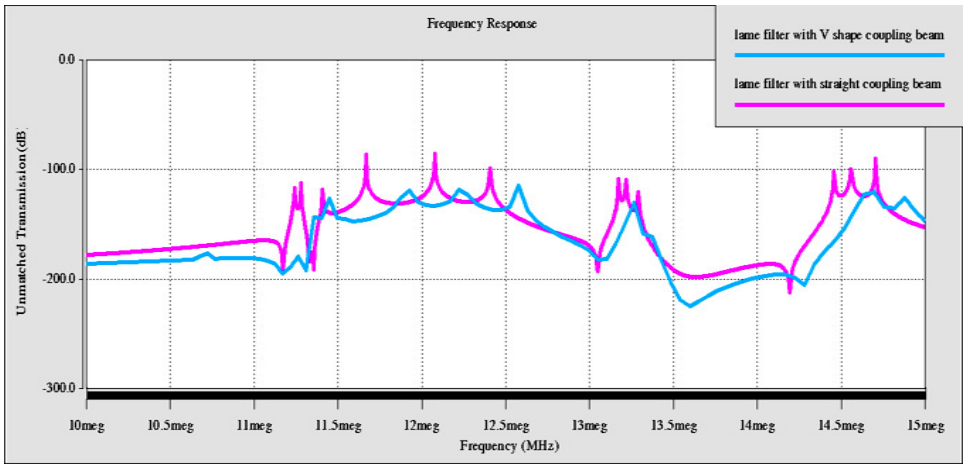

Figure 5.16: Frequency response of both normal Vs V-shaped coupling beam filters

Table 5.3: Performance parameters of the MEMS bandpass filter

Parameter	Lame filter with V-shaped coupling beam	Lame filter with straight coupling beam
Insertion loss minimum (dB)	116	85
Insertion loss maximum (dB)	138	131
Bandwidth (MHz)	12.652-11.751= 0.901	12.46-11.8=0.66
40dB shape factor = 40dB Bandwidth / 3dB bandwidth	1.793/0.901=1.990	1.649/0.66=2.498

5.6 Conclusion

This chapter detailed discussion about micromechanical Lame resonators and filters working principle and theory behind is given. The MEMS bandpass filter for a band width of 1 MHz has been designed and simulated, with two different coupling beam. Mechanical simulation results found from CoventorWare tool have been found to match quite well with the theoretical values, hence confirming the frequency filtering action. Additionally, the analogous S parameter simulation of the MEMS bandpass filter is done with circuit simulators, The frequency response of the designed filter is verified. From Table 5.3 it is observed that V-shaped coupling beam Lame filter provides 22dB pass band ripple, Lame filter with straight coupling beam provides 46dB pass band ripple. Another performance parameter 40dB shape factor for this filters are 1.990,2.498 respectively, From this concluded that V-shaped coupling beam provides better selectivity. V-shaped coupling beam provides 3dB bandwidth of 0.901MHz near to the design Value 1MHz. Lame filter with straight coupling beam provides 3dB bandwidth of 0.66MHz.From the observation concluded that when low ripple is needed in Pass band then Lame filter with straight coupling beam can be replaced with V-shaped coupling beam.

References:

[1] B. Razavi, RF microelectronics, Prentice Hall, NJ, 1998.

[2] C.T.C. Nguyen, "Frequency-selective MEMS for miniaturized low-power communication devices," *IEEE Trans. Microwave Theory And Techniques*, vol. 47, pp. 1486-1503, 1999.

[3] L. Khine, M. Palaniapan, and W.K. Wong, "12.9 MHz Lamé-mode differential SOI bulk resonators," *International Conference on Solid-State Sensors, Actuators and Microsystems*, Lyon, France, 10-14 June, pp. 1753-1756. 2007.

[4] M.M. Shalaby, M.A. Abdelmoneum, and K. Saitou, "Design of spring coupling for high Q, high frequency MEMS filters for wireless applications," *IEEE Trans. Ind. Elec*., vol. 56, no. 4, pp. 1022-1030, 2009.

[5] J.Basu, T.K.Bhattacharyya, R.R.Chaudhuri, A.L. Roy ," A Microelectromechanical Disk Resonator-based Bandpass Filter for Wireless RF Applications," *IEEE Applied Electromagnetics Conference*, Kolkata ,18-22 Dec, 2011.

[6] K. Wang and C. T.C. Nguyen, "High-order medium frequency micromechanical electronic filters," *IEEE/ASME J. Microelectromech. Syst*., vol. 8, no. 4, pp. 534–557, 1999.

[7] R. A. Johnson, Mechanical filters in electronics, Wiley Series on Filters, John Willey & Sons, Canada,1983.

[8] F.D. Bannon, J.R. Clark, C.T.C Nguyen, " High-Q HF microelectromechanical filters. *IEEE J Solid-State Circuits* ., vol. 35, no. 4, pp. 512–526, 2000.

[9] Mehrnaz Motiee, Raafat R Mansour, Amir Khajepour, " Novel MEMS filters for on-chip transceiver architecture, modeling and experiments, " *J. Micromech. Microeng* ., vol. 16, no. 2, pp. 407–418, 2006.

[10] N. Lobotniu and E. Garcia, Mechanics of Micro electromechanical Systems: Kluwer Academic Publishers,Boston, 2005.

[11] F. Nabki, M. N. El-Gamal, and T. A. Dusatko, Wireless technologies circuits, systems and devices, CRC Press, Boca Raton, 2007.

[12] A. I. Zverev, Handbook of filter synthesis, John Wiley & Sons, New York, 1967.

[13] MEMS design and analysis tutorials, vol. 1: physical and system-level design, CoventorWare, Version 2008.

[14] R. Adler, "Compact electromechanical filters,' *Electronics*, vol. 20, pp.100–105, 1947.

[15] A. Ballato and J. G. Gualtieri, "Advances in high-Q piezoelectric resonator materials and devices," *Trans. Ultrason. Ferroelectr. Freq. Control*, vol. 41, pp. 834-844, Nov. 1994.

[16] T. V. Roszhart, "The effect of thermo elastic internal friction on the Q of micro machined silicon resonators," *Tech. Dig. IEEE 1990 Solid-State Sensor and Actuator Workshop*, Hilton Head Island SC, Jun. 4-7, 1990.

[17] D. S. Bindel, E. Quevy, T. Koyama, S. Govindjee, J. W. Demmel, and R. T. Howe, "Anchor loss simulation in resonators," *Proc. IEEE 2005 MEMS Conf*, Miami FL, Jan. 30 - Feb. 3, 2005.

Chapter - 6

Conclusions and Future Scope of work

6.1 Conclusions

The objectives of this thesis are as follows: (1) To select CMOS post–processing compatible material to fabricate MEMS resonators for oscillator and filtering functions in wireless front end architectures and (2) To design a novel MEMS High frequency band pass filters.

Materials selection is essential for the efficient design of various systems, like micro-electromechanical systems (MEMS). With the development of fabrication techniques, the numbers of materials that can be used for MEMS resonator have been increased. Three basic requirements for material selection in MEMS resonator are high *Q*, high resonant frequency, and low process temperature, which in turn depends on suitable material to be used for the disk and supporting beam.

In this thesis, Ashby method is used for material selection Process. For high *Q*, high resonant frequency and CMOS compatible process temperature, it is confirmed that poly$Si_{0.35}Ge_{0.65}$ is the best material for MEMS disk resonator because of high *Q* compared to the Nickel (Ni). Ashby approach results are validated with simulation both are showing poly$Si_{0.35}Ge_{0.65}$ is the best material for the MEMS disk resonator.

Bandpass Lame filter structure for achieving a center frequency of 12.9 MHz and a bandwidth of 1 MHz is designed with two types of coupling beam such as V-shaped coupling beam, straight coupling beam. Important filter parameters such as insertion loss, shape factor and *Q* factor were investigated with FEM analysis.

It is observed that V-shaped coupling beam Lame filter provides 22dB pass band ripple, Lame filter with straight coupling beam provides 46dB pass band ripple. Another performance parameter 40dB shape factors of these filters are 1.990,2.498 respectively, From this concluded that V-shaped coupling beam provides better selectivity. The V-shaped coupling beam provides 3dB bandwidth of 0.901MHz near to the design Value 1MHz. Lame filter with straight coupling beam provides 3dB

bandwidth of 0.66MHz.From the observation concluded that when low ripple is needed in Pass band then Lame filter with straight coupling beam can be replaced with V-shaped coupling beam.

6.2 Future Scope of work

Additional exploration of this work is further required in the following aspects. Firstly, the fabrication of the filter structure has to be done followed by their electrical characterization using a vector network analyzer. Secondly, the proposed triple- plate filter can be further improved by optimizing the placement and dimensions of the two coupling beams used in the design.

The proposed filter we are using a SOIMUMPs process from MEMSCAP for design, which is for general MEMS designs. Because of the relatively large air gap between the resonators and electrodes (2 μm) and other fixed dimensions such as structural layer thicknesses dictated by the SOIMUMPs process, the dc-bias voltage becomes very high in comparison with IC circuits. Using other fabrication techniques allowing sub micron gaps to lower the dc-bias in an IC compatible range is another challenge in RF MEMS design.

Testing of RF MEMS filter is another difficulty that needs to be addressed. In general, the tests should be done in a vacuum chamber to eliminate the effect of air damping on the filter performance. Also, a proper experimental setup is needed to perform the tests.

Last but not least, the MEMS resonator packaging technology is currently a major limitation in using the devices for commercial applications. MEMS resonators are fragile structures, which need to be protected by very clean, enclosed environments from any contaminant which would degrade their short- or long-term performance. Most resonators would greatly benefit from a vacuum packaging, which ensures low damping, thus high quality factors. The package should not degrade the MEMS performance through the addition of parasitic capacitances or stress-induced stiffness changes. Finally, the packaging should meet all above requirements while maintaining a low cost.

A1. MATLAB Code for Disk Resonator based Bandpass Filter

```
%simple model find theoretical frequency for various radius and various
mode
clear all;
Q=1000;
t =2/1000000;
d=1/1000000;
p = 2300;
E = 160000000000;
sig = 0.22;
R = 40/1000000;
alpha1= 1;
alpha2= 2.62;
alpha3= 4.17;
V=35;
x=sqrt(E/p);
f=((0.342*alpha1)/(R))*x;
disp('frequency is ')
 disp(f);
  a=((2*E)/(2+(2*sig)));
 b=((E*sig)/(1-sig));
 h=sqrt((((2*pi*f)^2)*p)/(a+b));
 X=h*R;
 Y=besselj(1,X);
 x=sym('r');%x = sym('x') creates the symbolic variable with name 'r'
and stores the result in x.
 c=h*x;
 arg=(x*power(besselj(1,c),2));
 Etot=int(arg,x,0,R);%int(expr, v, a, b) returns the definite integral
of expr with respect to v from a to b
 Etotal=double(Etot);
 Mre=(2*pi*p*t*Etotal)/(Y^2);
 disp('effective mass is');
 disp(Mre);
 Kre=((2*pi*f)^2)*Mre;
 disp('Kre is ')
 disp(Kre);
 % force calculation
 A=pi*R*t;
 disp('Area is ')
 disp(A);
 F=(((8.85E-12)*A*V*V)/(2*d*d));
 disp('Force is ')
 disp(F);
 eda = (V*(8.854E-12)*A)/(d*d);
 disp('eda is ')
 disp(eda);
 Cre = sqrt(Kre*Mre)/Q;
 disp('Cre is ')
 disp(Cre);
 Rx= Cre/( eda* eda);
 disp('Rx is ')
 disp(Rx);
 Cx =( eda* eda)/Kre;
```

```
 disp('Cx is ')
 disp(Cx);
 Lx=Mre/( eda* eda);
 disp('Lx is ')
 disp(Lx);
 % ONE PORT MEASUREMENT SET UP
 %STATIC CAPACITANCE
 Co1=((8.85E-12)*A)/(d);
 disp('Co1 is ')
 disp(Co1);
 Co=2*Co1;
 disp('Co is ')
 disp(Co);
  % Yin at resonance
  Yin=(1/Rx)+(j*2*pi*f*Co);
  disp(' Yin is ')
 disp( Yin);
  %PARALLEL RESONANCE FREQUENCY
  fp=f*sqrt(1+(Cx/Co));
  disp(' PARALLEL RESONANCE FREQUENCY is ')
 disp( fp);
  %DAMPING CALCULATION
  Bdk=1/(Q*2*pi*f);
  disp(' DAMPING  is ')
 disp( Bdk);
 kij=0.665;  %depends on filter order
 B=1E6;%bandwidth
 ksij=kij*(B/f)*Kre;
 disp(' required coupling beam stifness  is ')
 disp(ksij);
 %coupler length calculation
 %Ls=38.5/1000000;
 Ls=(1*sqrt(E/p))/(4*f)
 disp(' coupling beam length  is ')
 disp(Ls);
 Ws=(ksij*2*Ls)/(pi*E*t);
 disp(' coupling beam width  is ')
 disp(Ws);
 kri=Kre
 krj=Kre
 Kij=0.655
 BW=(f/Kij)*(ksij/sqrt(kri*krj))
 disp('  band width  is ')
 disp(BW);
 %calculate z0 using machanical parameters
 w=2.98/1000000;
 Ac=w*t;
  z0=1/(Ac*sqrt(p*E));%correct one from Mecahanical filter design book
 disp('  Z0 is ')
 disp(z0);
%  calculate capacitor Ca,Cb
Ca=-1/(2*pi*f*z0);
disp(' Ca  with transformr ')
 disp(Ca);
 disp(' Cb with transformer ')
 disp(Ca);
%  calculate capacitor Cc
 Cc=1/(2*pi*f*z0);
disp(' Cc with transformer ')
 disp(Cc);
%calculate  capacitor from Ksij
```

```
% Ca=( eda* eda)/ksij;
% disp(' Ca is ')
%  disp(Ca);
% find stifeness of the coupling beam for entension mode and torison
mode
kc=(2*pi*f)*(Ac*sqrt(p*E));
disp('  stifeness of the coupling beamis ')
disp(kc);
 etac=sqrt(kc/Kre);
 Cs12=(eda^2)/ksij;
 disp(' Ca without tranformer T model ')
 disp(Cs12);
 disp('  sigle coupling filter model Ca ')
 Cs12=1/ksij;
 disp(' Ca is ')
 disp(Cs12);
disp('coupling Termination resistance ')
Qres=233480; %from simulation result
Qfltrv=21797;
q =1.4328;
Rqv=Rx*((Qres/(q*Qfltrv))-1);
disp('Termination resistance is ')
disp(Rqv);
IL=20*log((Rx+Rqv)/Rqv);
disp('Insertion loss is ')
disp(IL);
```

A2. MATLAB code for Lame Resonator Based Bandpass Filter

```
E = 160000000000;
v = 0.064;
rho=2330;
% x =2*(1+v);
G=79.4e9;
% G = E/x;
% disp('G is')
% disp(G);
z = sqrt(G/rho);
% disp('z is')
% disp(z);
L = 320e-6;
% h = 25e-06;
y= 1/(sqrt(2)*L);
% disp('y is')
% disp(y);
f = z*y;
disp('theretical lame f  is')
disp(f);
% for SE MODE
z1=1-(8/(pi*pi));
% disp('theretical Z1s')
% disp(z1);
z2=v/(v-1);
% disp('theretical Z2s')
% disp(z2);
z3=z1*z2;
% disp('theretical Z3s')
% disp(z3);
z4=1+z3;
z5=z4*(E/(rho*(1-v)));
z6=1/(2*L);
z7=z6*sqrt(z5);
disp('theretical square extension f  is')
disp(z7);
h=25e-6;
me=(rho*h*L*L)/(2);
disp('theretical meq is')
disp(me);
F =z7;% we are feeding from simulation
xo =5.12e-11;% displacement we are feeding from simulation
VP=100;  % bias voltage we are feeding from simulation
ep=8.9e-12;
Le= 320e-06; % length of electrode from simulation
d=2e-6;% gap from simulation
 t =25/1000000;
co= (ep*4*Le*h)/(d);
disp('theretical C0 is')
disp(co);
% eda =(co*VP)/(d);
eda =(2*ep*Le*t*VP)/(pi*d*d);
disp('theretical eda is')
disp(eda);
keq=(pi*pi*E*t)/(2*(1+v));
disp('theretical Keq is')
disp(keq);
Lx=me/(eda*eda);
disp('theretical Lx is')
```

```
disp(Lx);
Cx=(eda*eda)/keq;
disp('theretical Cx is')
disp(Cx);
Q =759360;% Q from simulation
Rx=(sqrt(keq*me))/(Q*(eda*eda));
disp('theretical Rx is')
disp(Rx);
%  % Yin at resonance
%   Yin=(1/Rx)+(j*2*pi*f*co);
%   disp(' Yin is ')
%  disp( Yin);
%   %PARALLEL RESONANCE FREQUENCY
%   fp=f*sqrt(1+(Cx/co));
%   disp(' PARALLEL RESONANCE FREQUENCY is ')
%  disp( fp);
%   %DAMPING CALCULATION
%   Bdk=1/(Q*2*pi*f);
%   disp(' DAMPING  is ')
%  disp( Bdk);
 kij=0.665;  %depends on filter order
 B=1e6;%bandwidth
 ksij=kij*(B/f)*keq;
 %ksij coupling beam stifness
 disp(' coupling beam stifness  is ')
 disp( ksij);
 %coupler length calculation
 %Ls=38.5/1000000;
 Ls=(1*sqrt(E/rho))/(4*f);
 disp(' coupling beam length  is ')
 disp(Ls);
 Ws=(ksij*2*Ls)/(pi*E*t);
 disp(' coupling beam width  is ')
 disp(Ws);
 kri=keq;
 krj=keq;
 Kij=0.655;
 BW=(f/Kij)*(ksij/sqrt(kri*krj));
 disp('  band width  is ')
 disp(BW);
 disp('  V shape coupling beam design ')

ws=24e-6;
 Is=(ws*t*t*t)/12;
% %  Ls=23e-6;
 disp('Vshape coupling beam moment of inertia  is ')
 disp(Is);
% %  v2=Ls*Ls*Ls*kij*keq;
% %  B=(6*E*Is*f)/v2;
% %  disp('Vshape coupling beam  BW  is ')
% %  disp(B);
ksij=kij*keq*0.077;
Ls3=(6*E*Is)/(ksij);
disp('Vshape coupling beam Ls3  is ')
disp(Ls3);
Ls=31e-6;
disp('Vshape coupling beam Ls  is ')
disp(Ls);
ds=40e-6;
% theta=49.88;
% Rs=Ls* sin(theta);
```

```
% disp('Vshape coupling beam Rs  is ')
% disp(Rs);
% ws= 2.6138e-05
% Lsa=rho*t*ws*Ls ;
% disp('Vshape coupling beam Lsa  is ')
% disp(Lsa);
% Csc=kij*(B/f)*keq;
% disp('Vshape coupling beam Csc  is ')
% disp(Csc);
% FIndinding the termination resistance
Qres=8527338; %from simulation result
Qfltr=970889;
q =1.4328;
Rq=Rx*((Qres/(q*Qfltr))-1);
disp('Termination resistance is ')
disp(Rq);
IL=20*log((Rx+Rq)/Rq);
disp('Insertion loss is ')
disp(IL);

disp('Vshape coupling Termination resistance ')
Qres=8527338; %from simulation result
Qfltrv=586194;
q =1.4328;
Rqv=Rx*((Qres/(q*Qfltrv))-1);
disp('Termination resistance is ')
disp(Rqv);
IL=20*log((Rx+Rqv)/Rqv);
disp('Insertion loss is ')
disp(IL);
```

List of Publications

Publication in Journals

[1] G.M. Sundaram, Mahesh Angira, Navneet Gupta and Kamaljit Rangra, "Material Selection for CMOS Compatible High Q and High Frequency MEMS Disk Resonator using Ashby Approach," *International Journal of Nanoelectronics and Materials*. [accepted]

[2] G.M. Sundaram, Mahesh Angira and Kamaljit Rangra," Design of VHF MEMS Disk Resonator," *International journal of Systems and Technologies*, vol.5, no 2, pp 18- 25, 2012. (ISSN 0974-2107).

[3] Mahesh Angira, G.M. Sundaram and Kamaljit Rangra, "A Novel Approach for Low Insertion Loss, Multi-band, Capacitive Shunt RF–MEMS Switch," *Wireless Personal Communications*, vol 83, no 3, pp 2289-2301, 2015. (ISSN: 0929-6212)

Publication in Conferences

[1] G.M. Sundaram, M. Angira, Navneet Gupta and K. Rangra, " A MEMS Disk Resonator-based Band pass Filter Electrical Equivalent Circuit Simulation," *International Conference on Emerging Technologies: Micro to Nano-2015 (*ETMN 2015*),*" Jaipur, India 24-25 October 2015.**[Published in Conference proceedings of American Institute of Physics (AIP)**].

[2] G.M. Sundaram, M. Angira and K. Rangra, "VHF MEMS Disk Resonator Design and Simulation," in *International Conference on RF and Signal Processing Systems*, Vijaywada, India, 2013, pp. 159-163

[3] G.M. Sundaram, M. Angira and K. Rangra, "Voltage Controlled MEMS Tunable Resonator Design and Analysis," in *International Conference on Smart Structures & Systems*, Chennai, India, 2013, pp. 1-3.

[4] G.M. Sundaram, M. Angira and K. Rangra, "Design and simulation of two port RF MEMS resonators," in *International Conference on Computer Communication and Informatics*, Coimbatore, India, 2012, pp. 1-3. [A**vailable in IEEE Xplore digital library**]

[5] G.M. Sundaram, M. Angira and K. Rangra, "An Approach For Motional Resistance Minimization in RF MEMS Disk Resonator," in *National conference on Recent Trends in Communication and Signal Processing*, Coimbatore, India, 2014, pp. 1-4.

Brief biography of the Candidate

G.Meenakhsi Sundaram did his B.E. in Electronics and Communication Engineering (2000) from Govt. College of Engineering, Tirunelveli, Tamil Nadu and M.E. Communication Systems (2004) from MEPCO Schlenk Engineering College, Sivakasi, Tamil Nadu. I am presently working as Lecturer in Electrical & Electronics Engineering (EEE), BITS-Pilani, Pilani Campus. I have teaching experience of more than 12 years at under graduate and graduate levels. My research areas are MEMS Resonator and Filter Design and Analysis etc.

Brief biography of the Supervisor

Dr. Kamaljit Rangra received his Ph.D. from University of Trento, Italy and Master degree in Microelectronicsfrom Birla Institute of Technology and Science (BITS)Pilani, India. He is currently working as Chief Scientist, Semiconductor Device Area at CSIR-Central Electronics Engineering Research Institute (CEERI), Pilani, Rajasthan.

His research area includes Radio frequency MEMS, MEMS based IR & Inertial Sensors and vacuum microelectronics. He has been associated with various projects such: (1) Design, fabrication & characterization of RF MEMS switches; (2) HRD under NPMASS Project (Maintaining Si- Wafer fabrication Facility for supporting HRD; (3) Innovative high k-dielectric RF -MEMS switch development; (4) Advanced Microsensors & Microsystems: Design, Development & Applications; (5) Design, development and packaging of RF MEMS switches; (6)Digital micro-mirror devices (DMD); (7) Development of Medium Power RF MEMS Ohmic Contact Switch and (8) Pattern Up Plating (PuP) process for MIC fabrication. Some of the project have successfully been completed while a few are in progress.

His teaching responsibilities include – Professor AcSIR new Delhi, Ex-Adjunct Professor , Bengal Engineering and Science University, Shibpur (West Bengal) and Tutor/Resource person CSIR- Human Resource Development Centre, at Ghaziabad. He is also Associate Editor of ISSS Journal and reviewer for (i) International Journal of Applied Electromagnetics and Mechanics, IOS Press , The Netherlands; (ii) AEÜE - International Journal of Electronics and Communications (Elsevier B.V.); (iii) Elsevier Journal of Materials and Design.

He has about 80 international journal publications to his credit in addition to several conference proceedings. He has successfully guided two doctoral students and presently guiding nine Ph.D candidates. He is Fellow of IETE (1998), Institution of Engineers (IE) 2014, Metrology Society of India (MSI) 2012, member and Secretary (local Chapter), Semiconductor Society of India (SSI) and Secretary (local Chapter) Indian Physics Association (1995).